1-28-2015

A High Power Microwave Zoom Antenna With Metal Plate Lenses

Julie Lawrance

Julie Lawrance
Candidate

Electrical Engineering
Department

This dissertation is approved, and it is acceptable in quality and form for publication:

Approved by the Dissertation Committee:

Dr. Christos Christodoulou , Chairperson

Dr. Edl Schamilaglu

Dr. Mark Gilmore

Dr. Mahmoud Reda Taha

A HIGH POWER MICROWAVE ZOOM ANTENNA WITH METAL PLATE LENSES

by

JULIE LAWRANCE

B.A., Physics, Occidental College, 1985
M.S. Electrical Engineering, 2010

DISSERTATION

Submitted in Partial Fulfillment of the
Requirements for the Degree of

Doctor of Philosophy
Engineering

The University of New Mexico
Albuquerque, New Mexico

December, 2014

A HIGH POWER MICROWAVE ZOOM ANTENNA WITH METAL PLATE LENSES

by

Julie Lawrance

B.A., Physics, Occidental College, 1985

M.S., Electrical Engineering, University of New Mexico, 2010

Ph.D., Engineering, University of New Mexico, 2014

ABSTRACT

A high power microwave antenna with true zoom capability was designed and constructed with the use of metal plate lenses. Proof of concept was achieved through experiment as well as simulation. This concept comprises a horn feed antenna and two metal plate lenses. Good agreement was found between experiment and simulation. This antenna provides true zoom capability in the TEM mode with continuously variable diameter pencil beam output and approximately 10% bandwidth.

Carbon Fiber Reinforced Polymer (CFRP) composites were demonstrated through experiment and simulation to have sufficient conductivity to replace metal for the lens elements and would provide a stronger, lighter weight alternative to metal. Such compounds should be considered for lower frequency applications to minimize overall system weight. In addition, the lower conductivity of these materials may help to mitigate possible spurious modes induced by longitudinal electric fields in the near field of the horn feed antenna.

TABLE OF CONTENTS

1. INTRODUCTION 1

2. BACKGROUND 4

3. ZOOM ANTENNA CONCEPT 6

3.1 Theory of Metal Plate Lenses 6

3.1.1 Parallel Plates as Waveguide Array 6

3.1.2 Index of Refraction of Waveguide Array 7

3.1.3 Shaping Array to Achieve Desired Focal Length 9

3.2 Zoom Antenna Concept 13

4. RESULTS AND ANALYSIS 20

4.1 Preliminary Experimental Results: Low Power 5GHz Lens 20

4.2 Simulated Results: 10GHz Zoom Antenna Concept 29

4.2.1 Simulation of Feed Horn 29

4.2.2 Simulation of Horn and Lens 1 38

4.2.3 Simulation of Horn and Both Lenses 53

4.3 Experimental Results: Low Power 10GHz Zoom Antenna 73

4.3.1 Experimental Setup for Zoom Antenna Measurements 74

4.3.2 Results of Zoom Antenna Measurements 76

4.3.3 Validation of Code: Comparison of Experimental with Simulated Results for 5GHz Lens 80

4.4 High Power Demonstration: L-Band Lens 84

4.5 Evaluation of Carbon Fiber Reinforced Polymer Composites 91

4.5.1 Experimental Results: Impulse Tests 93

4.5.2 Simulations to Explore Minimum Conductivity Required for Lens Plates 99

4.6 Analysis/Mitigation of Spurious Modes 109

4.7 Phase Error Analysis 120
4.8 Reflection at Air-Lens Interface 125
4.9 Bandwidth 127
4.10 Magnification Range/ Zoom Ratio 129
4.11 Maximum Power Handling Capability 135
5. SUMMARY AND CONCLUSIONS 138
6. REFERENCES 140

LIST OF FIGURES

Figure 1. Parallel Plate Waveguide Array 7
Figure 2. Sign Convention for a Bi-concave Lens 9
Figure 3. Front and Back Faces of the Parallel Plate Waveguide Array 11
Figure 4. Illustration of bi-concave, spherical metal plate lens 12
Figure 5. Collimation of beam with lens placed one focal length away from phase center of horn 14
Figure 6. Focus of beam to an Airy Disc in the focal plane when S1>f 15
Figure 7. Collimation of beam by placing a second lens, with focal length f', one focal length away from the focal plane of Lens 1 17
Figure 8. By moving Lens 1 further away from phase center of horn and re-positioning Lens 2, a broader collimated beam is achieved 18
Figure 9. Design and construction of prototype lens 21
Figure 10. Lens center plate 22
Figure 11. 5GHz prototype lens plates prior to assembly 24
Figure 12. Test setup showing fully assembled lens, transmit and receive horn antennas 25
Figure 13. Measured electric field at fixed location of receive antenna; 26
Figure 14. Gain of horn and lens 27
Figure 15. Horn Antenna Used in Simulations 31
Figure 16. Waveguide port at input to waveguide 31
Figure 17. Gaussian voltage waveform applied to waveguide port (9.8-10.2GHz) 32
Figure 18. Power spectral density of 10GHz Gaussian excitation 33
Figure 19. Fields radiated from horn antenna 34
Figure 20. 3-D Radiation Pattern of 10GHz horn antenna 35
Figure 21. E-Plane radiation pattern 36
Figure 22. H-Plane radiation pattern 36
Figure 23. Electric field along boresight (mouth of horn at y=188mm) 37
Figure 24. Biconcave Lens 1 with focal length of 254mm and diameter of 304.8 mm ... 39
Figure 25. Lens 1 at y = 800 mm, oriented with plates parallel to the electric field vector. 40
Figure 26. Electric Field (Ex) Contour Map Showing Beam Focus 41

Figure 27. Carpet Representation of Electric Field (Ex) in the Focal Plane of Lens 1 42
Figure 28. Boresight Measurement of Electric Field (Ex)..... 43
Figure 29. Electric Field Near the Focal Plane of Lens 1 (Lens 1 at y = 800mm) 44
Figure 30. Electric Field Across the Focal Plane in the E-plane 45
Figure 31. Electric Field Across the Focal Plane in the H-plane..... 46
Figure 32. Effective Focal Length of Lens (Designed for f=262mm) vs. S1 48
Figure 33. Boresight electric field showing beam collimation 49
Figure 34. Radiation pattern with lens 1 at y = 500 mm 49
Figure 35. S11 Measurement for Lens 1 at y = 500mm. 50
Figure 36. VSWR with lens 1 at y = 500mm..... 51
Figure 37. S11 of Horn/Lens combination with lens at y = 700mm 52
Figure 38. VSWR with lens 1 at y = 700mm..... 52
Figure 39. Amplitude Plot of Electric Field (Ex) in the E-Plane (Narrow Beam)..... 55
Figure 40. Simulated Boresight Measurement of Electric Field (Ex) – Narrow Beam.... 56
Figure 41. “Carpet” Representation of Electric Field (Ex) at y = 6500mm (Narrow Beam) 57
Figure 42. Electric Field (Ex) in the E-Plane at y = 6500 mm (Narrow Beam) 58
Figure 43. Electric Field (Ex) in the H-plane at y = 7000 mm (Narrow Beam)..... 58
Figure 44. Phase Plot of Electric Field (Ex) in the E-Plane (Narrow Beam) 59
Figure 45. Phase Plot of Electric Field (Ex) in the H-Plane at y = 6500 mm (Narrow Beam)..... 60
Figure 46. 3-D Radiation Pattern (Narrow Beam)..... 61
Figure 47. Far Field Radiation Pattern in the E-Plane (Narrow Beam)..... 62
Figure 48. Far Field Radiation Pattern in the H-Plane (Narrow Beam) 62
Figure 49. Amplitude Plot of Electric Field (Ex) in the E-Plane (Broad Beam)..... 64
Figure 50. Simulated Boresight Measurement of Electric Field (Ex) – Broad Beam 65
Figure 51. “Carpet” Representation of Electric Field (Ex) at y = 6500mm (Broad Beam) 66
Figure 52. Electric Field (Ex) in the E-Plane at y = 6500 mm (Broad Beam)..... 67
Figure 53. Electric Field (Ex) in the H-plane at y = 7000 mm (Broad Beam) 67
Figure 54. Phase Plot of Electric Field (Ex) in the E-Plane (Broad Beam)..... 68

Figure 55. Phase Plot of Electric Field (Ex) in the H-Plane at y = 6500 mm (Broad Beam) 69
Figure 56. 3-D Radiation Pattern (Broad Beam) 70
Figure 57. Far Field Radiation Pattern in the E-Plane (Broad Beam) 71
Figure 58. Far Field Radiation Pattern in the H-Plane (Broad Beam) 72
Figure 59. Test Setup for Exploring Beam Collimation 74
Figure 60. Test Setup; Lenses Positioned for Beam Collimation 75
Figure 61. Boresight Measurements of 10GHz Low Power Demonstrator Zoom Antenna 76
Figure 62. E-Plane Measurements (Lenses Positioned for Narrow Collimated Beam) .. 77
Figure 63. H-Plane Measurements (Lenses Positioned for Narrow Collimated Beam 78
Figure 64. E-Plane Measurements (Lenses Positioned for Broad Collimated Beam) 79
Figure 65. H-Plane Measurements (Lenses Positioned for Broad Collimated Beam) 79
Figure 66. Experimental normalized S21 measurement across focal plane of 5GHz lens in the E-plane 81
Figure 67. Simulated Electric Field Across Focal Plane for 5GHz Lens in the E-Plane.. 82
Figure 68. Comparison of Simulated to Experimental Results..... 83
Figure 69. L-Band Lens for High Power Demonstration 84
Figure 70. Boresight Measurements With and Without Lens..... 85
Figure 71. Low Power Measurements; Electric Field across E-Plane in the Focal Plane of the Lens 86
Figure 72. Low Power Measurement: Electric Field Across H-Plane in the Focal Plane of the Lens 87
Figure 73. High Power Measurements: Boresight Electric Field Through Focal Plane... 88
Figure 74. High Power Measurements: E-Field Across E-Plane in Focal Plane of Lens. 89
Figure 75. High Power Measurements: Electric Field Across H-plane in Focal Plane of Lens..... 89
Figure 76. Test Setup for Impulse Measurements 93
Figure 77. Transmit and Receive Antennae Used in Impulse Tests 94
Figure 78. Special PBG1 Pulse Source Used in Impulse Tests 95
Figure 79. Tek. DPO 7254 Oscilloscope in Screened Enclosure 96

Figure 80. Absorber Box with Copper Sample for Impulse Tests 97
Figure 81. Results of Impulse Tests 98
Figure 82. Simulated Design of LBand Horn and Lens to Explore Effect of Varying Conductivity of Plates 99
Figure 83. Gaussian Excitation (Time Domain) 101
Figure 84. Power Spectral Density of Gaussian Excitation (Frequency Domain) 102
Figure 85. Conductivity of CFRP/CNT Compared to Aluminum 103
Figure 86. Skin depth of CFRPC and Aluminum 104
Figure 87. Simulated Boresight Measurements with Lens Plate Material of Varying Conductivity 105
Figure 88. Simulated Boresight Measurement for Various Conductivities: Close Up of Focal Region. 106
Figure 89. E-Plane Measurements Across Focal Plane 108
Figure 90. H-Plane Measurements Across Focal Plane 108
Figure 91. Gain of 10GHz Horn Antenna at 30GHz 110
Figure 92. X-Band Horn with Field Monitor in the Near Field (y = 200mm) 112
Figure 93. Near Field Electric Field (E_x) 113
Figure 94. Transverse Electric Fields (Ez) 114
Figure 95. Longitudinal Electric Field (E_y) 115
Figure 96. Longitudinal Fields Ey in the X-Y Plane 116
Figure 97. Illustration of Mismatch Between Radius of Curvature of Lens and Incident Phase-Front 120
Figure 98. Difference Between Phase Front and Curvature of Lens 1 122
Figure 99. Phase Across E-Plane in the Focal Plane 123
Figure 100. Phase Across H-Plane in the Focal Plane 124
Figure 101. Variation in Index of Refraction with Frequency 127
Figure 102. Zoom Antenna Concept 129
Figure 103. Magnification for Varying S1/f1 and f2/f1 133
Figure 104. Source Power Requred to Induce Air Breakdown in the Focal Region 137

LIST OF TABLES

Table 1. Feed Horn Parameters..... 30
Table 2. Lens 1 Design Parameters..... 38
Table 3. Location of Focal Plane and Effective Focal Length for Decreasing S1..... 47
Table 4. Lens 2 Design Parameters..... 53
Table 5. Lens Positions Corresponding to Narrow and Broad Collimated Beams..... 53
Table 6. Properties of Metals..... 91
Table 7. Design Parameters for LBand Horn and Lens..... 100
Table 8. Attenuation Due to Conductor Loss for Al and CFC..... 118
Table 9. Excel Spreadsheet Created to Design 10GHz Zoom Antenna..... 132

1. INTRODUCTION

A true zoom antenna produces a collimated beam of electromagnetic (EM) energy with a planar wavefront and with continuously variable diameter. This type of antenna provides beam control in terms of spot size and power density on target. A true high power microwave (HPM) zoom antenna greatly extends the range of an HPM source and is useful for such applications as target acquisition and tracking, communications, and electronic attack. Until now, true zoom antenna capability for high power microwave applications did not exist.

The zoom antenna concept presented herein consists of a horn feed antenna and two metal plate lenses. These lenses are particularly well suited to this application. While aluminum was originally the metal of choice for these lenses, newly emerging carbon fiber compounds (CFCs) were demonstrated to have sufficient conductivity for this application. These compounds have lower density than aluminum; they provide a lightweight alternative to metal for lens construction, which becomes important for applications at lower frequencies.

This effort comprises design and demonstration – through experiment and simulation - of a true zoom antenna concept for HPM applications. This is a narrowband antenna with approximately 10% bandwidth which produces a linearly polarized collimated beam with continuously variable diameter (achieved by axial translation of the lenses relative to each other and relative to the feed horn). The zoom antenna can be designed for a wide range of frequencies from hundreds of megahertz (MHz) to tens of gigahertz (GHz). It

has excellent power handling capability: ranging from tens of megawatts (MW) at 10GHz to several gigawatts (GW) at 1GHz.

This is a practical system that could be implemented in the field near-term. Design considerations and analysis are focused on minimizing complexity and cost of fabrication. However, if minimizing weight is an issue, carbon fiber compounds should be considered for lens construction.

A background of the zoom antenna concept and metal plate lens is provided in Section 2.

The theory of the metal plate lens is presented in Section 3 along with design considerations for shaping of the lens to achieve the desired focal length. The zoom antenna concept is also described in detail in this Section.

Section 4 presents results of experiment and simulation. Section 4.1 presents preliminary experimental results of a low power 5GHz lens designed and constructed simply to explore focusing capability of a metal plate lens. Section 4.2 presents the results of simulation of the zoom antenna concept at 10GHz using CST Microwave Studio and shows simulations of beam collimation for minimum and maximum beam diameter. Results of cold tests conducted on a low power zoom antenna designed and constructed to explore zoom capability at 10GHz are presented in Section 4.3. Section 4.4 describes the results of high power experiments on a metal plate lens designed for L-Band operation. Evaluation of carbon fiber compounds (CFCs) as lightweight alternatives to metal plates for the lenses is presented in Section 4.5: this includes a description of desired physical and electrical characteristics of lens plates and includes simulated and

experimental results conducted to evaluate the effect of replacing metal plates with carbon fiber compounds. Section 4.6 presents and analysis of spurious modes in the system. Phase error analysis is presented in Section 4.7; with emphasis on minimizing complexity and cost of the zoom antenna system. Analysis of reflection at the air-lens interface- due to backscatter from the metal plates and mode-mismatch is presented in Section 4.8. Section 4.9 presents an analysis of the bandwidth of the system. Design considerations to optimize magnification range of the complete zoom antenna for a specific application is presented in Section 4.10. Section 4.11 presents analysis of the maximum power handling capability of the zoom antenna system.

Summary and conclusions are presented in Section 5.

All references are listed in Section 6.

2. BACKGROUND

Historically, the term “zoom antenna” has been erroneously applied to reflector antennas that are used to broaden the beam through a defocusing effect; there are a number of these types of antennas described in available literature and existing patents; some examples are given in [Ref 1-3]. These are not technically zoom antennas. While Cassegrain and Gregorian (reflector) antennas can produce a collimated beam of electromagnetic energy; they cannot provide continuously variable diameter of this collimated beam. True zoom capability cannot be achieved with any of these reflector type antennas.

A true high power microwave (HPM) zoom antenna therefore requires the use of lenses. Dielectric lenses are not a good option for HPM applications because they are lossy at high frequencies and because they become prohibitively heavy at lower frequencies on the order of a few gigaherz. Metal plate lenses are particularly well-suited to the HPM zoom antenna application.

The concept of the metal plate lens was proposed by W.E. Kock [Ref. 4] in the 1940’s; however, it has found limited application since. An example is found in [Ref. 5] for satellite communications at high frequencies. More detailed discussion of these lenses are found in [Ref. 6-9]. According to Krauss, [Ref. 10], one of the major benefits of parallel plate waveguide lenses (or what he refers to as “E-plane metal plate lens antennas”) over parabolic reflectors is that the tolerance of this type of lens is much higher than the surface contour requirements of a parabolic reflector such that, “a relatively large amount

of warping and twisting can be tolerated". This is a major benefit for a practical system that can be implemented in the field, and, in fact, this was demonstrated to be true in experiments presented herein.

A drawback of these lenses, according to Krauss, is their small bandwidth. He derives in [Ref. 7] a bandwidth on the order of 5%; however it was found in these experiments that the usable bandwidth is closer to 10%.

Single metal plate lenses have been designed and implemented by HAM radio operators to extend the range of radar guns [Ref. 11]. They have also been implemented in experiments designed to explore interaction of HPM energy with plasmas. It is thought that they were once used as boosters in telecommunications systems; however documented evidence of this is not readily available.

Implementing these lenses in a high power microwave zoom antenna has not been proposed or demonstrated prior to this work.

3. ZOOM ANTENNA CONCEPT

The zoom antenna concept is presented in this Section, beginning with a description of the theory of the metal plate lenses that provide the zoom capability.

3.1 Theory of Metal Plate Lenses

Metal plate lenses are essentially shaped parallel plate waveguide arrays designed to operate in the TE1 mode of propagation. This array will appear – to an incident TEM wave with electric field parallel to the plates – to have an index of refraction less than 1. The array can then be shaped according to optics equations to yield a metal plate lens with the desired focal length.

3.1.1 Parallel Plates as Waveguide Array

A simple parallel plate waveguide array is illustrated in Figure 1. A narrowband TEM wave incident on this structure will propagate through it in the TE1 mode if the spacing "a" between the conducting plates is slightly more than half a wavelength of the incident wave. Arrows indicate direction of the electric field vector (**E**) and direction of propagation (**k**). To ensure higher order modes are cutoff, the spacing "a" between the plates should be on the order of 0.6-0.8λ.

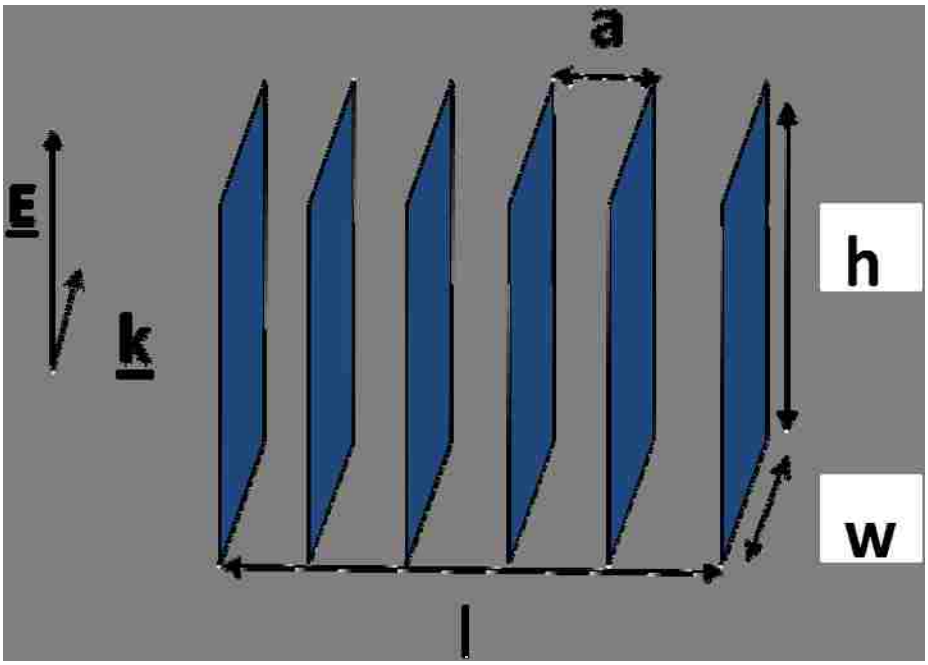

Figure 1. Parallel Plate Waveguide Array

The width of the plates, indicated by "w" in Figure 1 must be at least 1.5 λg to ensure propagation of the TE1 mode, where λg is the waveguide wavelength.

3.1.2 Index of Refraction of Waveguide Array

From optics, the index of refraction, n, of a medium is determined by the ratio of the wave velocity in a vacuum, c, to the wave velocity in the medium, v_{med}, or

$$n = \frac{\text{c}}{v_{\text{med}}} \qquad [1]$$

In waveguide, the phase velocity, v_{ph}, is greater than the speed of light and is determined by

$$v_{\mathrm{ph}} = \frac{\mathrm{c}}{\sqrt{1 - \left(\frac{f_c}{f}\right)^2}} \quad [2]$$

Where f_c is the cutoff frequency and f is the frequency in vacuum.

For the TE1 and TM1 mode of propagation in parallel plate waveguide, the cutoff frequency is determined by

$$f_c = \frac{\mathrm{c}}{2\mathrm{a}} \quad [3]$$

This can be re-written as

$$f_c = \frac{\lambda \mathrm{f}}{2\mathrm{a}} \quad [4]$$

Where λ is the free space wavelength. Substituting [4] into [2], yields

$$n = \frac{v_0}{v_{ph}} = \sqrt{1 - \left(\frac{\lambda}{2a}\right)^2} \quad [5]$$

Therefore, this array of conducting plates appears as a rectangular volume whose index of refraction is less than 1 for an incident TEM wave with electric field vector parallel to the plates and when the dimension "a" is such that ½ λ < a λ.

3.1.3 Shaping Array to Achieve Desired Focal Length

This array can then be shaped into a spherical lens to achieve the desired focal length according to the lensmaker's equation:

$$\frac{1}{f} = (n-1) * (\frac{1}{R1} - \frac{1}{R2} + \frac{(\mathrm{n}-1)\mathrm{d}}{nR1R2}) \quad [6]$$

Where f is the focal length, d is the thickness of the lens, and R1 and R2 are the radii of curvature of the front and back faces of the lens, with sign convention shown, for a concave lens, shown in Figure 2.

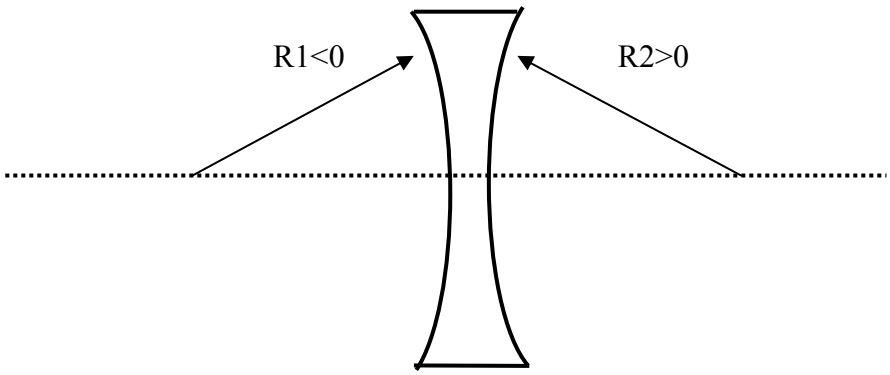

Figure 2. Sign Convention for a Bi-concave Lens

For the design of lenses developed for simulation and experiment in this effort, the thin lens approximation , given by

$$\frac{1}{f} = (n-1) * (\frac{1}{R1} - \frac{1}{R2}) \quad [7]$$

was assumed. In fact, it is common practice in designing optical zoom lenses to start with a thin lens layout. [Ref. 12].

The parallel plate waveguide array can then be shaped by moving a sphere of radius R1 into the front face of the array as indicated in Figure 3, in axial alignment with the plates, and subtracting the sphere volume from the array volume and repeating this on the back face with a sphere of radius R2.

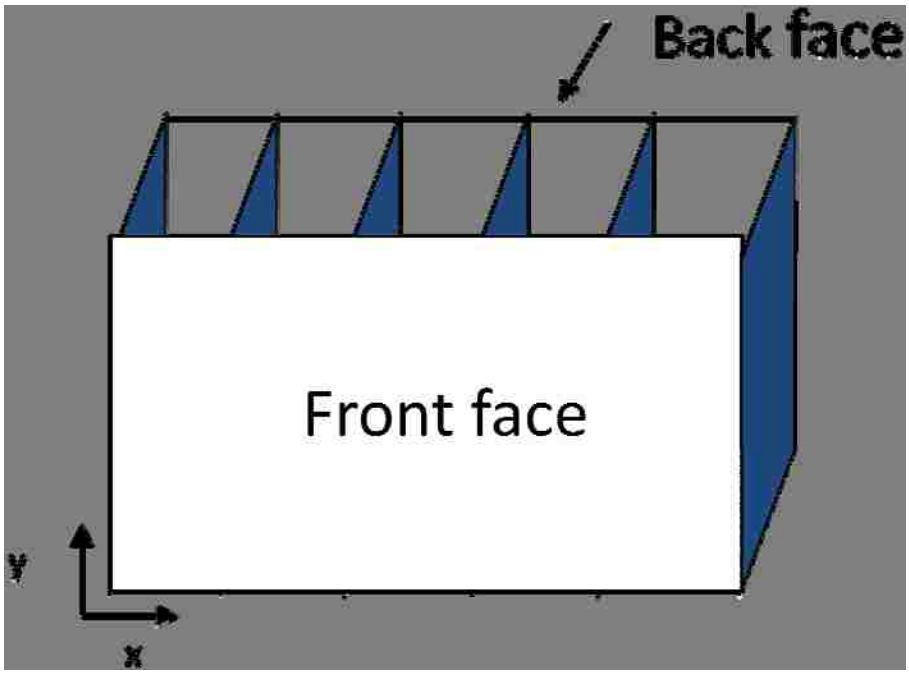

Figure 3. Front and Back Faces of the Parallel Plate Waveguide Array

The result is a biconcave metal plate lens, as shown in Figure 4, with a focal length determined by Equation 7. Because the index of refraction of a metal plate lens is less than 1, a bi-concave metal plate lens is equivalent in terms of its focusing properties, to a biconvex dielectric lens with index of refraction greater than 1.

The lens is thinnest at the middle of the center plate. In designing these lenses, one must ensure that this is at least 1 ½ λg to ensure propagation of the wave through this part of the lens in the TE1 mode.

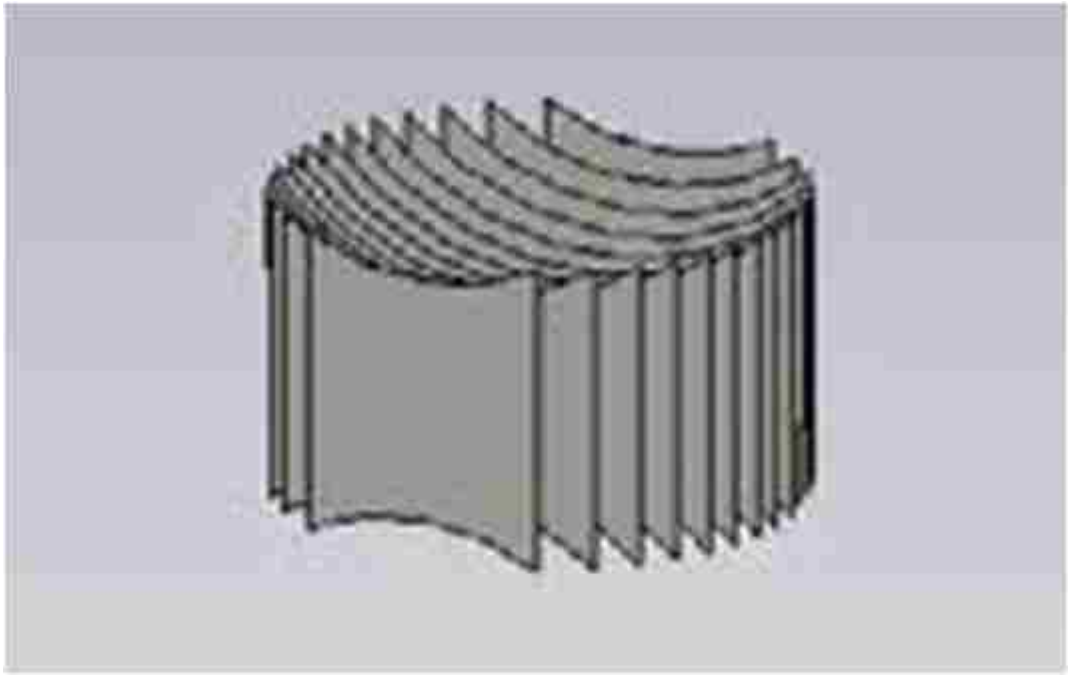

Figure 4. Illustration of bi-concave, spherical metal plate lens

3.2 Zoom Antenna Concept

This zoom antenna is a system comprising a pyramidal horn and two metal plate lenses which can be translated on axis to achieve zoom capability. These lenses operate on the principle of EM waves travelling through the lens with a phase velocity that is faster than the speed of light as opposed to dielectric lenses that operate on the principle of EM waves travelling slower than the speed of light in the dielectric medium.

A waveguide horn antenna (typically under vacuum for very high power operation) is an appropriate radiator for an HPM source. If one were to measure the electric field along boresight of this system, one would see high fields in the waveguide. These would decrease as the electromagnetic energy propagates through the flared horn, then fall as $1/r^2$ as it propagates away from the antenna. The radiated beam flares out from the mouth of the horn antenna with a half power beam width that is inversely proportional to the gain of the antenna. The phase front of the wave radiated from the horn is close to spherical over its half power beamwidth and is centered at the phase center of the horn for a given frequency. While the phase center is different in the E- and H- planes for a pyramidal horn antenna, this difference is very small for a moderate gain pyramidal horn antenna [Ref .13] and it is within the tolerance of the zoom antenna system as will be demonstrated herein.

This diverging beam from the transmit horn antenna can be collimated or focused by a single metal plate lens. This is governed by the lens equation:

$$\frac{1}{f} = \frac{1}{S1} + \frac{1}{S2} \qquad [8]$$

where S1 is the distance from the phase center of the horn antenna to the center of the lens. If the lens were designed with a focal length of f and placed with its axis along boresight of the horn antenna at a distance of one focal length from the phase center of the horn, as shown in Figure 5, the beam emerging from the lens would be collimated.. This is because at S1 = f, S2 = ∞. This is indicated in Figure 5 by the dashed lines to the right of the lens.

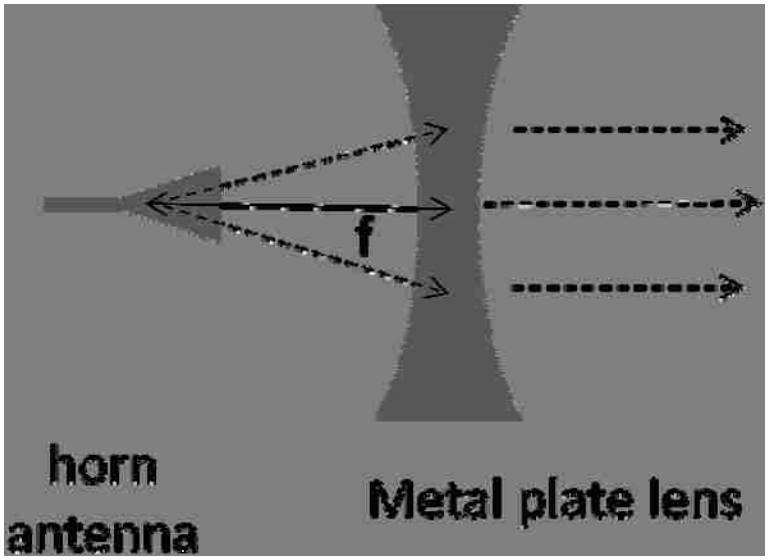

Figure 5. Collimation of beam with lens placed one focal length away from phase center of horn

Because the beam diverges as it radiates from the horn antenna, the lens diameter must increase with focal length in order to intercept most of the radiated beam. The peak

electric field in the collimated beam therefore decreases as the focal length increases and the diameter of the collimated beam increases, assuming the lens is made large enough to intercept the entire beam..

Now, if the lens is placed more than one focal length away at a distance of S1, it will focus the beam to an Airy disk in the focal plane located at S2 as shown in Figure 6, where S2 is determined from Equation 8.

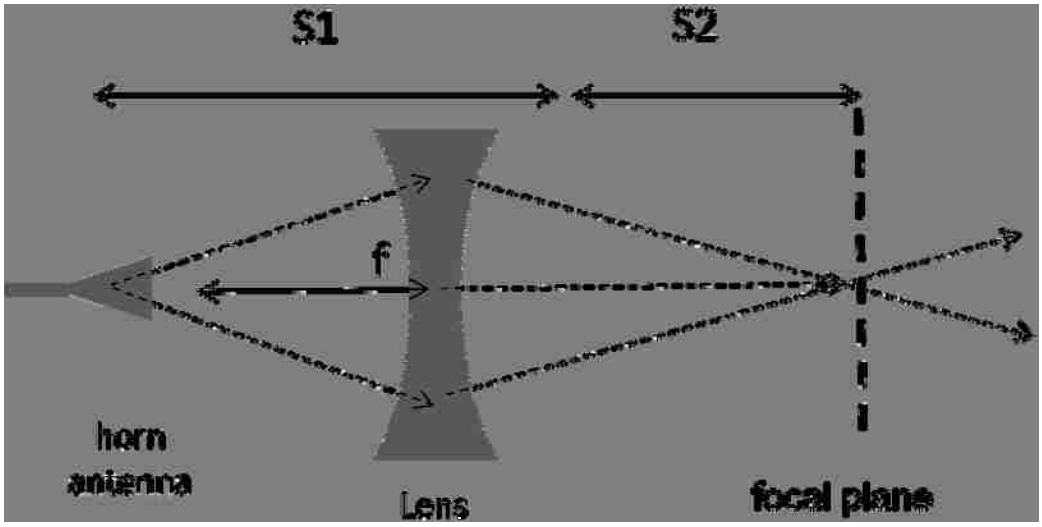

Figure 6. Focus of beam to an Airy Disc in the focal plane when S1>f

The diameter of the disk is diffraction limited to

$$X = 1.2\frac{\lambda * f}{d} \quad [9]$$

Where f is the focal length and d is the diameter of the lens.

The angle of divergence of the beam as it propagates away from the airy disk along boresight is the same as the angle of convergence of the beam as it propagates from the lens towards the focal plane.

Now, place a second lens, with focal length f' at a distance of f' from the focal plane of the first lens, keeping everything else fixed. RF energy will diverge from the focal plane of the first lens as it propagates towards the second lens and will be collimated by the second lens as indicated in the drawing of Figure 7. The beam, as it propagates away from the second lens will have a diameter that corresponds to the diameter of the beam intercepted by the second lens at this location.

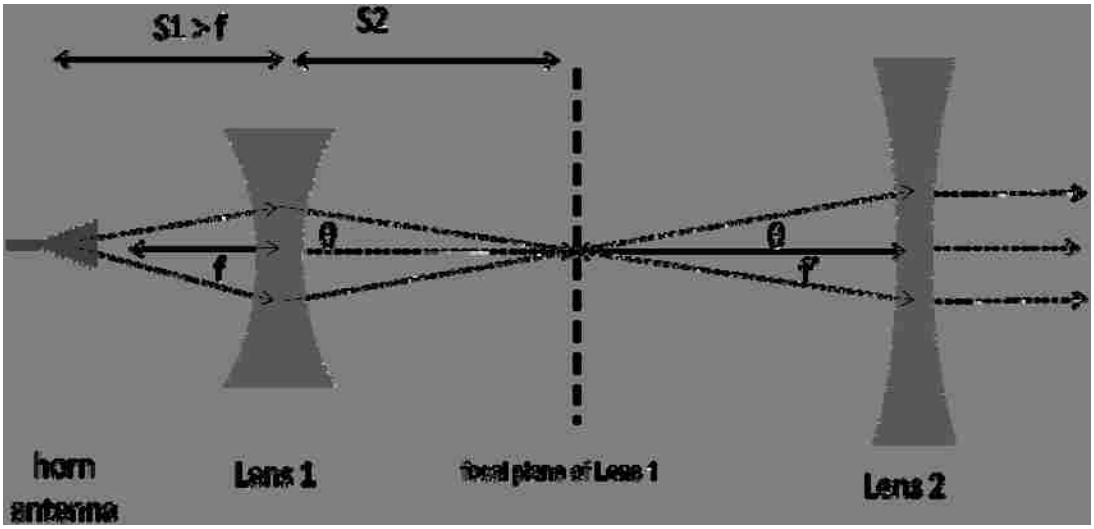

Figure 7. Collimation of beam by placing a second lens, with focal length f', one focal length away from the focal plane of Lens 1

If the first lens is then placed a little farther away from the radiating horn antenna so that S1 in Equation 8 increases. The diameter of the beam incident on the first lens will be larger than it was before. The location of the focal plane according to Equation 8 will be closer to lens 1than before, as shown in Figure 8.

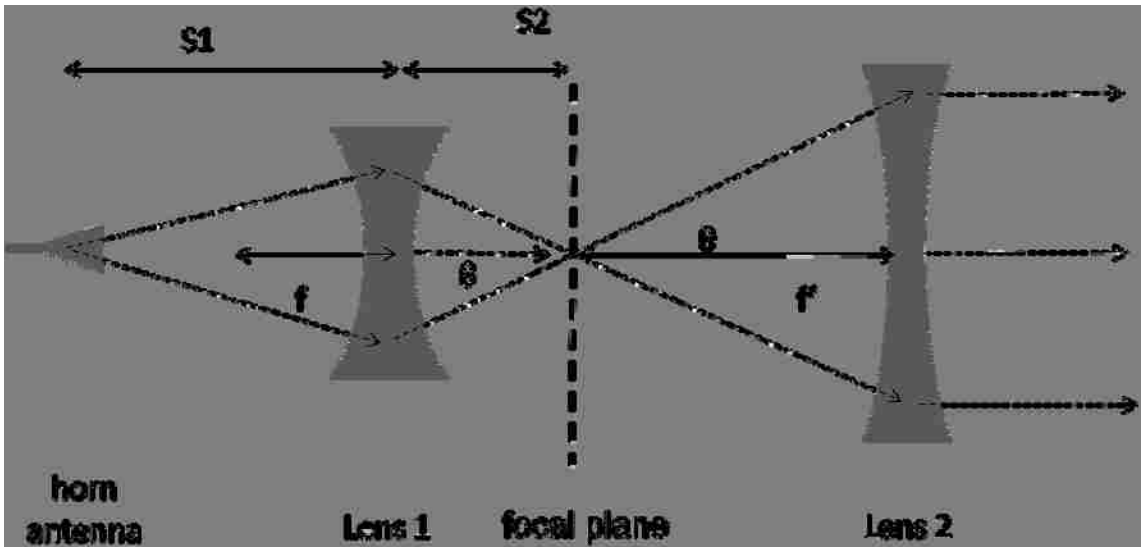

Figure 8. By moving Lens 1 further away from phase center of horn and re-positioning Lens 2, a broader collimated beam is achieved

The angle of convergence of the beam as it propagates towards the focal plane of the first lens is greater than it was before, as is the angle of divergence of the beam as it propagates from the focal plane towards the second lens. The second lens will always be placed one focal length (f') from the focal plane of lens 1 so that the HPM beam that emerges is collimated. In this case, the diameter of the collimated beam is larger.

This is the concept of the zoom lens antenna; i.e., with a radiating horn antenna and two lenses, one can collimate HPM energy radiating from the horn and vary the diameter of the collimated beam by varying the distance of lens 1 from the horn and adjusting the second lens so that it is always one focal length (f') from the focal plane created by lens 1.

For practical applications, minimizing lens size minimizes weight. Minimizing translation range of lens 1 makes implementation of the antenna system easier. In addition, the diameter of lens 1 must be large enough to intercept the full half power beamwidth of the feed horn. To minimize the size of lens 1, therefore, the focal length of lens 1 should be kept relatively small. Shorter focal lengths are more readily achieved with a bi-concave lens, according to the lensmaker's equation; however the diameter of lens 1 is limited by the focal length; i.e., for a given focal length, the radius of the lens is limited to the radius of curvature of the spherical face of the lens required to achieve that focal length..

The result is that the ideal gain of a feed horn for this zoom antenna is close to 16dBi. For a more highly directive horn antenna, the first lens must be translated over longer distances to achieve a given range of magnifications. If it is less highly directive, the diameter of this lens must be very large to intercept at least the full half power beamwidth at a given location. Design considerations are discussed in more detail in Section 4.10.

4. RESULTS AND ANALYSIS

All experimental and simulated results are presented in this section. All simulations were run using CST Microwave Studio.

4.1 Preliminary Experimental Results: Low Power 5GHz Lens

To explore focal properties of the metal plate lens, a low power 5GHz prototype bi-concave, spherical lens was designed and constructed using insulated foam sheathing and heavy duty aluminum foil, as shown in Figure 9. Spray adhesive was used to attach the foil to the foam sheathing. The sheathing itself is extruded polystyrene and has a dielectric constant very close to that of air. This is necessary to yield an index of refraction for the lens of less than 1. The sheathing then acts simply as structural support and as an "air" spacer for the aluminum foil plates. The thickness of the foam sheathing then determines the spacing "a" between the plates and was chosen to yield and index of refraction of n=0.6 at a frequency of 5GHz. The spherical radius of curvature for this lens was 40.6 cm, yielding a focal length of 52 cm.

Figure 9. Design and construction of prototype lens

The center plate is shown in Figure 10. The minimum width of this plate was 10.2 cm, which is greater than one and a half times the free space wavelength at 5GHz (λ=6cm), which, since it is greater than the guide wavelength, ensures sufficient lens width in this region of the lens. The radius of curvature of the center plate was 40.6 cm. To construct this plate, one would use a compass set for the desired radius of curvature of the lens and place one end at a point "P" from center of the lens determined by R1 plus half the

minimum width of the plate. This point “P” is then the fixed point of reference for constructing the remaining plates.

Figure 10. Lens center plate

For constructing these lenses by hand, it is important to note that, for the face of the lens to transcribe a sphere of radius R1, such that it would focus in the E- and H- planes, the radius of curvature of the plates decreases as one moves away from the center plate. In fact, the radius of curvature of the nth plate from the center plate is determined by

$$R_n = R1\cos(\theta) \quad [10]$$

where

$$\theta = \sin\left(\frac{na}{R1}\right) \quad [11]$$

If all of the plates had radius of curvature of R1, the lens would only focus in the E-plane.

The radius of curvature of plates successively far from the center plate decreases. To construct these plates, one must apply equations [10] and [11] to determine the radius of curvature of a given plate, n steps from the center plate, and maintain the fixed point of reference relative to the center of the plates.

The resulting set of plates comprising the lens are shown in Figure 11, with the center plate on the left and plates successively far away from the center plate in the upper and lower rows in the picture. Great care was then taken to align the plates properly.

Figure 11. 5GHz prototype lens plates prior to assembly

Low power experiments were then conducted in an anechoic chamber, by making S21 measurements with a network analyzer with port 1 connected to a transmit antenna and port 2 connected to a receive antenna, shown in Figure 12.

The transmit antenna had a gain of 15 dBi and is shown to the right in Figure 12. The lens was placed at a distance from the transmit antenna so that the half power beam width of the transmit antenna at that location entirely illuminated the aperture of the lens. This was greater than a focal length away from the phase center of the transmit antenna. The

receive antenna, with a gain of 6dBi, was placed at the center of the focal plane of the lens.

Figure 12. Test setup showing fully assembled lens, transmit and receive horn antennas

The frequency was swept from 4.5 to 5.5 GHz. Figure 13 shows the measured electric field with and without the lens in place, with both the transmit and receive antennas fixed. With the lens in place, the electric field peaks at 5GHz at a value of close to 1.7V/m (indicated by the green curve in Figure 13). By simply removing the lens, the

electric field at 5GHz drops to 0.28 V/m, as indicated by the red curve. The blue curve is a theoretical curve calculated from the radar range equation.

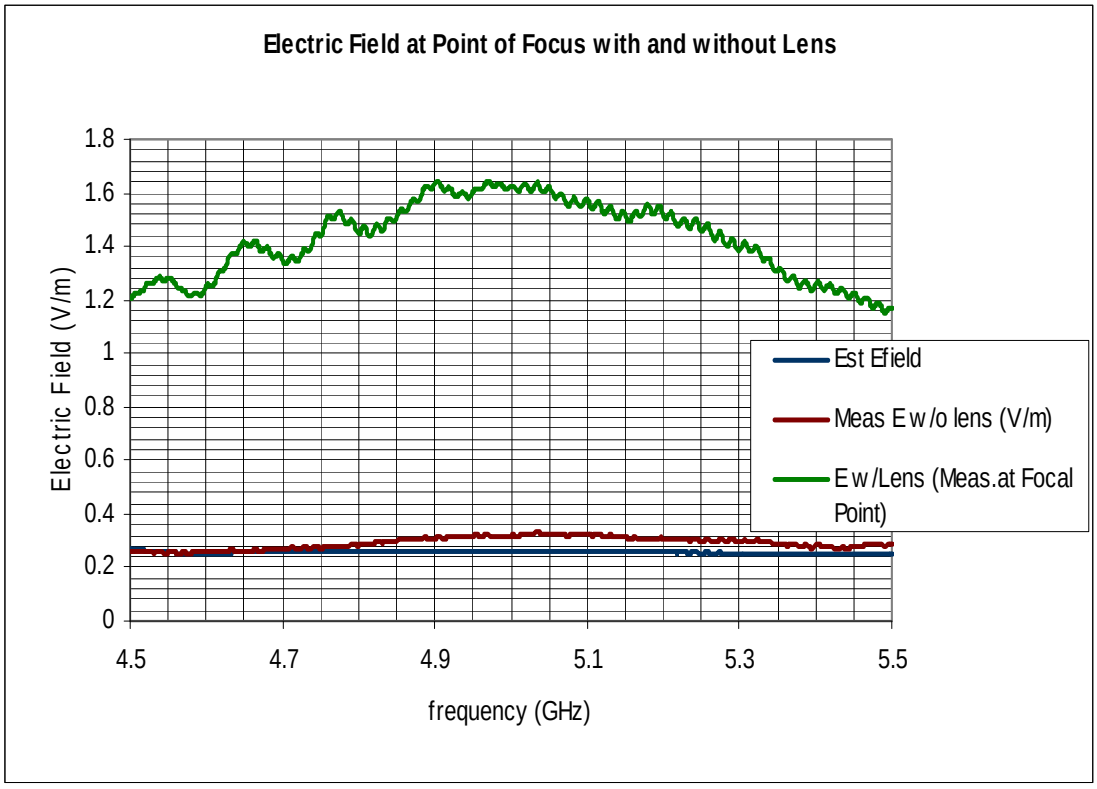

Figure 13. Measured electric field at fixed location of receive antenna; with and without lens

Figure 14 presents the gain of the lens (blue curved) and the combined gain of the lens and horn antenna. From these experiments, it was determined that the gain of the lens was close to 15dB above the 15dBi gain of the horn antenna, resulting in a total gain of the horn –plus- lens combination of close to 30dBi.

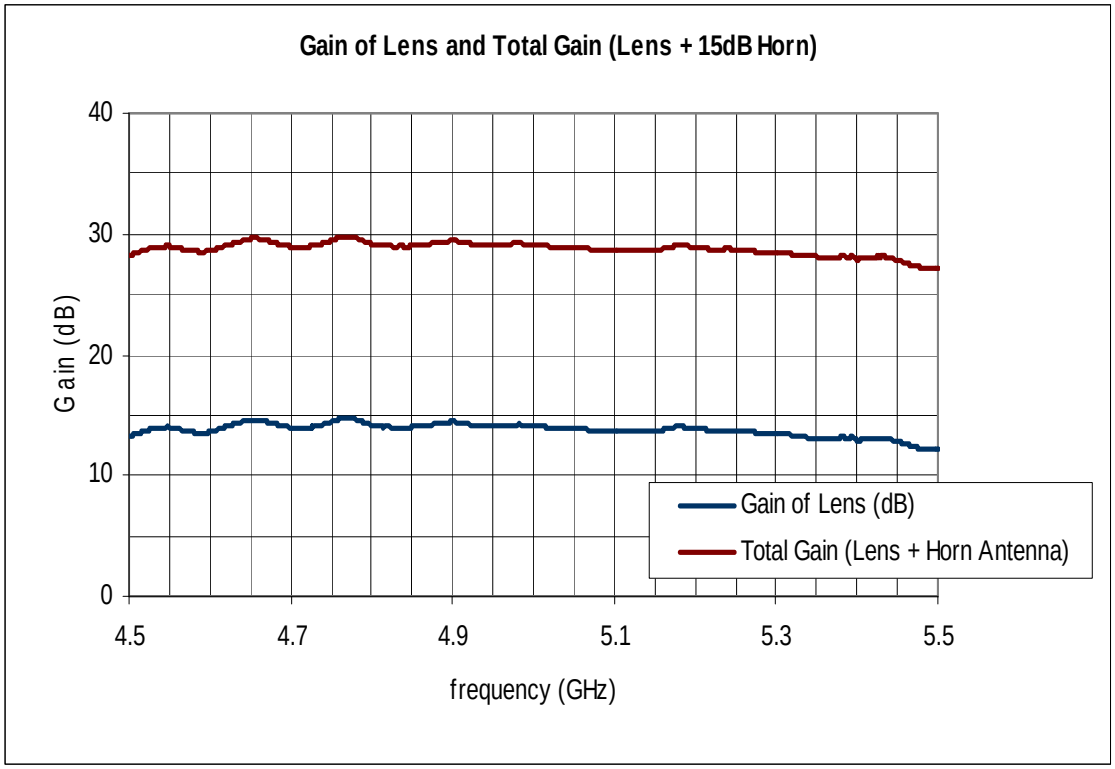

Figure 14. Gain of horn and lens

This lens is an aperture antenna. The gain of an aperture antenna is given by

$$G = \frac{4\pi A\eta}{\lambda^2} \qquad [12]$$

Where η is the antenna efficiency. Assuming 100% efficiency, the maximum gain of this particular lens was calculated to be 30dBi. The results indicate 70% efficiency of this hand-built lens!

This showed good promise. The next step was to demonstrate the full zoom concept. Because antenna dimensions decrease with increasing frequency, it was decided to demonstrate the zoom antenna concept through simulation and experiment at 10 GHz, due to relative ease of fabrication at the higher frequency.

It is important to note here that the gain of the system is quite good over the entire range from 4.5-5.5 GHz, indicating a usable bandwidth for the lens of close to 10%. Further discussion on the bandwidth of this zoom antenna system is presented in Section 4.9.

4.2 Simulated Results: 10GHz Zoom Antenna Concept

As stated previously, this zoom antenna concept comprises a horn antenna and two metal plate lenses, which, when translated along boresight relative to each other and relative to the phase center of the horn antenna, provide a collimated beam output with continuously variable diameter. Simulations were conducted with CST Microwave Studio to explore relevant radiative properties of the horn antenna, the horn plus a single lens, and finally the horn plus both lenses.

4.2.1 Simulation of Feed Horn

In all of the simulations herein, wave propagation is in the y-direction and the electric field is in the x-direction. The simulation parameters are shown in Table 1. The waveguide horn was constructed with a waveguide feed with dimensions of a=10.16 mm and b=22.86 mm, corresponding to standard gain x-band rectangular waveguide dimensions. The length of the waveguide was 50 mm and was chosen to be sufficiently long for the TE1 mode to get set up in the waveguide. The horn dimensions were chosen to be 52.07 mm and 71.12 mm, for the E- and H- dimensions at the aperture and a length of 138.43 mm, corresponding to the dimensions of a standard gain pyramidal horn with a gain of 16dBi.

Description	Size (mm)
Waveguide E	10.16
Waveguide H	22.86
Waveguide Length	50
Horn E	52.07
Horn H	71.12
Horn Length	138.43
Horn Wall Thickness	2

Table 1. Feed Horn Parameters

This structure was then fed via a waveguide port at the waveguide input located at y=0. With these dimensions, the aperture of the horn antenna is located at y = 188.43 mm. The simulated horn antenna is shown in Figure 15; the waveguide port input is shown in Figure 16.

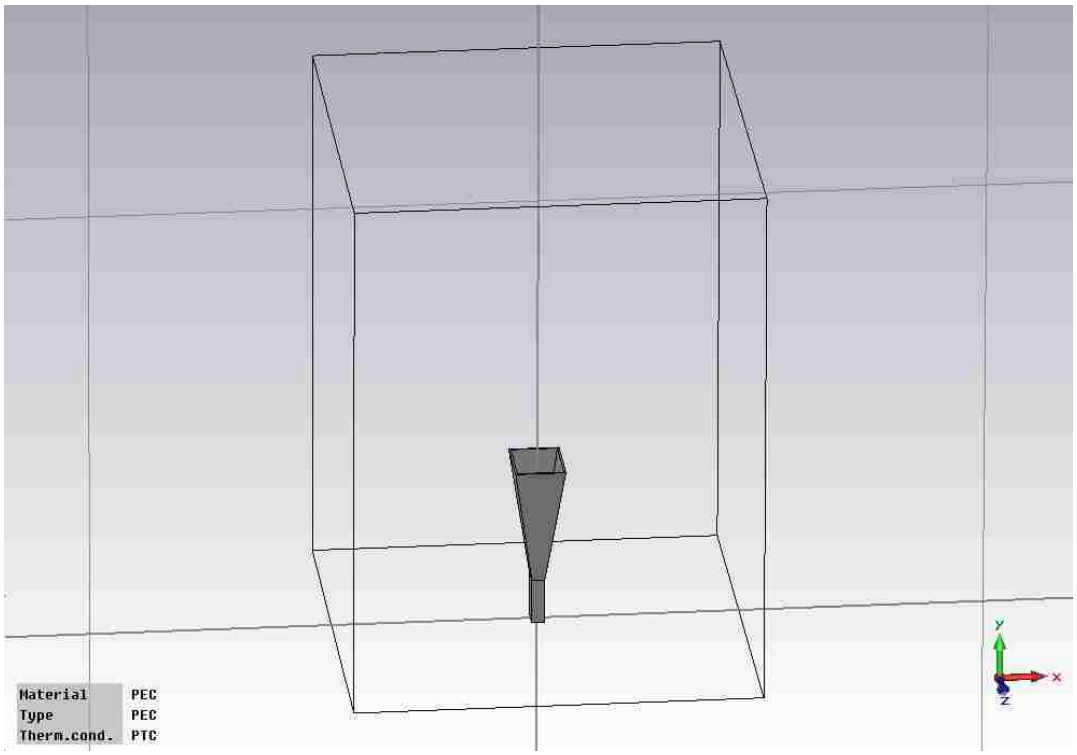

Figure 15. Horn Antenna Used in Simulations

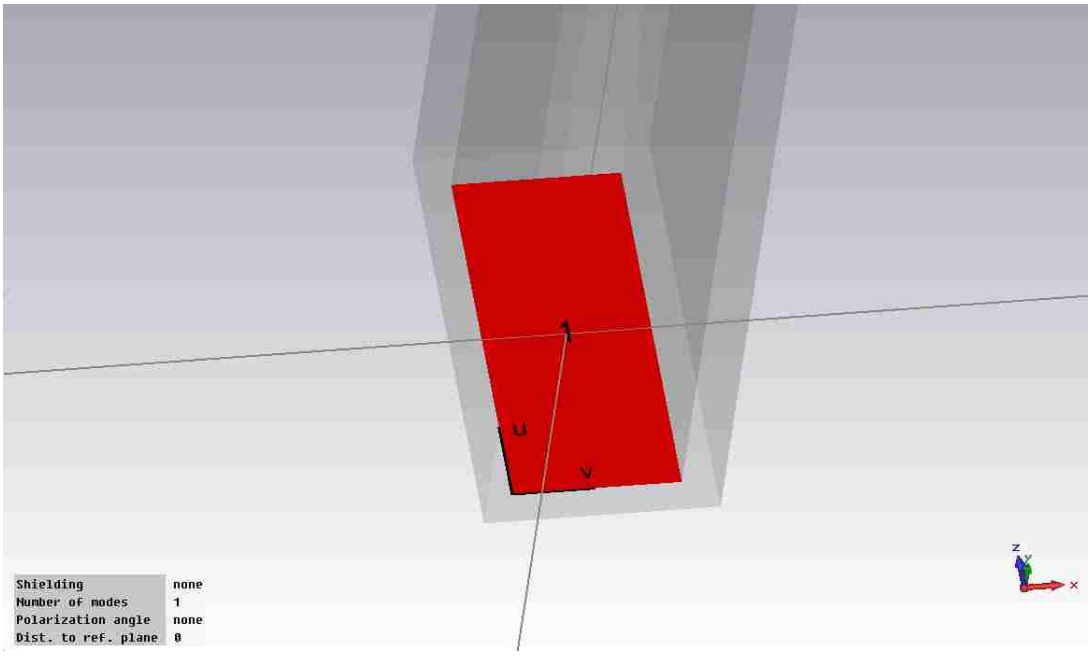

Figure 16. Waveguide port at input to waveguide

A Gaussian excitation from 9.8 to 10.2 GHz was used with a total power of 1 Watt. It is shown in the time domain in Figure 17. The power spectral density of this excitation is shown in Figure 18. The power peaks at 10 GHz, and falls to 1/e of its value at 9.8 and 10.2 GHz as indicated in Figure 18.

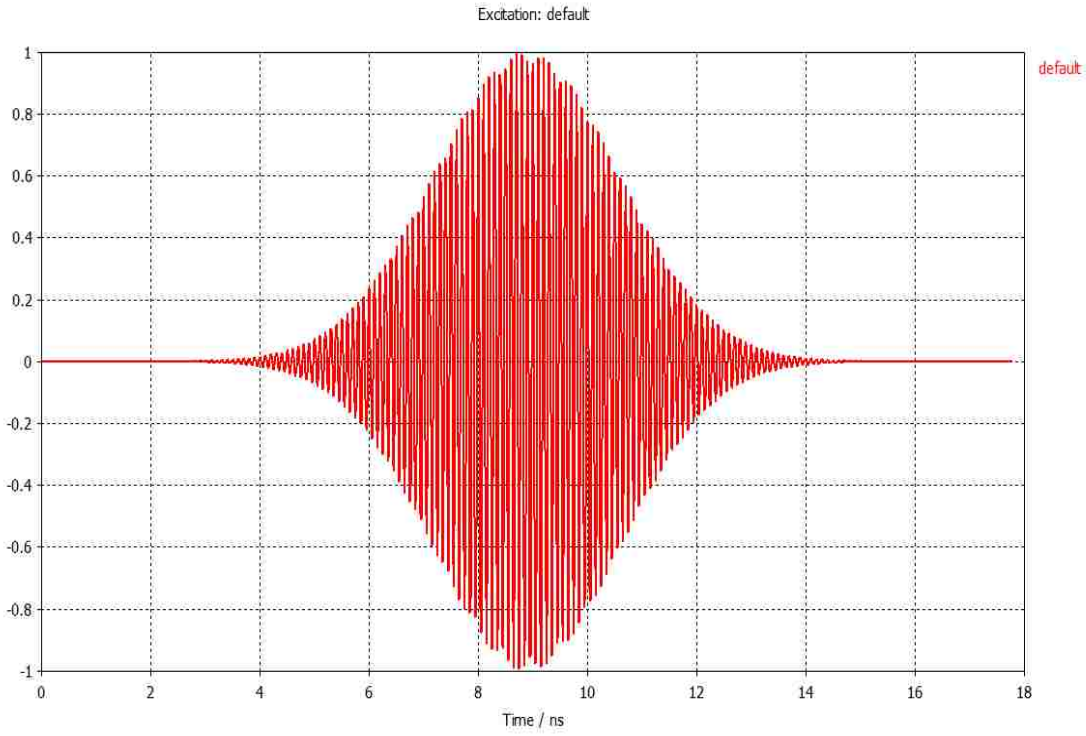

Figure 17. Gaussian voltage waveform applied to waveguide port (9.8-10.2GHz) [vertical axis: amplitude (V)]

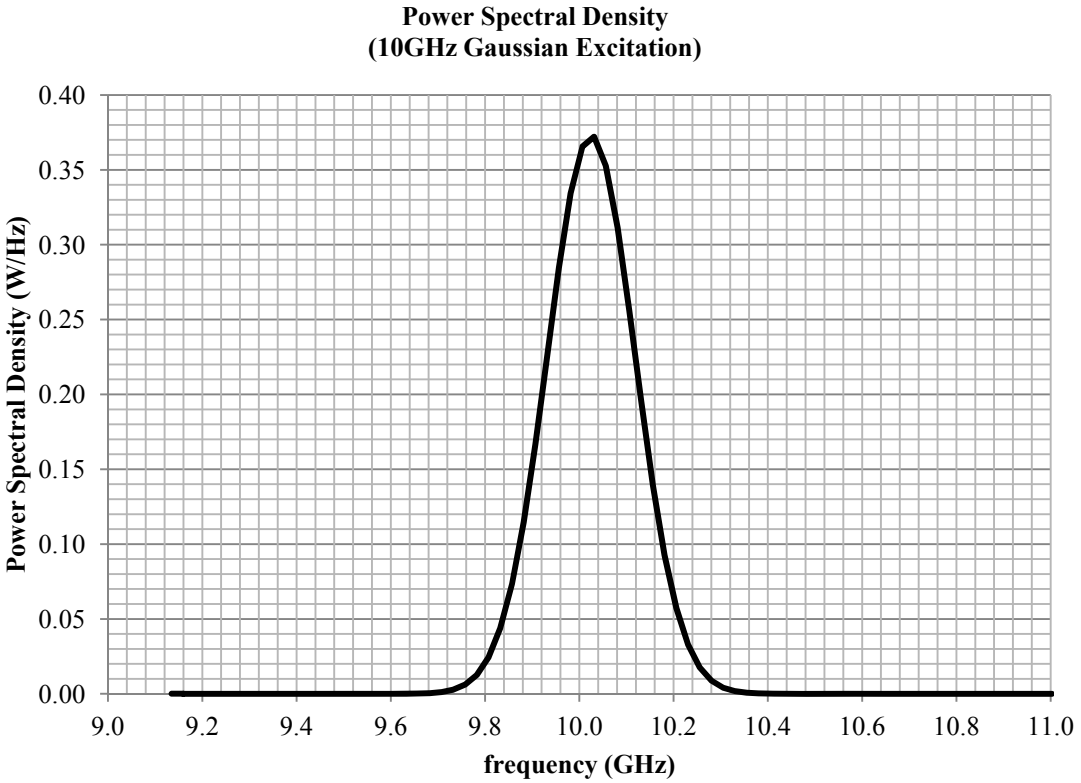

Figure 18. Power spectral density of 10GHz Gaussian excitation

The radiated electric field is shown in Figure 19. High electric fields (Ex) exist within the waveguide, decrease through the flared horn section, then propagate away from the aperture of the horn in the y-direction in a spherical radiation pattern.

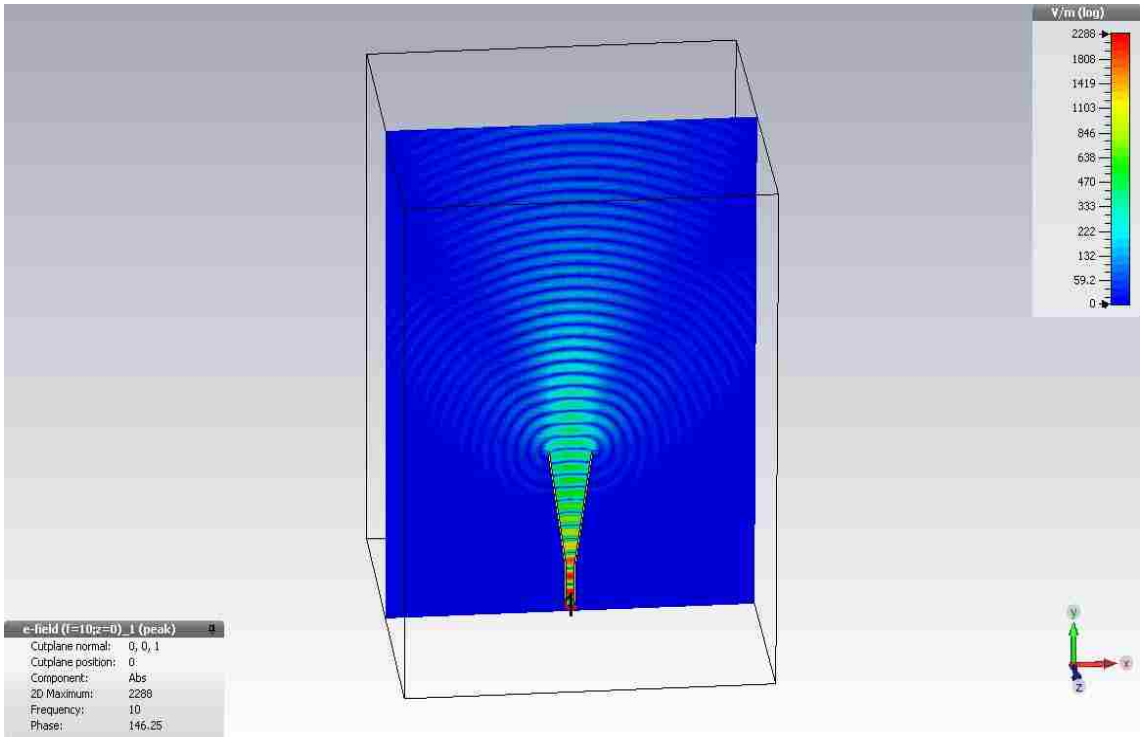

Figure 19. Fields radiated from horn antenna

The 3-D radiation pattern is shown in 3-D in Figure 20. The maximum gain of this horn antenna along boresight was determined to be just over 16 dBi, as expected for the chosen horn dimensions and showing excellent agreement between simulated results and theory.

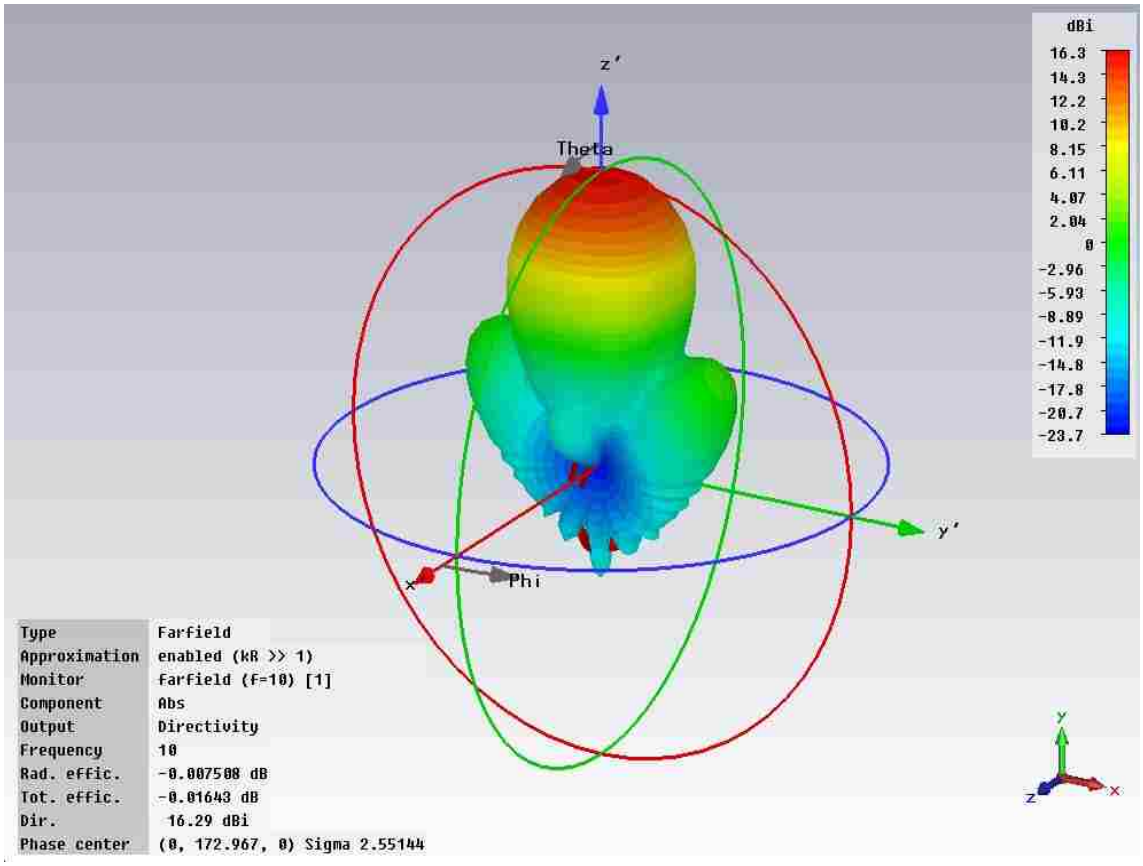

Figure 20. 3-D Radiation Pattern of 10GHz horn antenna

Note location of phase center at y=173 mm plus or minus a few mm. It is important to note that the phase center of a horn antenna is not the same for the E- and H- planes. However, in most cases, these are sufficiently close (i.e.., much less than a wavelength) that this has a negligible effect on the focusing properties of the lens.

The radiation pattern in the E- and H-planes is shown in Figures 21 and 22, respectively. While the radiation pattern is slightly broader in the E-plane, the half power beamwidth is very close to 30 degrees for both the E- and H- planes.

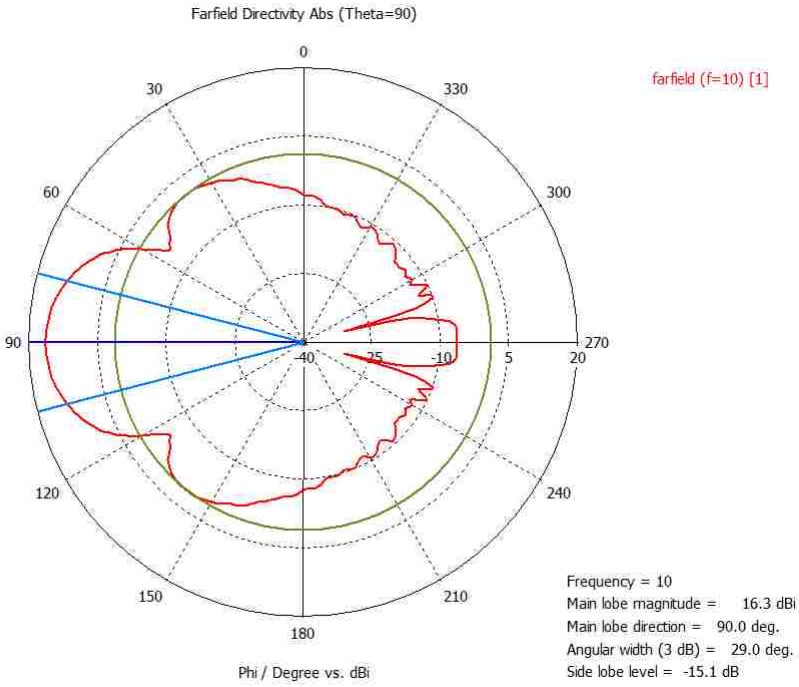

Figure 21. E-Plane radiation pattern

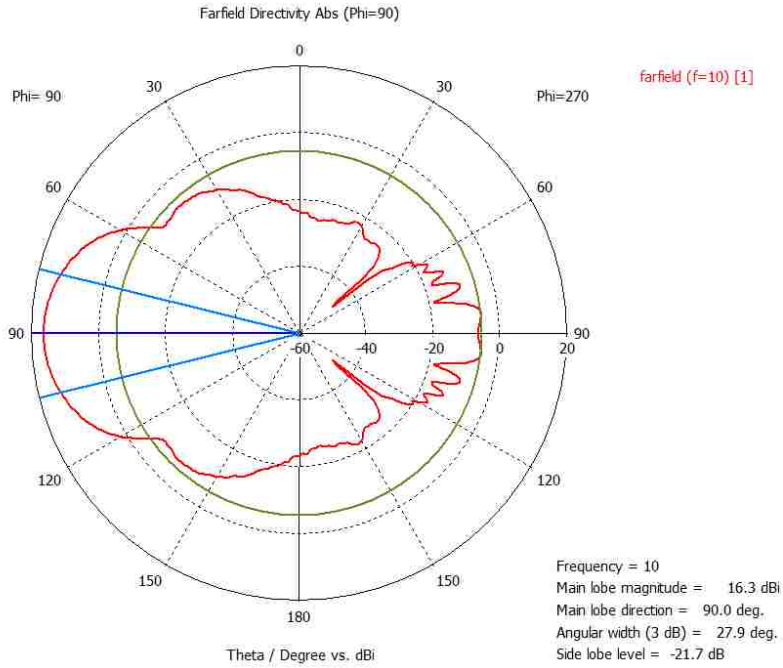

Figure 22. H-Plane radiation pattern

Figure 23is a simulated measurement of the x-directed electric field along boresight. This measurement indicates high fields within the waveguide falling as it moves outward along the tapered horn section, then propagating away from the horn, beyond y = 188 mm. The electric field falls as 1/R away from the horn antenna.

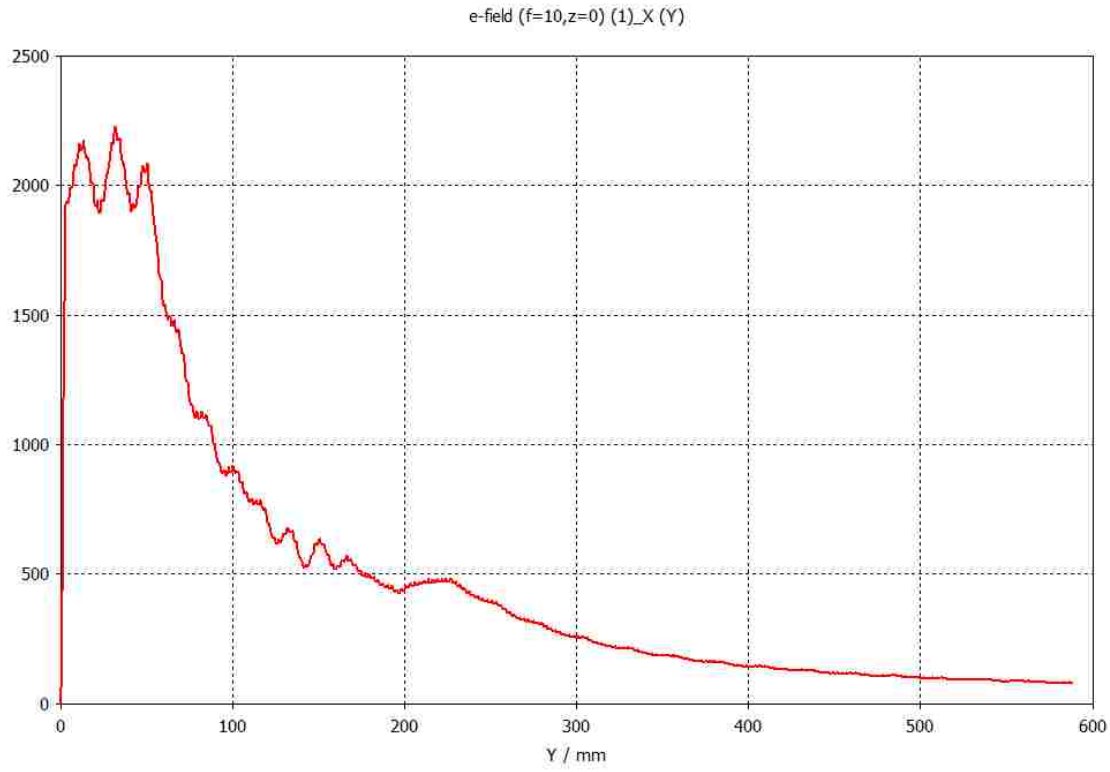

Figure 23. Electric field along boresight (mouth of horn at y=188mm) [vertical axis: Electric Field (V/m)]

4.2.2 Simulation of Horn and Lens 1

A biconcave first lens was then constructed with the electrical properties of Aluminum and with the parameters listed in Table 2. The plate thickness was chosen to be that of heavy duty aluminum foil, or .0254 mm. At 10GHz, the free space wavelength is λ=30 mm; the plate spacing of 19.05 mm was chosen to yield an index of refraction of n = 0.6. The minimum width of the center plate was greater than three wavelengths.

Description	Size (mm)
Plate length	406
Plate width	254
Plate thickness	.0254
Plate spacing	19.05
Radius of curvature (R1, R2)	203.2
Minimum width of center plate	101.6

Table 2. Lens 1 Design Parameters

The resulting lens aperture diameter was then 304 mm and the focal length was 254 mm. These parameters were selected to correspond to those used in the construction of the

low power lenses to experimentally demonstrate the zoom concept, as presented in Section 4.1.

The simulated lens itself is shown in Figure 24. It is bi-concave, although only one face is visible in the rendering, has a focal length of 254 mm and an aperture diameter of 304.8 mm.

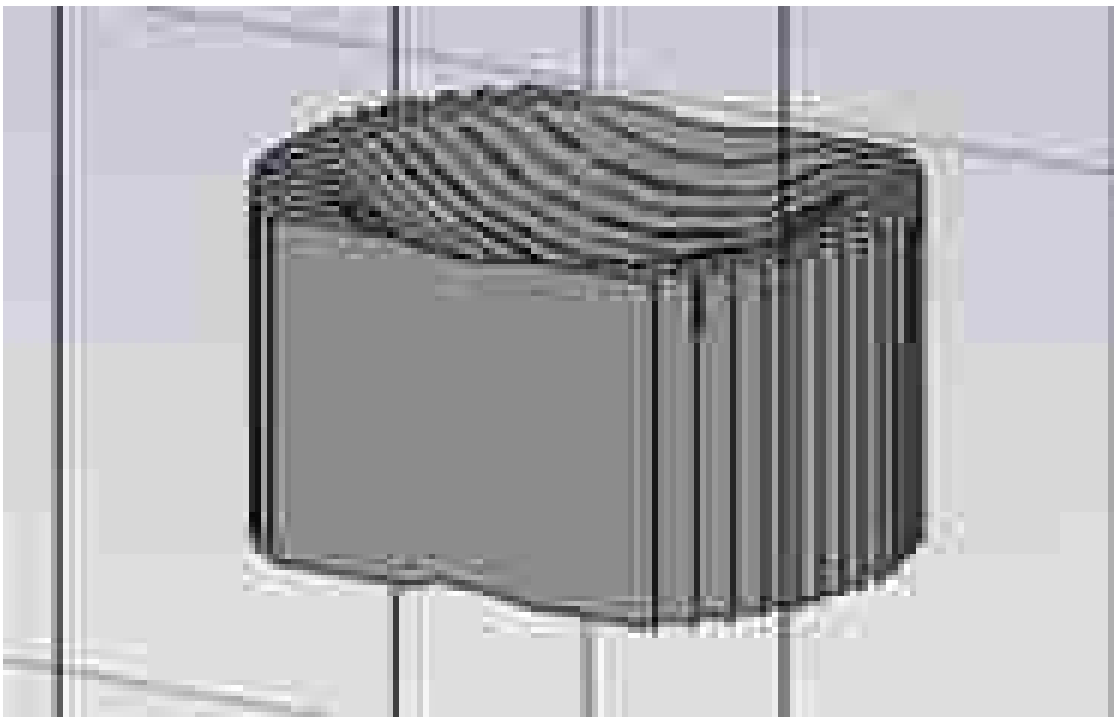

Figure 24. Biconcave Lens 1 with focal length of 254mm and diameter of 304.8 mm

This lens was then placed at y = 800 mm, axially aligned with boresight of the simulated horn antenna, as indicated in Figure 25. Because the aperture of the horn is at y = 174mm. this corresponds to S1 = 636 mm.

Electric field is oriented in the x-direction and propagation is in the y-direction. The lens is oriented with plates parallel to the electric field vector.

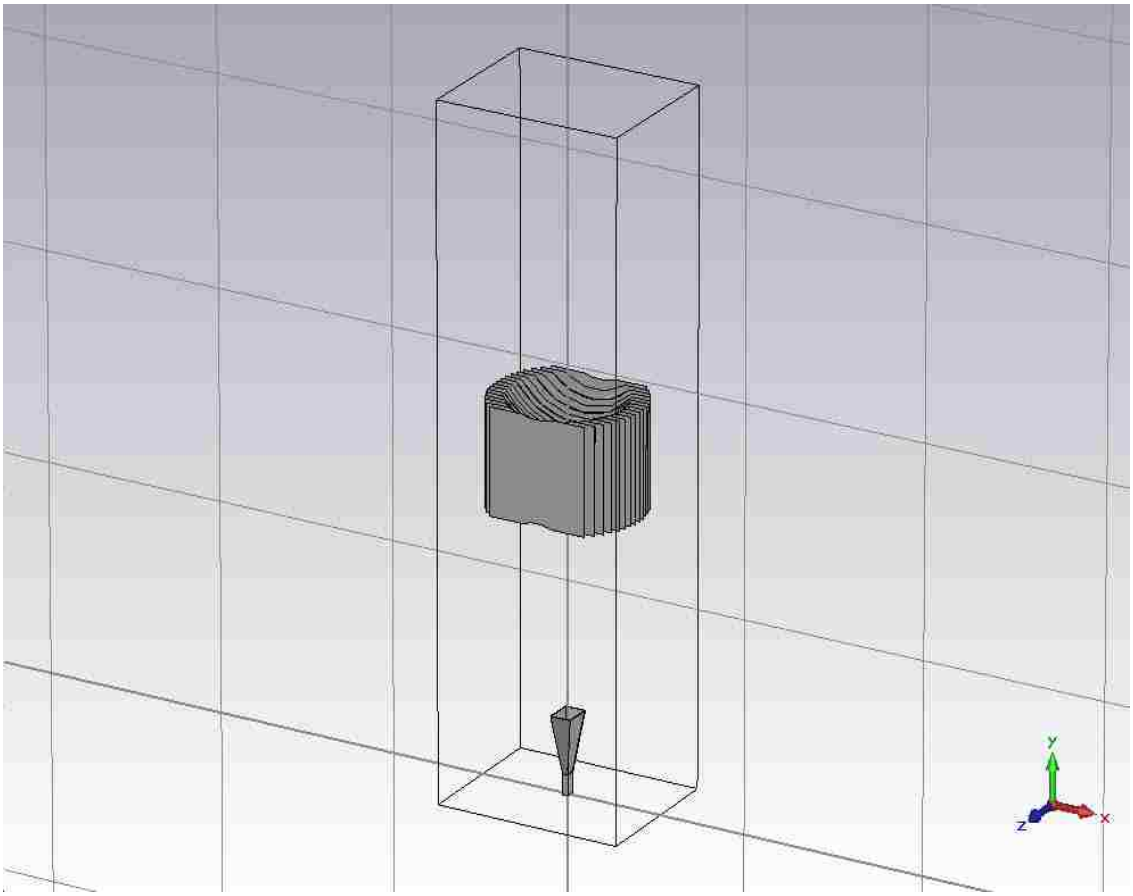

Figure 25. Lens 1 at y = 800 mm, oriented with plates parallel to the electric field vector.

The simulated electric field in the x-y plane is shown in Figure 26. Note the shape of the beam in the region near the focal plane beyond lens 1; rather than having a single plane of focus, it extends along a length of high field intensity. The focal plane is centered in this tubular region of high electric field. The length of this region in the y-direction is

referred to as the “confocal parameter” or “waist length ” [Ref. 14] and is determined from

$$b = \frac{2\pi w_0^2}{\lambda} \qquad [13]$$

where w_0 is the diameter of the beam waist (Airy disc).

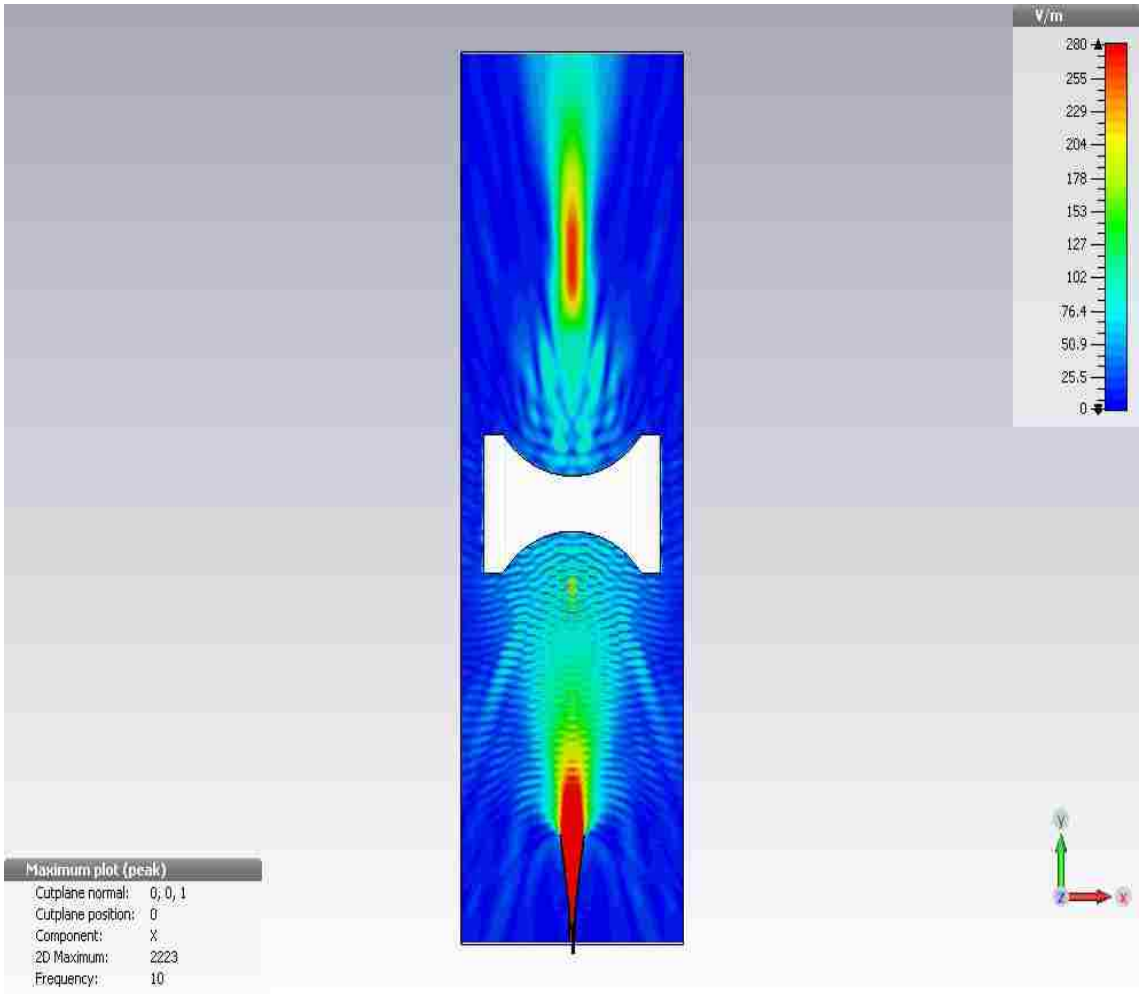

Figure 26. Electric Field (Ex) Contour Map Showing Beam Focus

Figure 27 shows a “carpet” representation of the electric field in the focal plane , which illustrates the width of the Airy disc in the focal plane of lens 1, and reveals that focusing is indeed achieved in this plane when lens 1 is farther than a focal length away from the phase center of the transmit horn antenna.

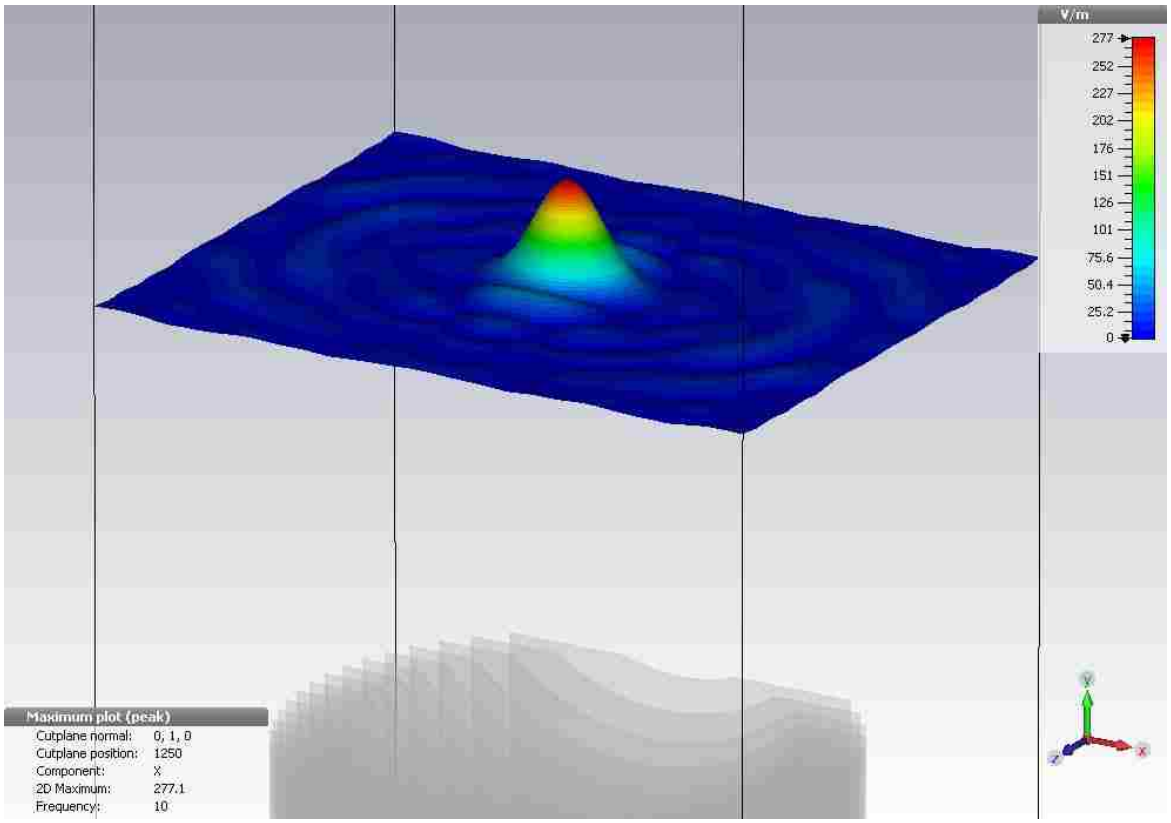

Figure 27. Carpet Representation of Electric Field (Ex) in the Focal Plane of Lens 1

The simulated boresight electric field measurement is shown in Figure 28. The electric field drops to zero along the width of the aluminum center plate of the lens over an interval corresponding to the width of the center plate along the boresight axis.

Between the aperture of the horn antenna and the lens (i.e, for 188 mm < y < 800mm), backscatter and reflection from the lens can be observed, when compared to the boresight electric field of Figure 23 without the lens. This is caused by the mode mismatch at the air-lens interface in going from the TEM mode in air with an index of refraction of n = 1 to that of the waveguide (TE1 mode with n = 0.6), as well as reflection off the metal plates this is described in more detail in Section 12.

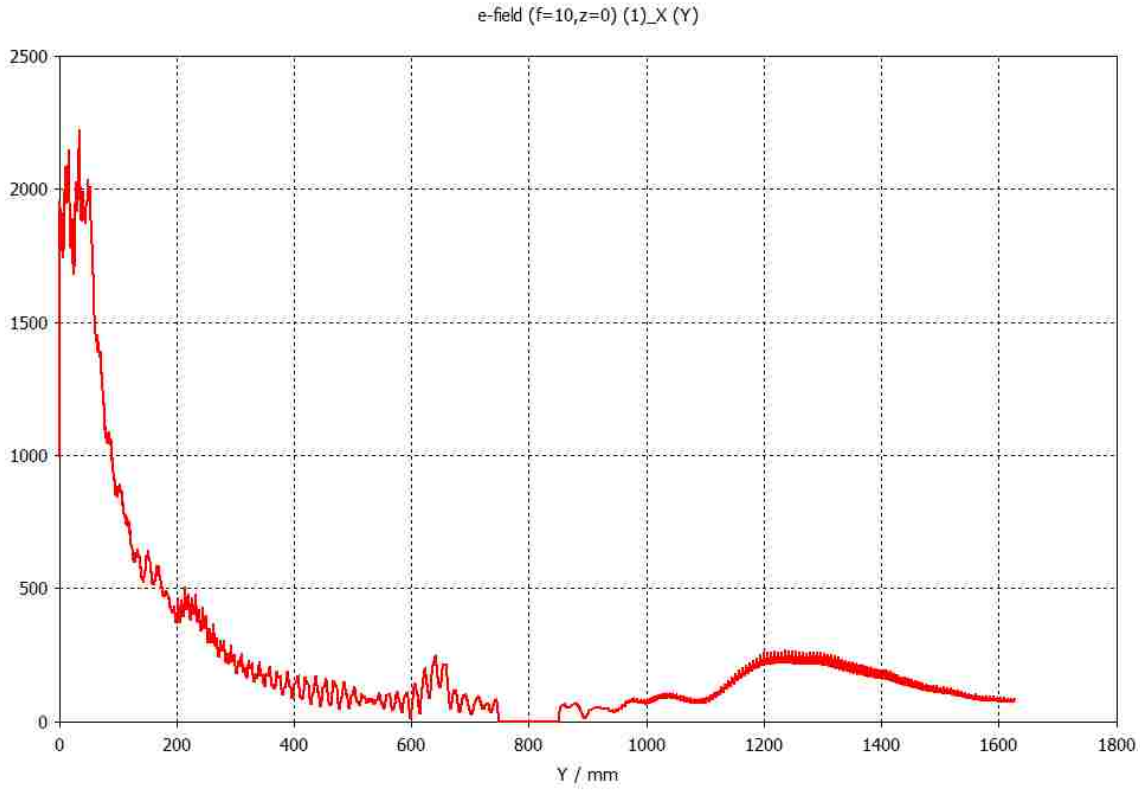

Figure 28. Boresight Measurement of Electric Field (Ex)

[vertical axis: Electric Field (V/m)]

Figure 29 is a close up of the boresight electric field in the region of the focal plane. The electric field starts to increase at near y = 1100 mm and continues to increase to y = 1200 mm. This is the region of the focal plane . It is not sharply defined at a single point; relatively high fields exist in the regions from y = 1200 mm to y = 1300 mm and a little beyond, indicating a depth of focus of about about 150 mm.

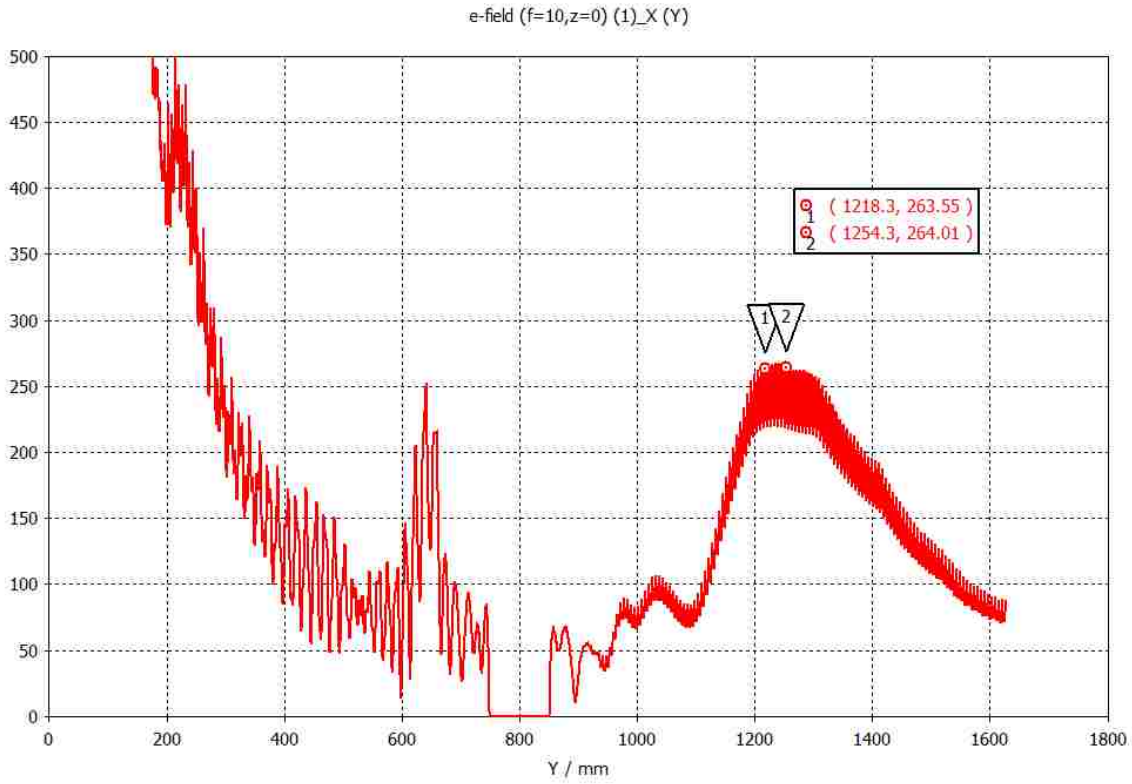

Figure 29. Electric Field Near the Focal Plane of Lens 1 (Lens 1 at y = 800mm) [vertical axis: Electric Field (V/m)]

The electric field measurements across the the E- and H- planes of the focal plane is shown in Figures 30 and 31, respectively. The half power beam width in the E- plane is about 42 mm, or close to 1.4 λ. In the H- plane, this width is closer to 1.3 λ, slightly narrower, as expected; however the shape of the Airy disc is very close to circular, within one tenth of a wavelength.

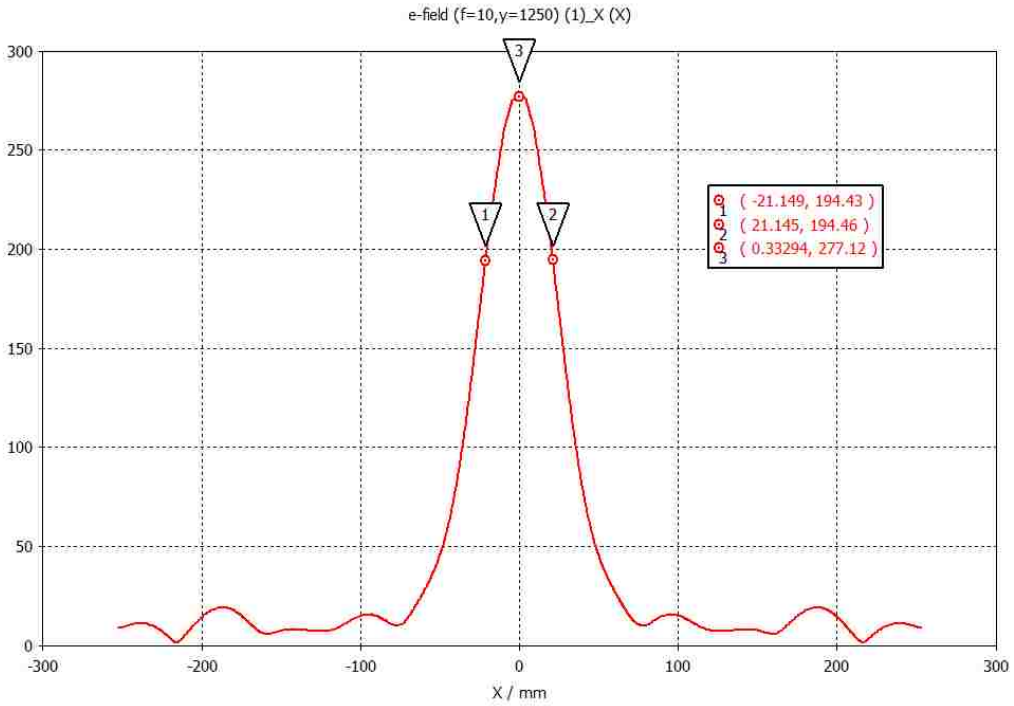

Figure 30. Electric Field Across the Focal Plane in the E-plane

[vertical axis: Electric Field (V/m)]

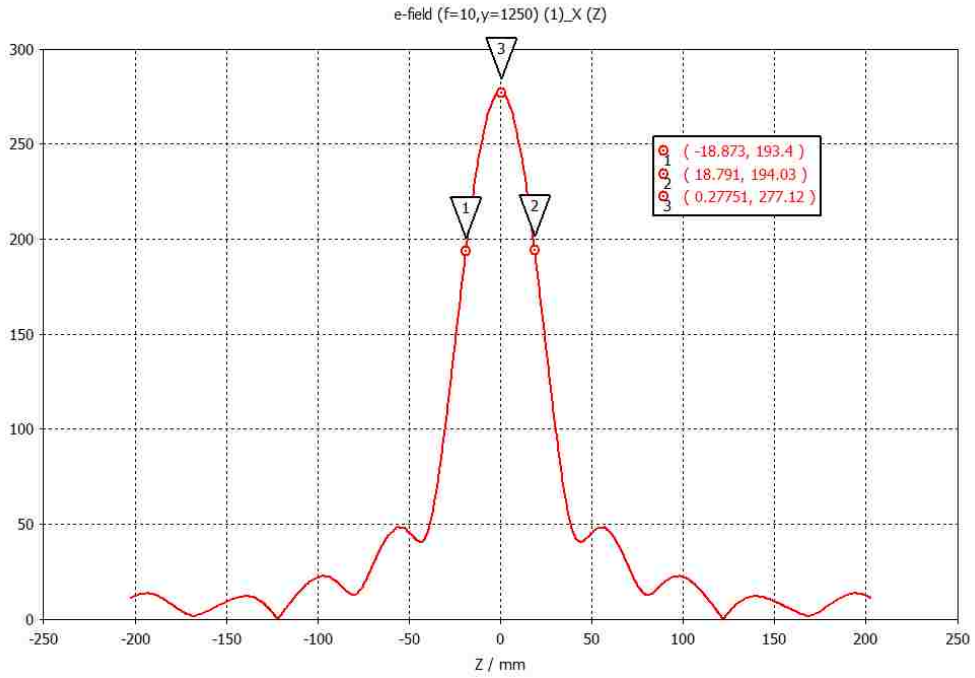

Figure 31. Electric Field Across the Focal Plane in the H-plane

[Vertical axis: Electric Field (V/m)

Note the relative peak in the field between the horn and the lens, located at just over y = 600mm in Figure 29. This standing wave in the system is the combined effect of backscatter from the metal plates and reflection due to mode mismatch at the air-to-lens interface. This standing wave ratio increases as the horn-to-lens 1 separation decreases and results in a slight decrease in the effective focal length of the lens as it moves closer to the horn aperture (i.e., as S1 decreases).

Table 3 lists the location of the focal plane for a range of lens locations from y=550mm to y=900mm, and includes calculation of the effective focal length, f(eff) in the far right column. Note that this focal length decreases as the horn-to-lens distance decreases.

Location of Lens 1 (mm)	S1 (mm)	Location of focal plane (mm)	S2 (mm)	f(eff) (mm)
900	726	1310	410	262
800	626	1250	450	262
700	526	1200	500	256
600	426	1199	599	248
550	376	1244	694	243

Table 3. Location of Focal Plane and Effective Focal Length for Decreasing S1.

These results are plotted in Figure 32. This is the result of interaction of the reflected fields with the lens which becomes significant as the lens approaches the horn apertures. While it is important to be aware of this effect in designing this system, there is not much that can be done to mitigate this effect .

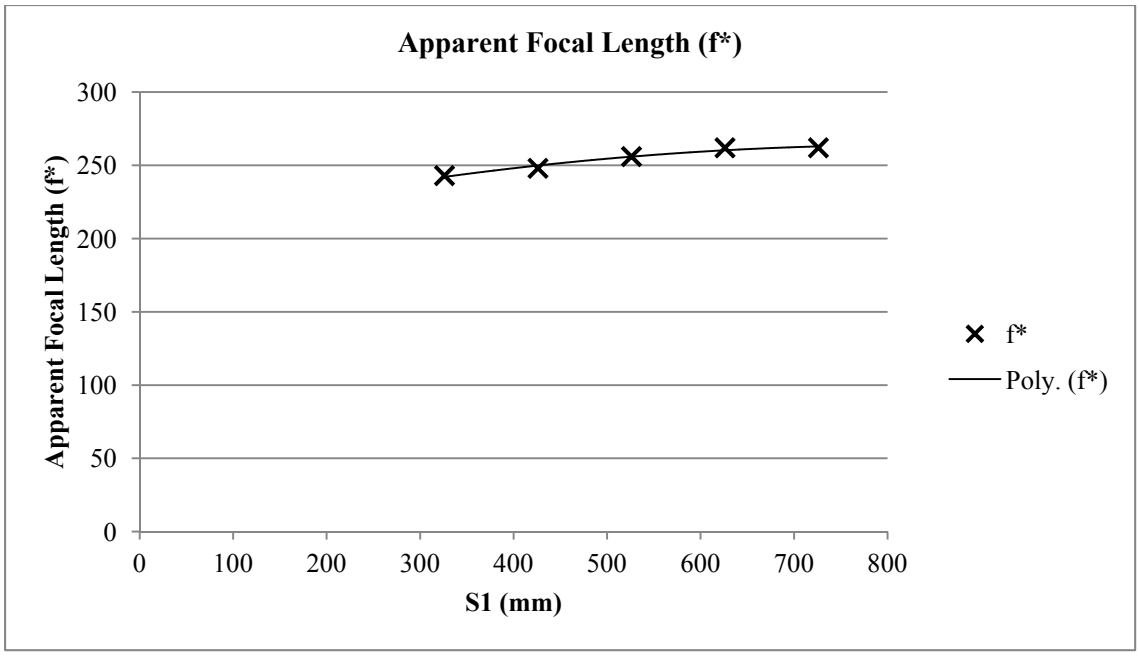

Figure 32. Effective Focal Length of Lens (Designed for f=262mm) vs. S1

With lens 1 positioned very close to a focal length from the phase center of the horn feed antenna, the beam is collimated. This is illustrated in the simulated boresight measurement of Figure 33 and the corresponding 3-D radiation pattern shown in Figure 34.

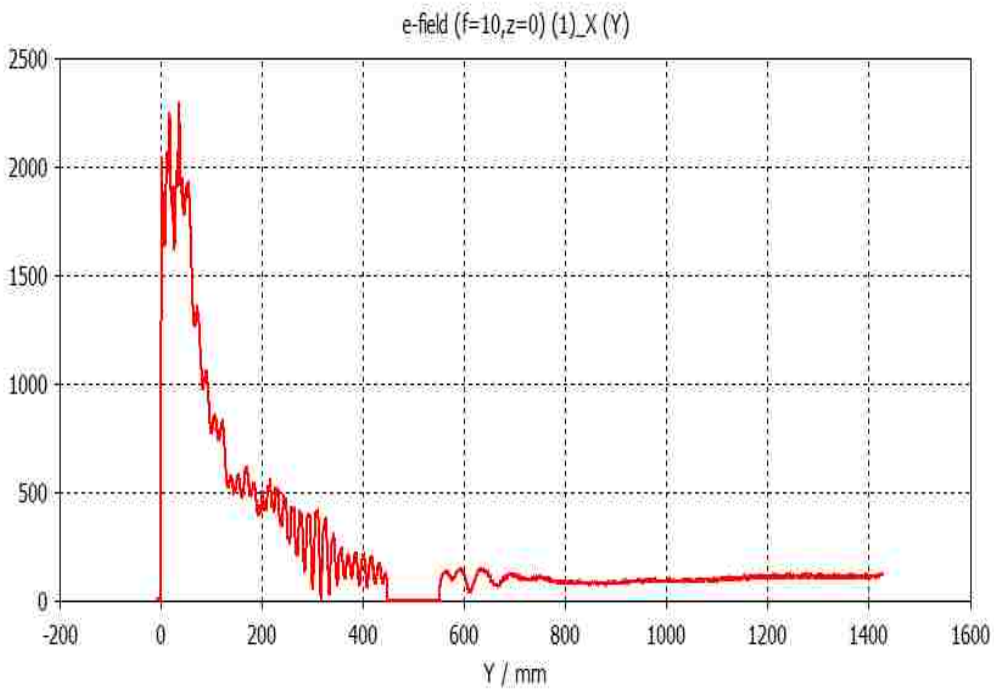

Figure 33. Boresight electric field showing beam collimation

[vertical axis: Electric Field (V/m)]

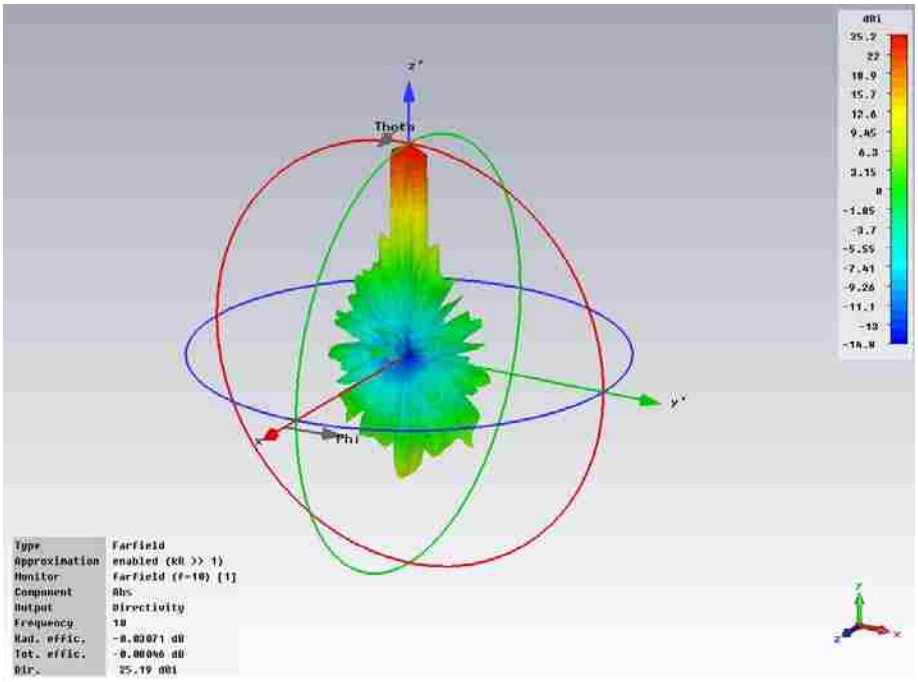

Figure 34. Radiation pattern with lens 1 at y = 500 mm

The focal length of this first lens determines the minimum S1; as a minimum, it cannot be closer to the phase center of the horn antenna than its focal length. The aperture determines maximum S1; the lens should not be further from the phase center of the horn than the half power beam width at that location. For this lens, minimum S1 corresponds to lens location at y = 500 mm. The simulated S11 measurement for this location is shown in Figure 3.

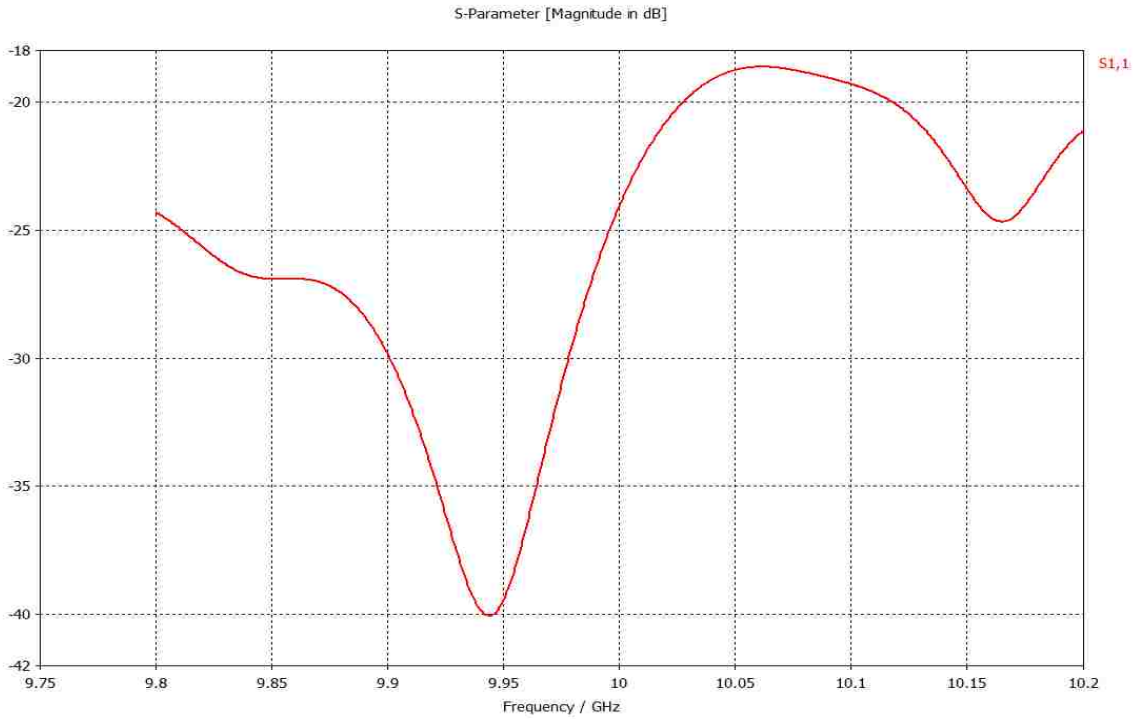

Figure 35. S11 Measurement for Lens 1 at y = 500mm.

[vertical axis: S21(dB)]

This is the worst case scenario. At the center frequency (10GHz), S11 = -24 dB. This is an acceptable value for S11. Further, it is less than -19 dB across the entire frequency range of 9.8 to 10.2 GHz.

The VSWR of the system with the lens at this location is shown in Figure 36. It is somewhat high at a value of 1.15; however it is still within an acceptable range for antenna design.

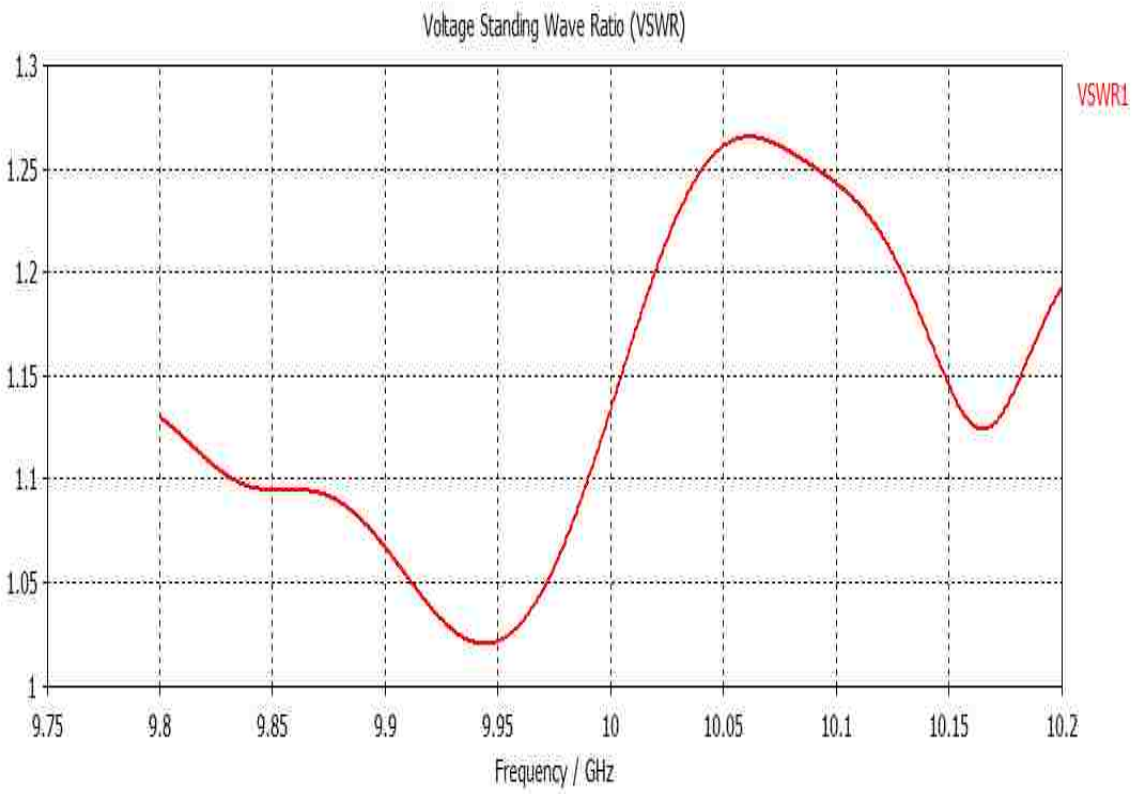

Figure 36. VSWR with lens 1 at y = 500mm

For comparison, the S11 and VSWR measurements of the system with the lens at y = 700mm is shown in Figures 37 and 38, respectively. S11 drops to -25dB, and VSWR to 1.12; again acceptable values for antenna design.

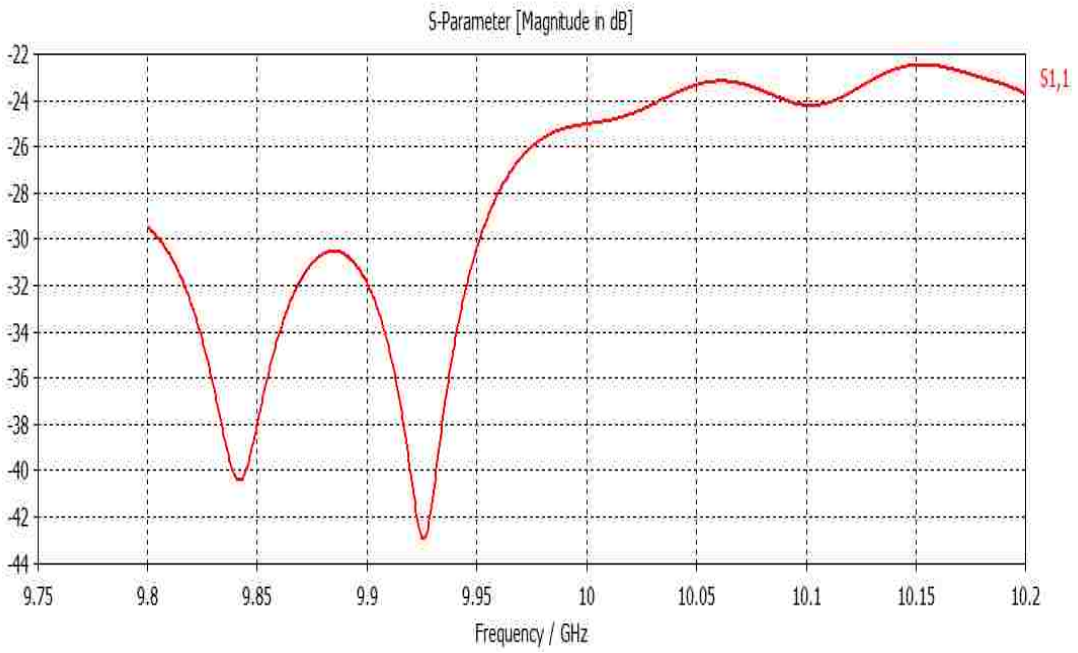

Figure 37. S11 of Horn/Lens combination with lens at y = 700mm

[vertical axis: S21(dB)]

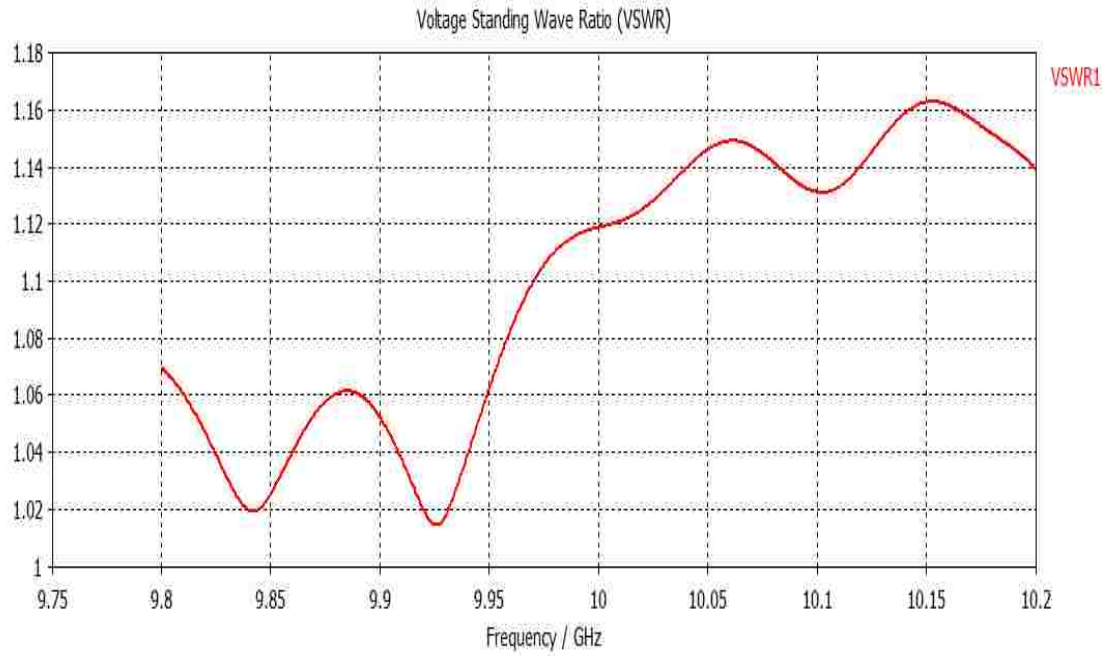

Figure 38. VSWR with lens 1 at y = 700mm

4.2.3 Simulation of Horn and Both Lenses

Lens 2 was then designed with the parameters indicated in Table 4. This was a plano-concave lens, with R1 = -558.8 mm and R2 = ∞.

Name	Value (mm)
Radius of Curvature	558.8
Plate Height	762
Minimum Width of Plate	101.6
Plate Thickness	.0254
Plate Width	406.4

Table 4. Lens 2 Design Parameters

This was chosen to be a plano-concave lens in order to achieve both a relatively large diameter and focal length. The diameter of the lens was 762 mm and the focal length was chosen to be 1397 mm.

	Lens 1 Location (mm)	Lens 2 Location (mm)
Narrow Beam	550mm	2550mm
Broad Beam	750mm	2570mm

Table 5. Lens Positions Corresponding to Narrow and Broad Collimated Beams

Simulations were run with the same time-domain excitation as shown in Figure 17. The lenses were positioned as shown in Table 5, corresponding to lens 1 positions for which the collimated beam output were maximum (at S1 = 750mm) and minimum (at S1 = 550mm).

4.2.3.1 Simulated Results Narrow Beam

The simulated results for narrow-beam lens positioning are shown in Figure 39, which is an amplitude plot of the electric field in the E-plane, with lens 1 at y = 550 mm and lens 2 at 2550 mm. High fields are present near the horn and along the focal region of lens 1. The beam flares out from the focal plane of lens 1 towards lens 2 and becomes collimated by this lens, as can be seen near the top of the figure.

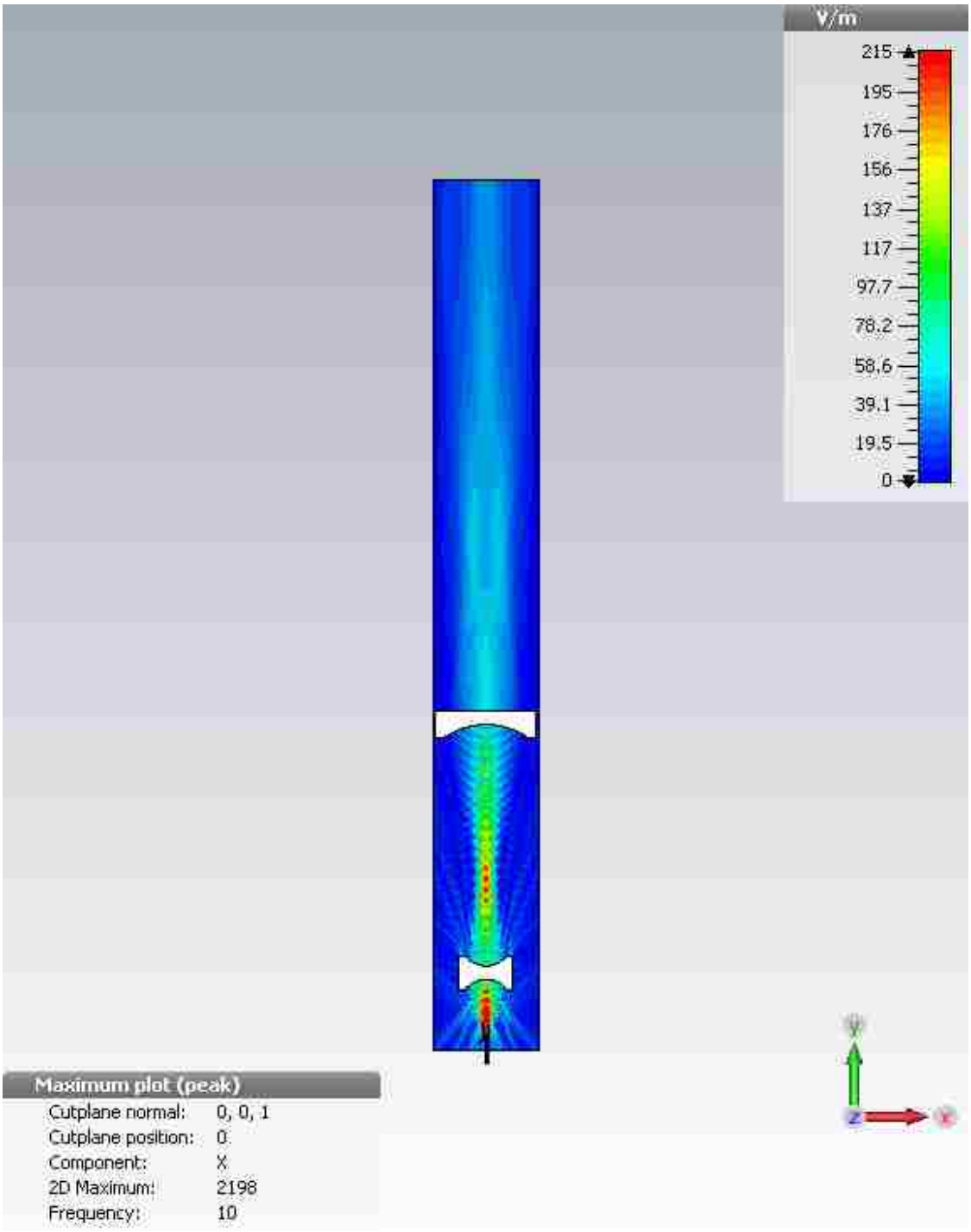

Figure 39. Amplitude Plot of Electric Field (Ex) in the E-Plane (Narrow Beam)

The simulated boresight measurement with the lenses thus positioned is shown in figure 40. The boresight electric field drops to zero at the center plates of the lenses as can be seen at y = 550 mm and y = 2550 mm, corresponding to positions of lenses 1 and 2, respectively. The focal region of lens 1 can be seen near y = 1200 mm. Beyond lens 2, at y > 2600mm, the electric field holds steady at close to E = 50 V/m, indicating collimation of the beam.

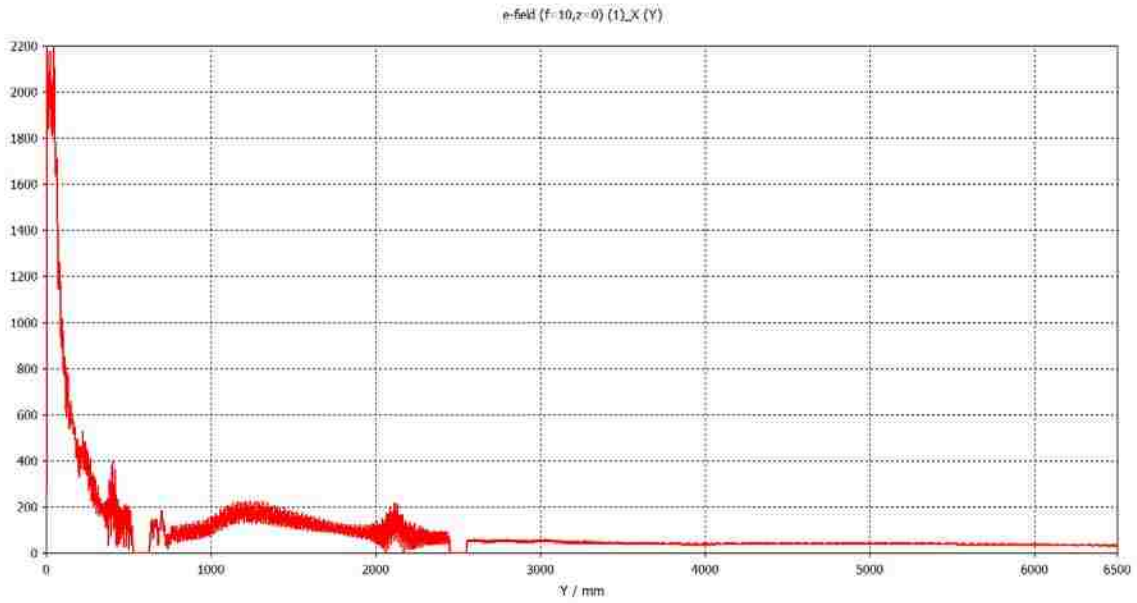

Figure 40. Simulated Boresight Measurement of Electric Field (Ex) – Narrow Beam [vertical axis: Electric Field (V/m)

A “carpet” representation of the electric field (ex) in the 2-D plane at y = 6500 mm is shown in Figure 41. These fields indicate a well behaved collimated beam, with close to constant amplitude across the E- and H- planes; tapering off nicely at the outer edges.

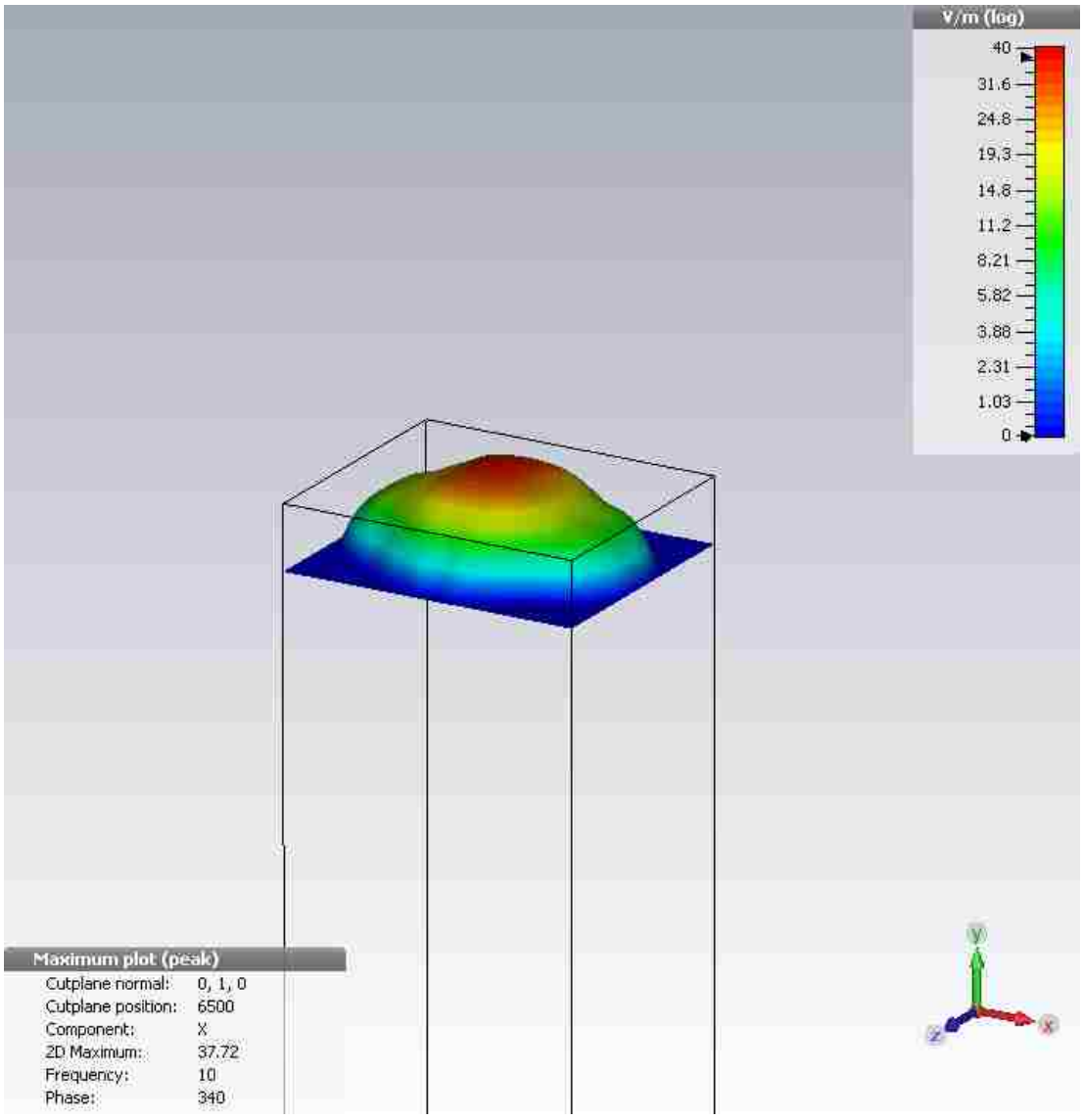

Figure 41. "Carpet" Representation of Electric Field (Ex) at y = 6500mm (Narrow Beam)

The simulated electric field measurement across the E- and H- planes in this plane are presented in Figure 42 and 43, respectively. The half power beam width in the E-plane is approximately 120 mm, in the H- plane it is slightly larger, at about 130mm.

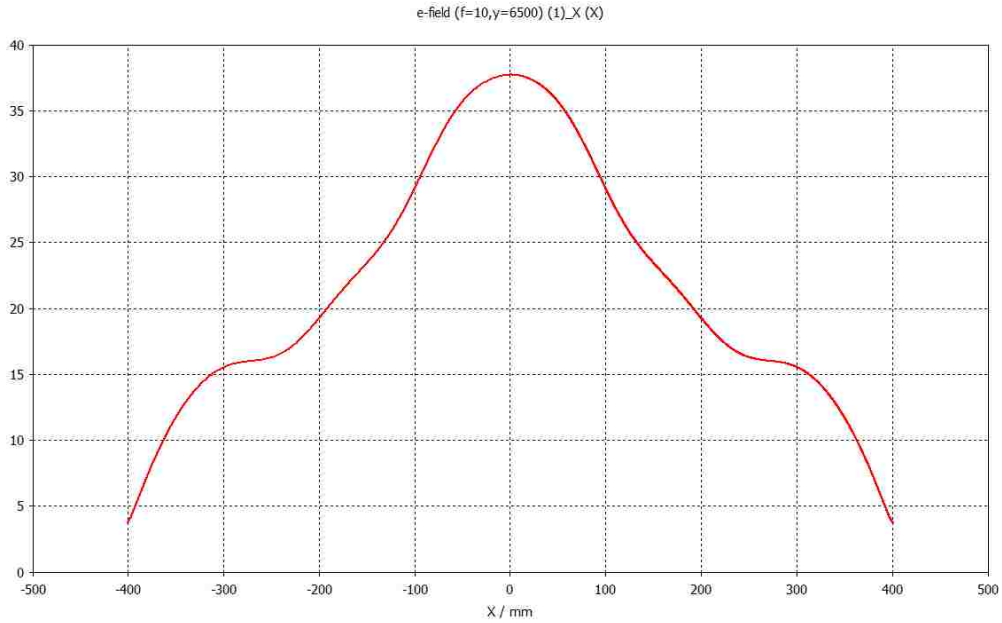

Figure 42. Electric Field (Ex) in the E-Plane at y = 6500 mm (Narrow Beam)

[vertical axis: Electric Field (V/m)

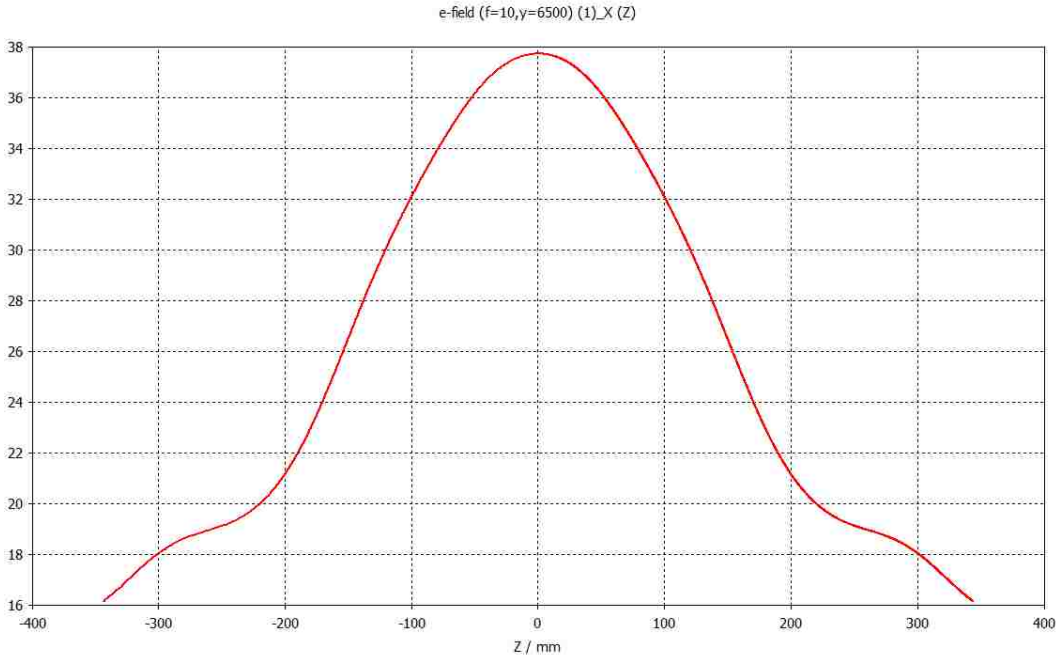

Figure 43. Electric Field (Ex) in the H-plane at y = 7000 mm (Narrow Beam)

[vertical axis: Electric Field (V/m)]

Figure 44 is a phase plot of the electric field (Ex) in the E-plane, showing a narrow collimated beam with a very close to planar phase front in the far field across the beam in this plane for -120 mm < y < 120mm .

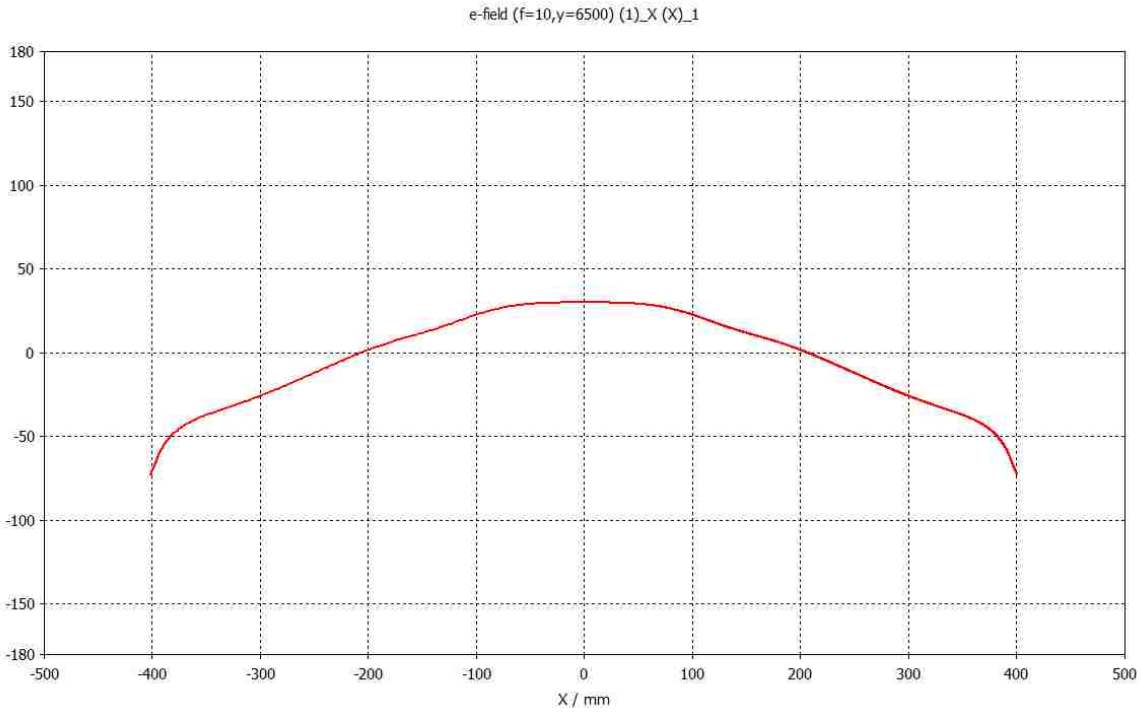

Figure 44. Phase Plot of Electric Field (Ex) in the E-Plane (Narrow Beam) [vertical axis: Phase (degrees)]

Figure 45 is a phase plot of the electric field (Ex) in the H- plane at y = 6500 mm, showing a very flat phase front across the H-plane from -130 mm < y < 130 mm.

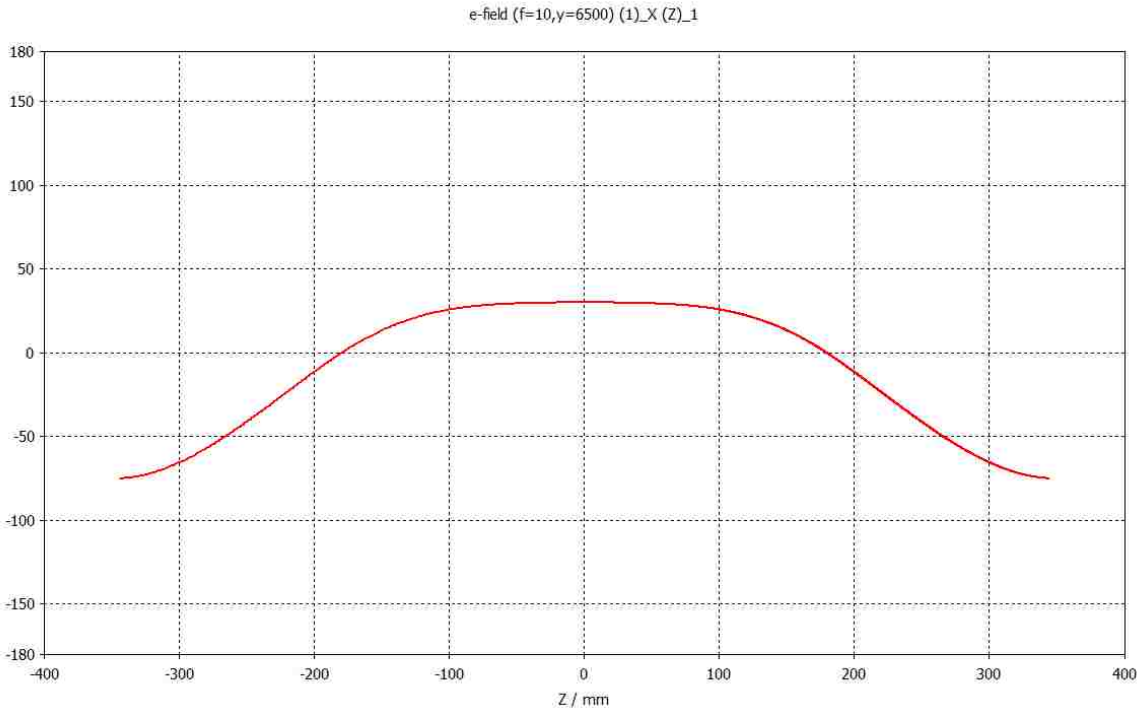

Figure 45. Phase Plot of Electric Field (Ex) in the H-Plane at y = 6500 mm (Narrow Beam)

[vertical axis: Phase (degrees)]

The far field 3D radiation pattern is shown in Figure 46. The gain of the system is 32 dBi. Side and back lobes are present; however these are well below the main lobe. The largest lobe is the back lobe. The radiation pattern is extremely narrow in the direction of the main lobe in the far field.

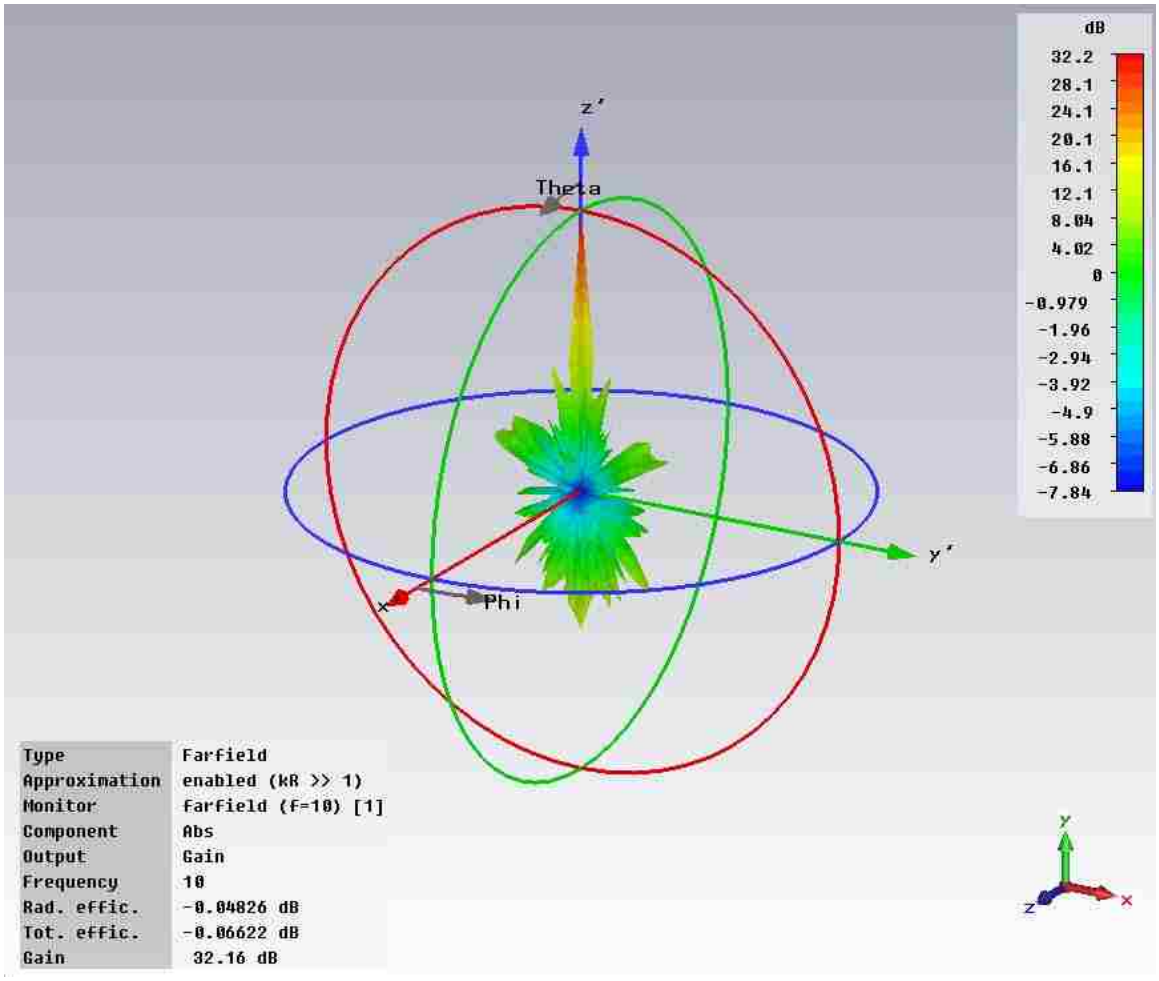

Figure 46. 3-D Radiation Pattern (Narrow Beam)

This can be seen more clearly in the 2-D polar plots of Figure 47 and 48, in the E- and H-planes, respectively. These indicate high gain, with a half power beam width on the order of 2.2° in both planes. Side and back lobes are everywhere at least 20 dB below the main lobe.

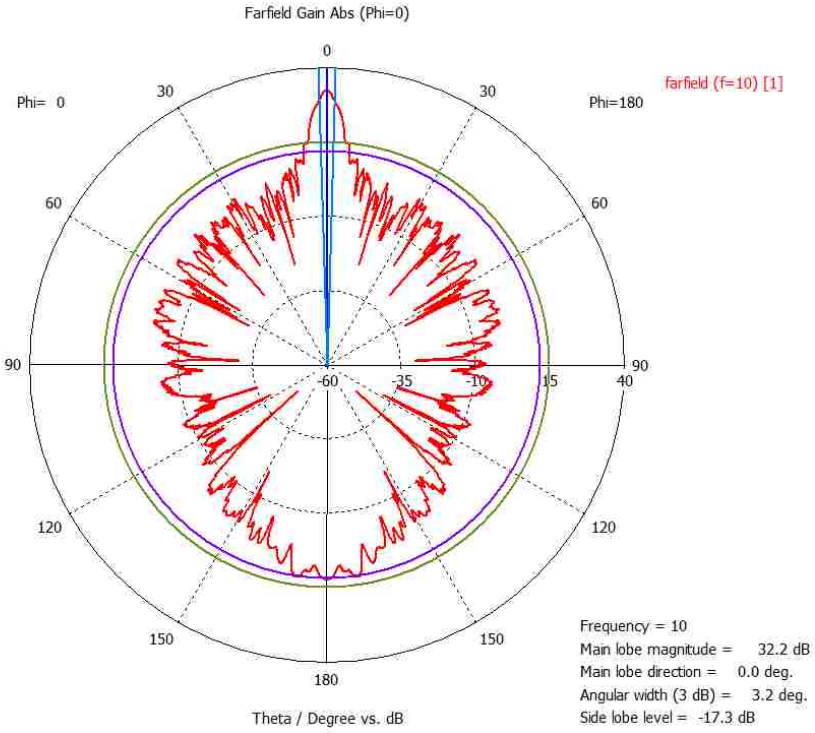

Figure 47. Far Field Radiation Pattern in the E-Plane (Narrow Beam)

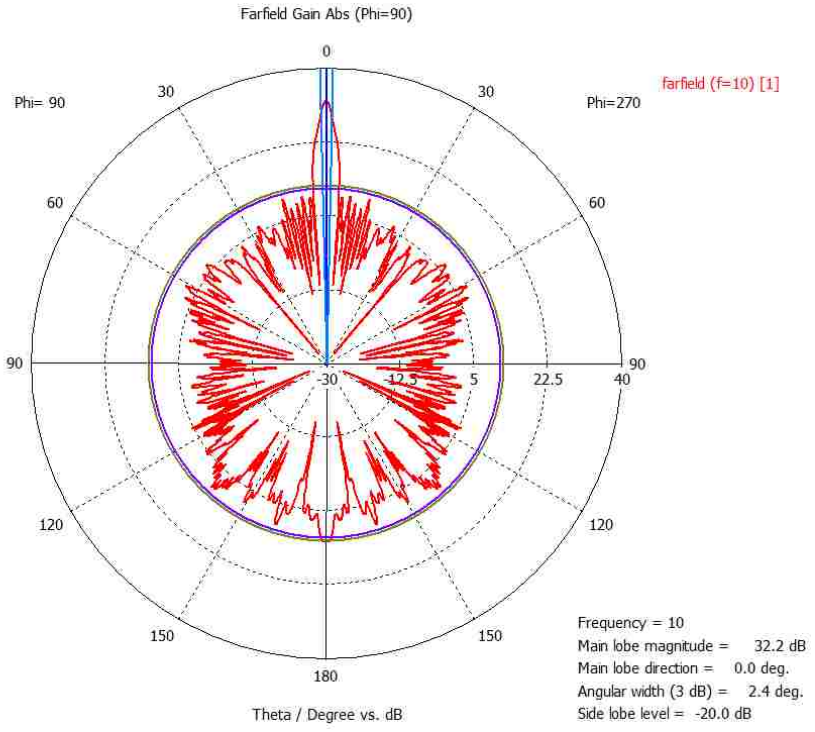

Figure 48. Far Field Radiation Pattern in the H-Plane (Narrow Beam)

4.2.3.2 Simulated Results Broad Beam

The simulated results for broad-beam lens positioning are shown in Figure 49, which is an amplitude plot of the electric field in the E-plane, with lens 1 at y = 750 mm and lens 2 at 2630 mm. High fields are present near the horn and along the focal region of lens 1. The beam flares out from the focal plane of lens 1 towards lens 2 and becomes collimated by this lens, as can be seen near the top of the figure.

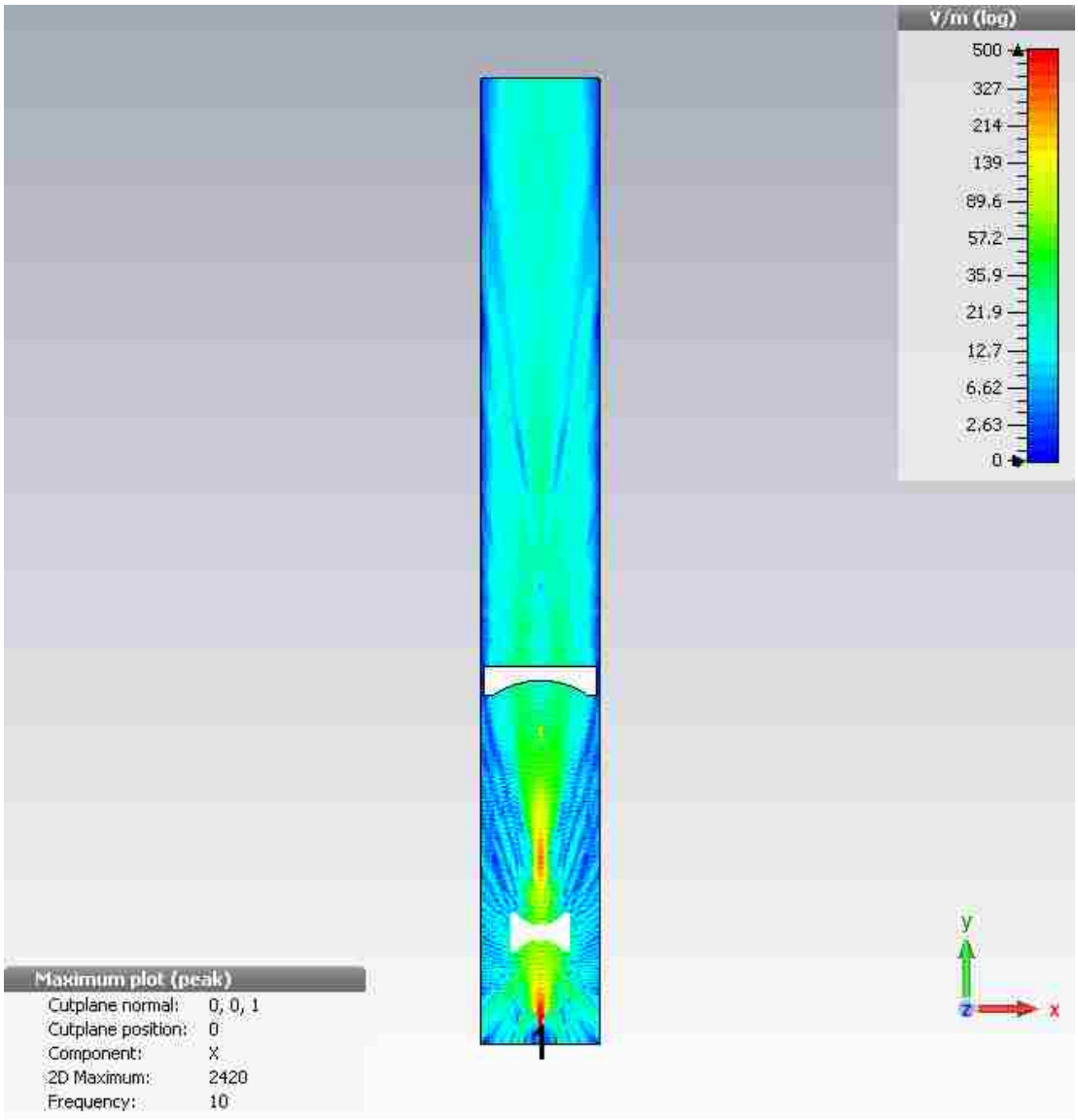

Figure 49. Amplitude Plot of Electric Field (Ex) in the E-Plane (Broad Beam)

The simulated boresight measurement with the lenses thus positioned is shown in Figure 50. The boresight electric field drops to zero at the center plates of the lenses as can be seen at y = 750 mm and y = 2570 mm, corresponding to positions of lenses 1 and 2, respectively. The focal region of lens 1 can be seen near y = 1225 mm. Beyond lens 2, at

y > 2700mm, the electric field holds steady at close to E = 18 V/m, indicating collimation of the beam.

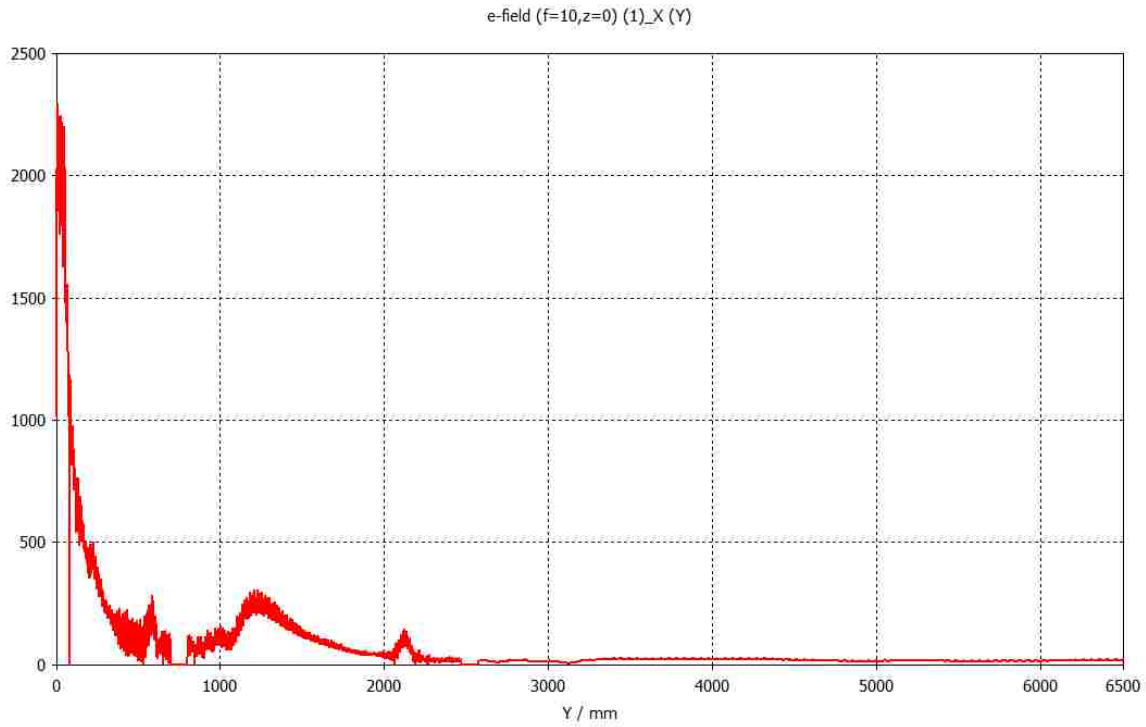

Figure 50. Simulated Boresight Measurement of Electric Field (Ex) – Broad Beam [vertical axis: Electric Field (V/m)]

A "carpet" representation of the electric field (ex) in the 2-D plane at y = 6500mm is shown in Figure 51.

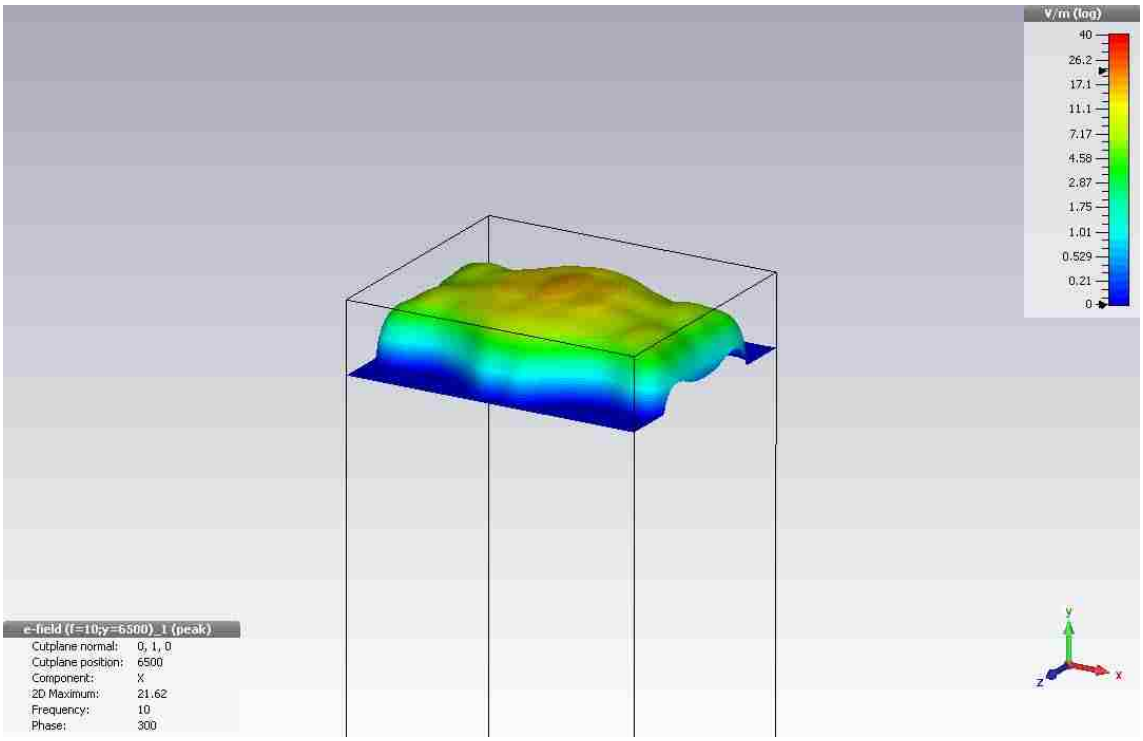

Figure 51. "Carpet" Representation of Electric Field (Ex) at y = 6500mm (Broad Beam)

The simulated electric field measurement across the E- and H- planes in this plane are presented in figure 52 and 53, respectively. The half power beam width in the E-plane is approximately 220 mm, in the H- plane it is broader, although not as sharply defined at approximately 400 mm.

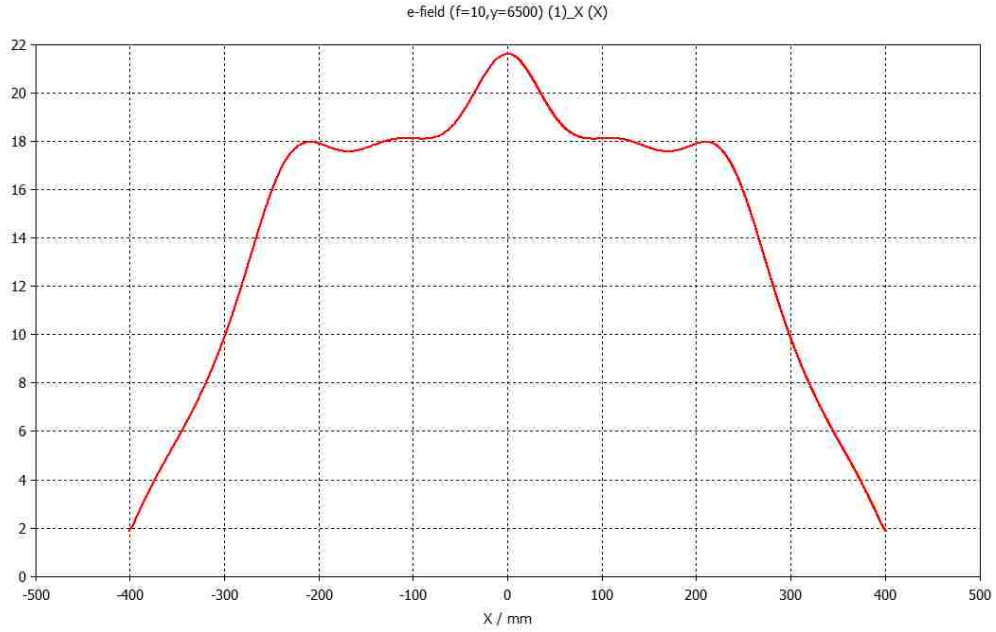

Figure 52. Electric Field (Ex) in the E-Plane at y = 6500 mm (Broad Beam) [vertical axis: Electric Field (V/m)]

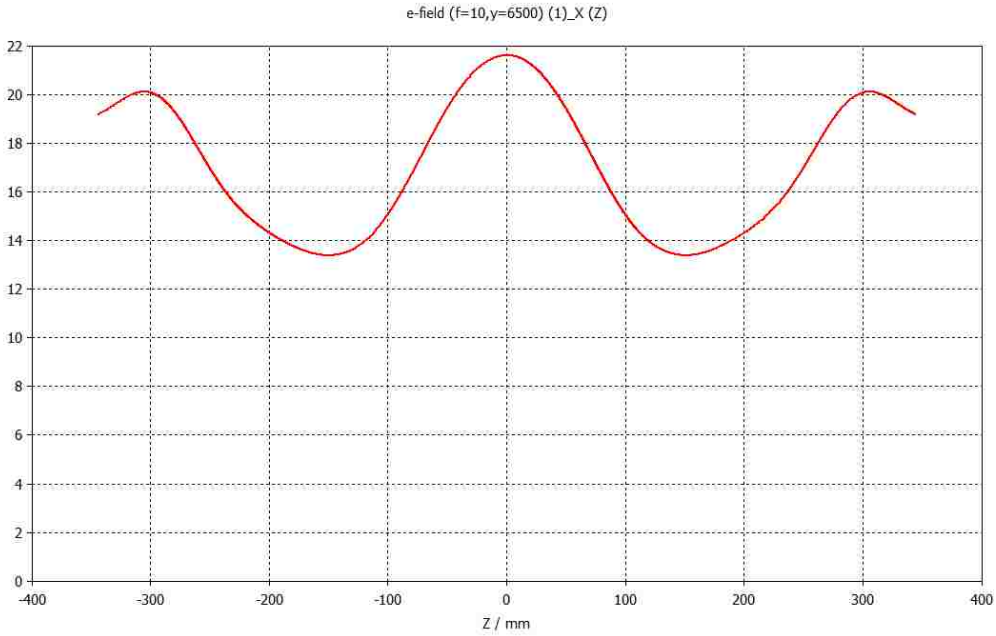

Figure 53. Electric Field (Ex) in the H-plane at y = 7000 mm (Broad Beam) [vertical axis: Electric Field (V/m)]

Figure 54 is a phase plot of the electric field (Ex) in the E-plane, showing a broad collimated beam with a very close to planar phase front in the far field across the beam in this plane for -250 mm < y < 250mm .

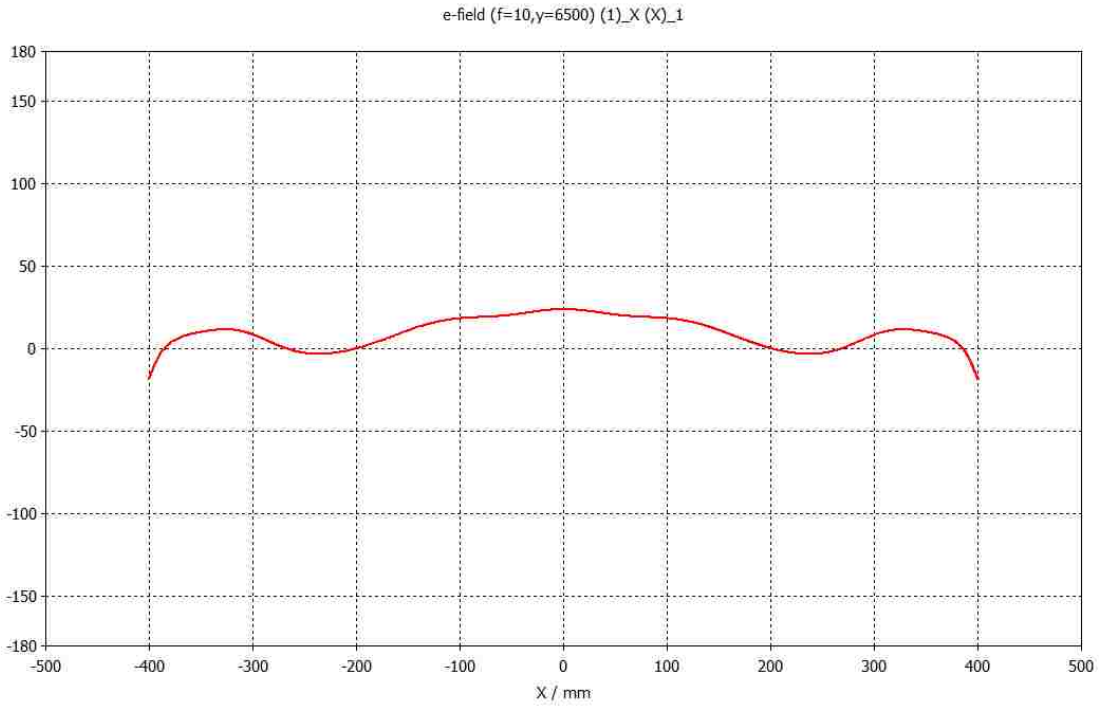

Figure 54. Phase Plot of Electric Field (Ex) in the E-Plane (Broad Beam) [vertical axis: Phase (degrees)]

Figure 55 is a phase plot of the electric field (Ex) in the H- plane at y = 6500 mm, showing a very flat phase front across the H-plane from -400 mm < y < 400mm.

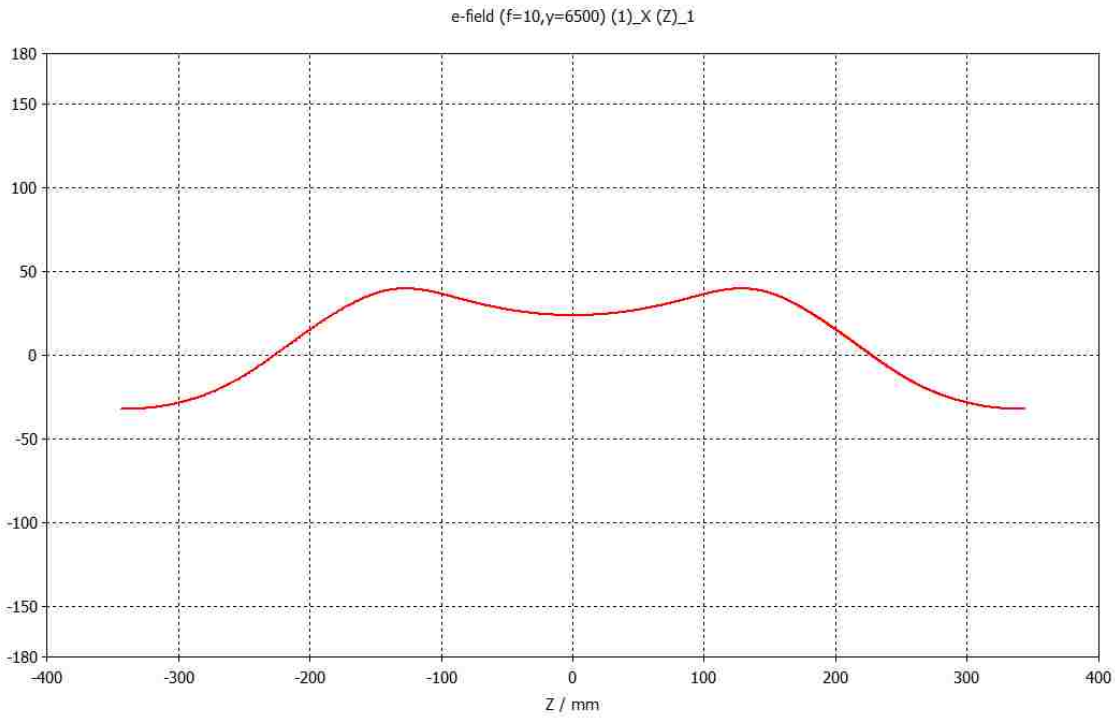

Figure 55. Phase Plot of Electric Field (Ex) in the H-Plane at y = 6500 mm (Broad Beam)

[vertical axis: Phase (degrees)]

The far field 3D radiation pattern is shown in Figure 56. The gain of the systems is 32 dBi. Side and back lobes are present; however these are well below the main lobe. The largest lobe is the back lobe. The radiation pattern is extremely narrow in the direction of the main lobe in the far field.

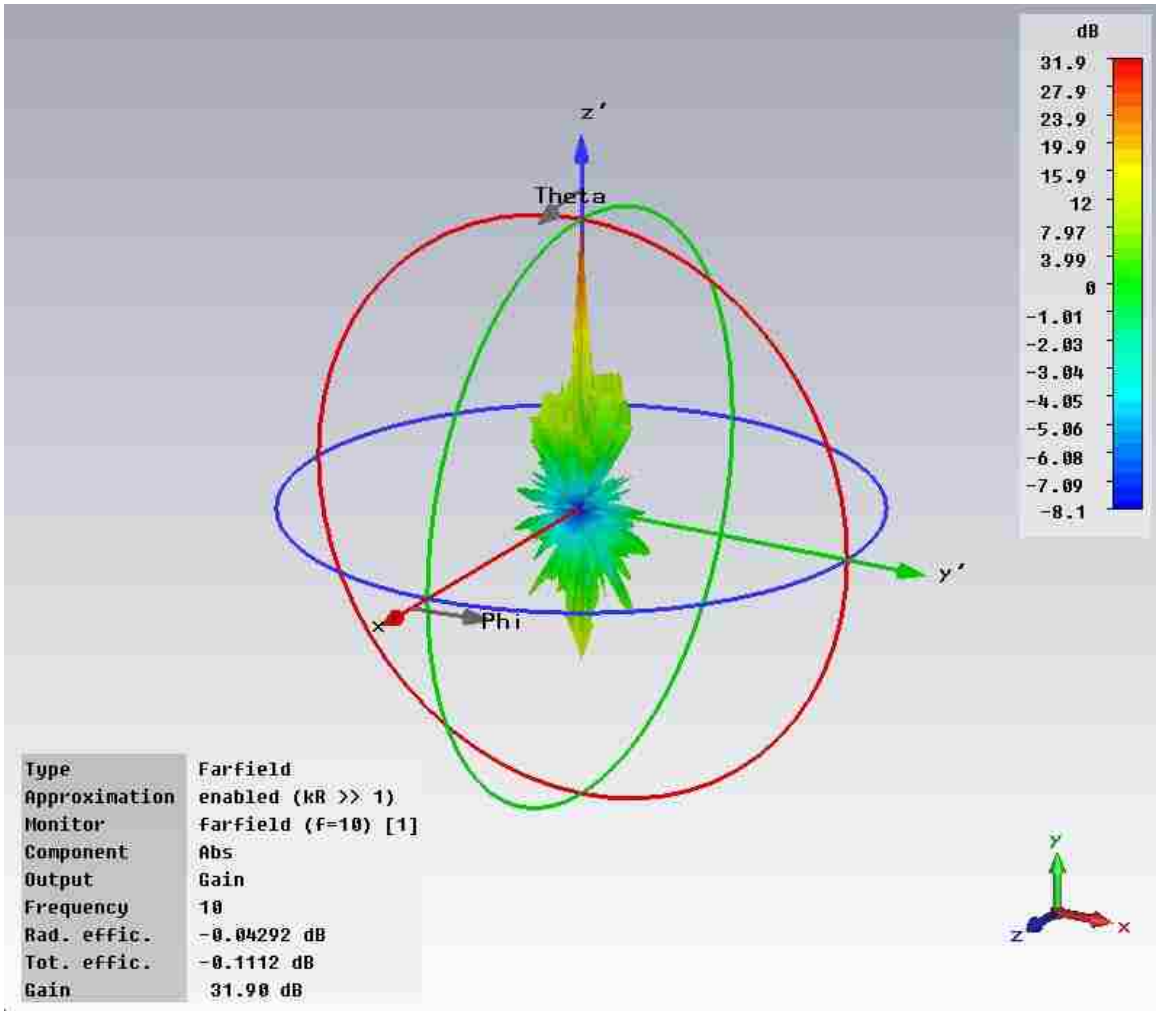

Figure 56. 3-D Radiation Pattern (Broad Beam)

This can be seen more clearly in the 2-D polar plots of Figure 57 and 58, in the E- and H-planes, respectively. These indicate high gain, with a half power beam width on the order of 2° in both planes. Side and back lobes are everywhere at least 20 dB below the main lobe.

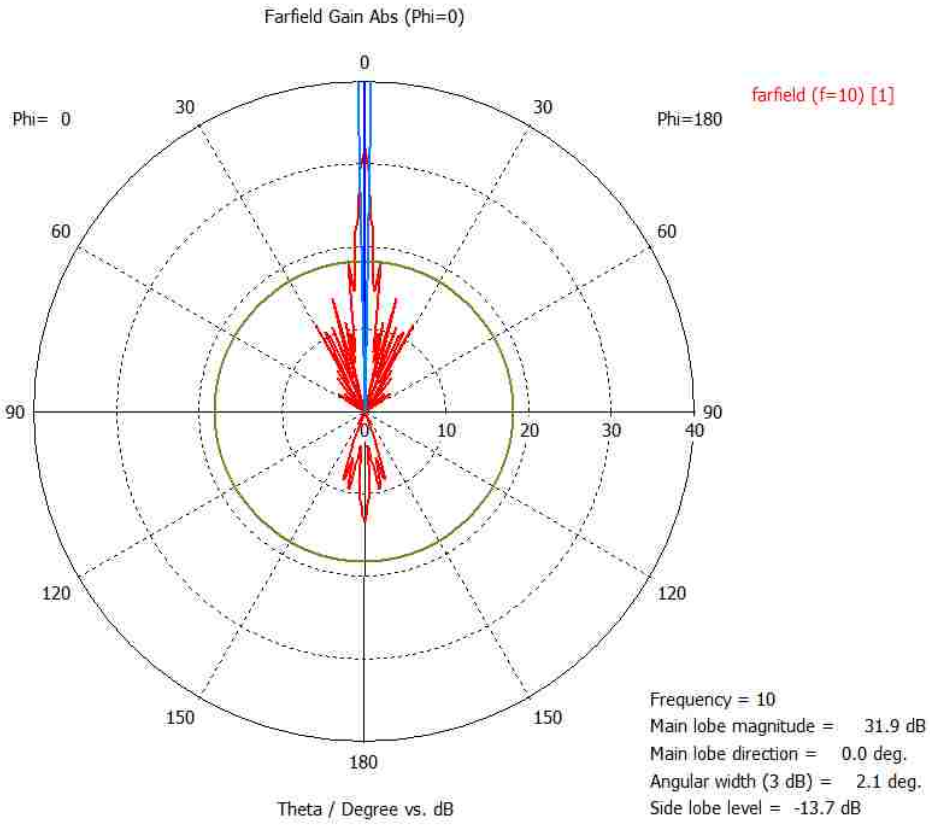

Figure 57. Far Field Radiation Pattern in the E-Plane (Broad Beam)

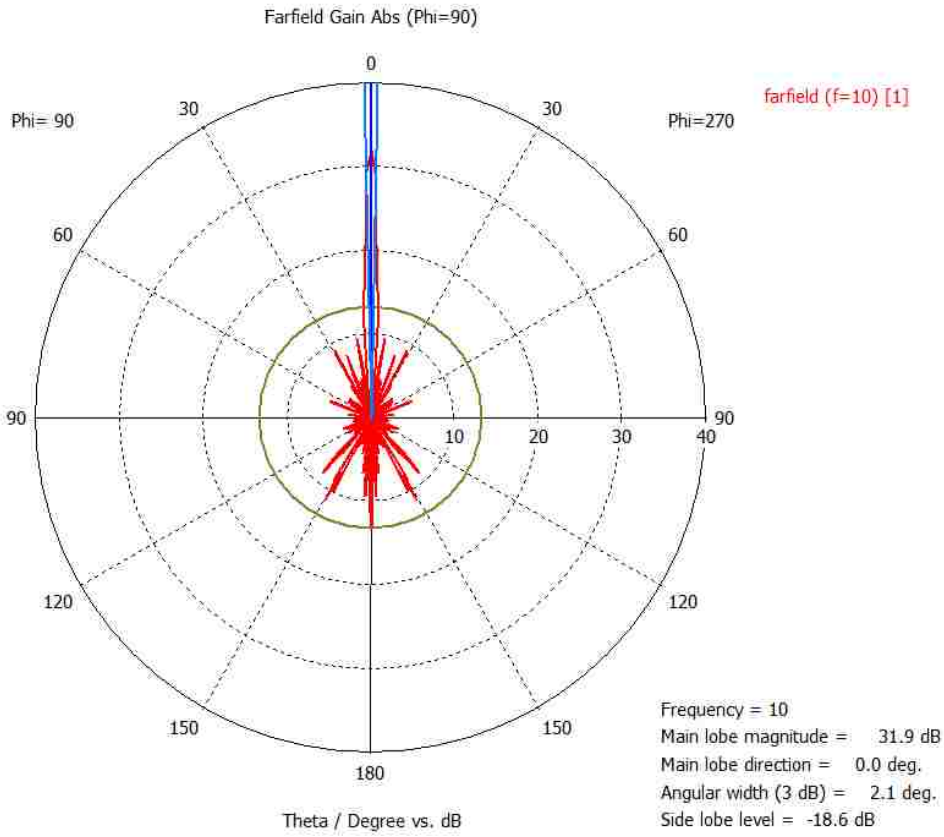

Figure 58. Far Field Radiation Pattern in the H-Plane (Broad Beam)

4.3 Experimental Results: Low Power 10GHz Zoom Antenna

The lenses for this demonstration were constructed with the same materials as described in Section 4.1with extruded polystyrene as spacer and support structure and heavy duty aluminum foil, having a thickness of close to .0254 mm, for the lens plates. The spacing of the plates was chosen to be 19.05 mm in order for the index of refraction to be n = 0.6.

The diameter and focal length of both lenses was chosen by an iterative process using an excel spreadsheet (see Section 4.10) containing appropriate equations for determining:

- focal lengths of both lenses based on their index of refraction and radii of curvature,
- S1and S2 for various positions of lens 1,
- Required diameter of lens 1 at various positions in order for it to intercept the half power beamwidth of the horn antenna at the farthest horn-lens separation
- required placement of lens 2 for varying positions of lens 1 and varying focal lengths for lens 2,
- required diameter of lens 2 for interception of the half power beamwidth, when placed a focal length from the location of the focal plane with lens 1 at its farther distance from the horn phase center.

and keeping in mind physical limitations such as:

- lens 1 cannot be closer to the phase center of the horn antenna than the thickness of the lens plus the distance from the phase center of the horn to its aperture
- measurements were to be made in an anechoic chamber 30 feet long

- both of these lenses were to be hand-built and therefore it was not desirable that they be untenably large or have a prohibitively large number of plates

Design of the two lenses for a given zoom application is discussed in further detail in the discussion of magnification range presented in Section 4.10.

4.3.1 Experimental Setup for Zoom Antenna Measurements

The test setup used to explore collimation of the beam is shown in Figure 59. An X-Band antenna with a gain of 16dBi was used as the transmit antenna. The receive antenna was a small 6dBi antenna. An Agilent N9912A-106 FieldFox Network Analyzer was used with ports 1 and 2 connected to the transmit and receive antennas, respectively.

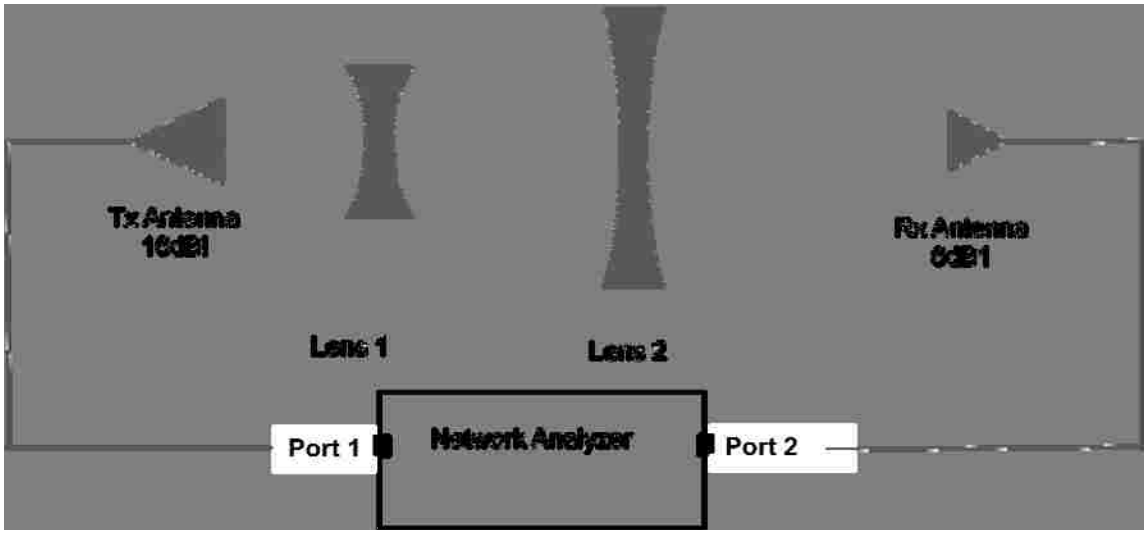

Figure 59. Test Setup for Exploring Beam Collimation

The lenses were positioned for beam collimation; i.e., lens 1 was placed a distance S1 from the phase center of the transmit horn antenna, the distance to the focal plane, S2, was calculated. The second lens was placed a focal length (f') from the focal plane of lens 1. This is illustrated in the photograph of Figure 60.

Figure 60. Test Setup; Lenses Positioned for Beam Collimation

Boresight and focal plane measurements were made for lens placement required to achieve the most narrow collimated beam for this lens pair as well as for the broadest collimated beam, by varying the location of the receive antenna.

4.3.2 Results of Zoom Antenna Measurements

The results of boresight measurements are shown in Figure 61. These measurements were made along boresight (the axis of the system) at regular intervals moving away from the location of lens 2. Measurements were made with the lenses in place (i.e., the upper curve marked by x's in Figure 61) and compared to measurements made with the receive antenna at the same locations, with the lenses removed (marked by diamonds in Figure 61.

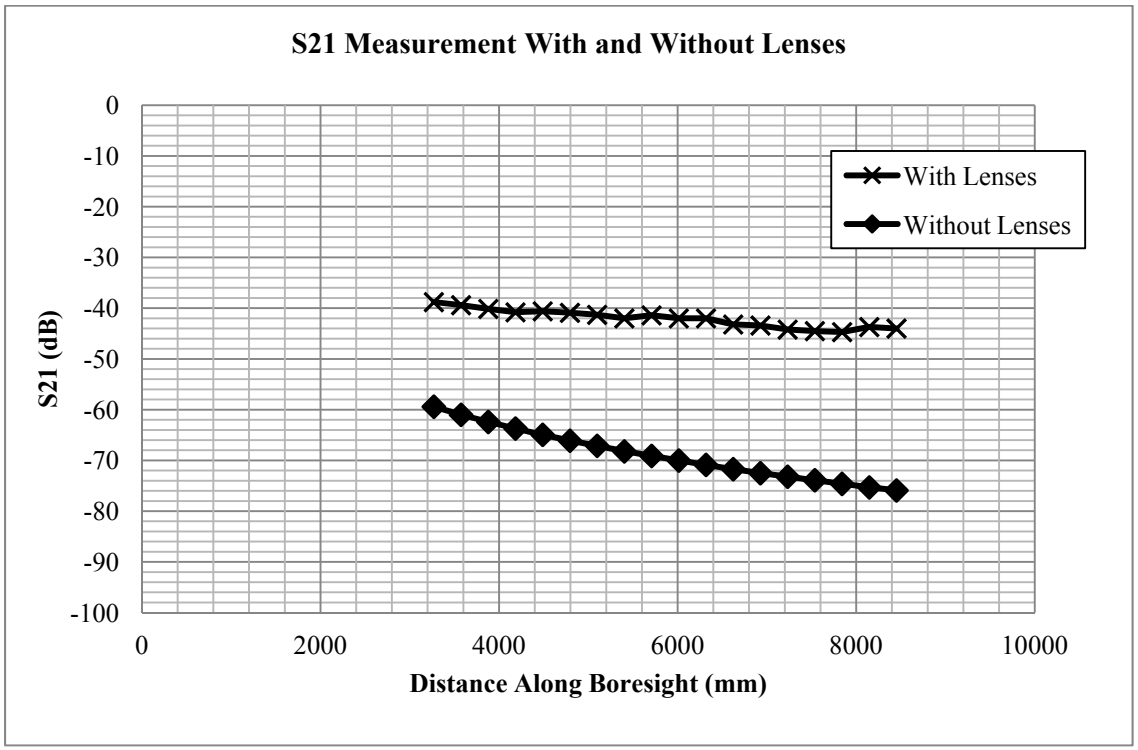

Figure 61. Boresight Measurements of 10GHz Low Power Demonstrator Zoom Antenna

The upper curve indicates beam collimation by remaining steady as the receive horn moves away from second lens; the lower curve shows the $1/R^2$ loss of power with increasing distance when the lenses are removed.

With the lenses in place, and positioned for beam collimation with a relatively narrow beam diameter, measurements were made across the E- and H-planes to explore the half power beam width of the collimated beam.

The results are shown in Figures 62 and 63, for the E- and H-planes, respectively. These measurements were normalized to the peak at the center of the beam. The half power beam width is close to 180 mm in the E-plane and 160mm in the H-plane. This corresponds to approximately 5 wavelengths, and is somewhat symmetric; to within 0.3 λ.

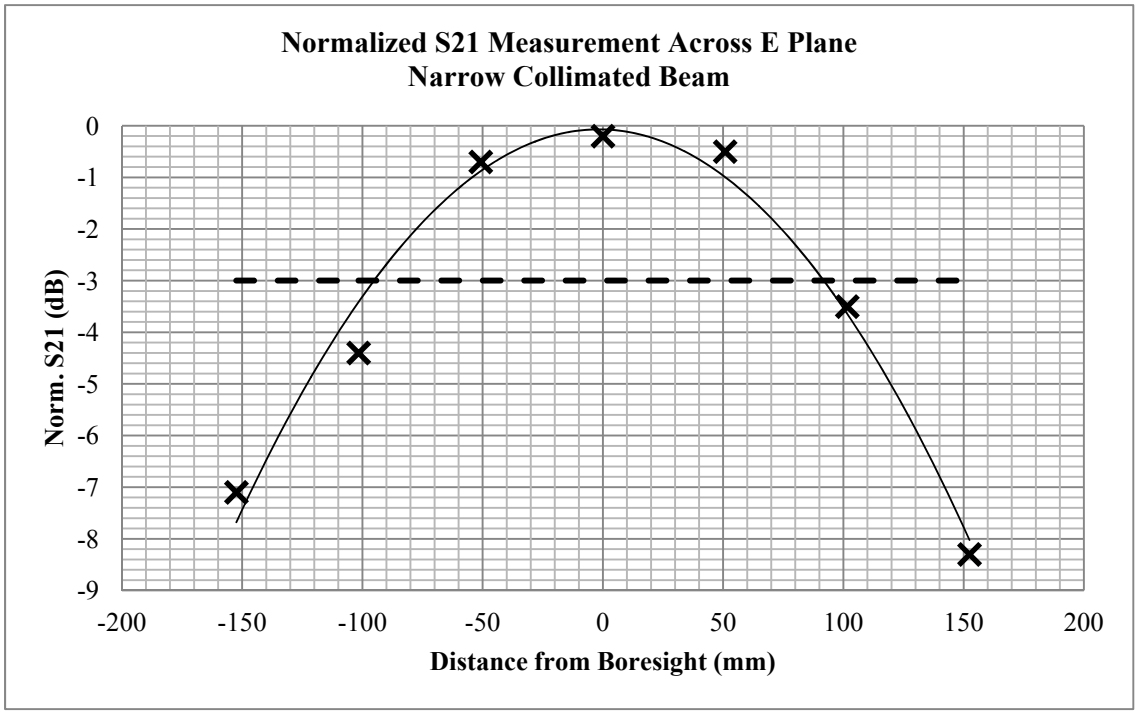

Figure 62. E-Plane Measurements (Lenses Positioned for Narrow Collimated Beam)

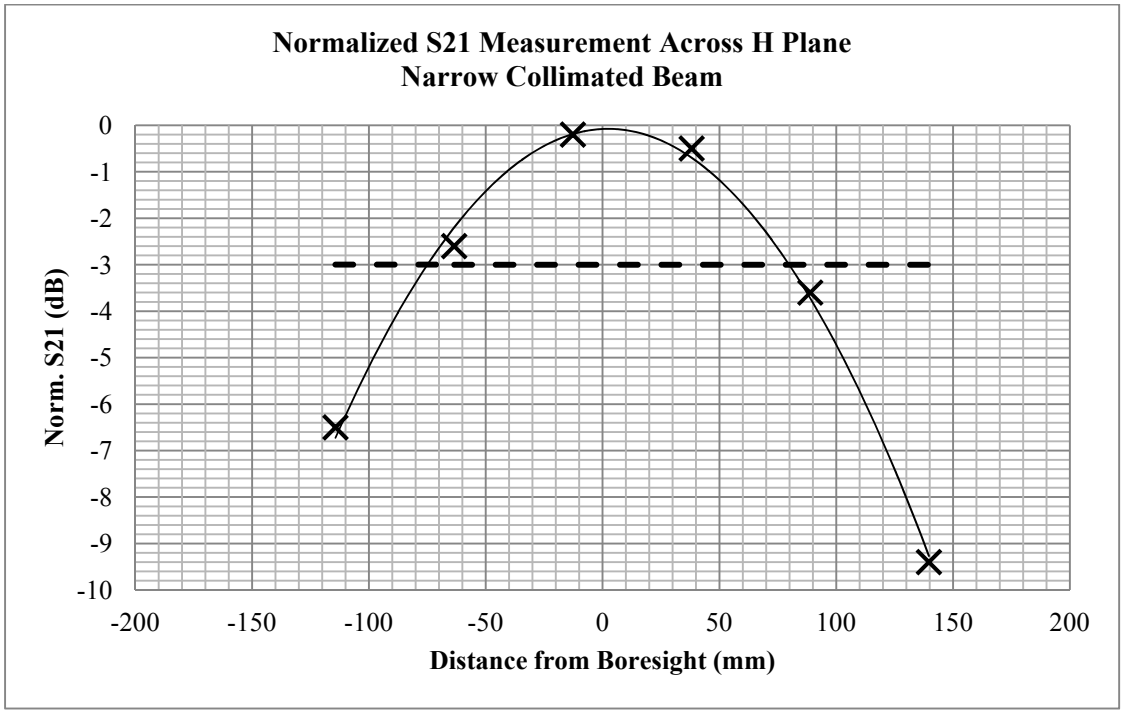

Figure 63. H-Plane Measurements (Lenses Positioned for Narrow Collimated Beam

The results of similar measurements made with the lenses positioned for a broader collimated beam are shown in Figures 64 and 65, for the E- and H-planes, respectively. These results indicate a half power beamwidth in the E-plane of 640mm and in the H-plane of 640mm; again, symmetrical about the axis of the system to within less than a wavelength.

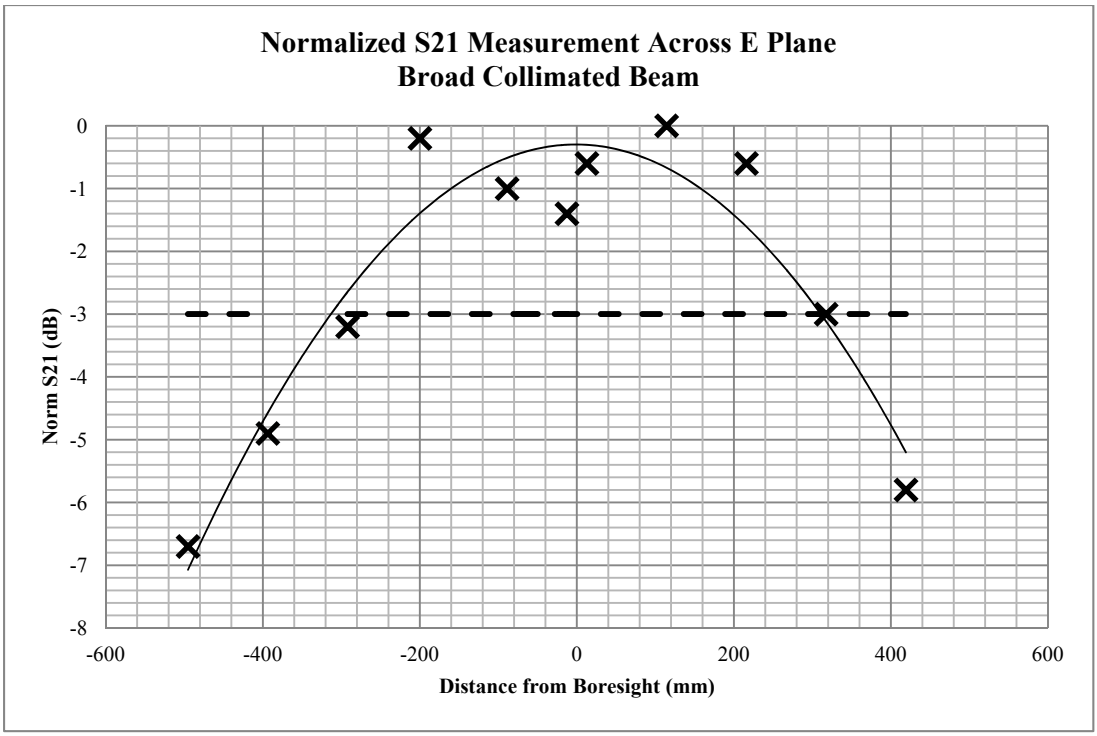

Figure 64. E-Plane Measurements (Lenses Positioned for Broad Collimated Beam)

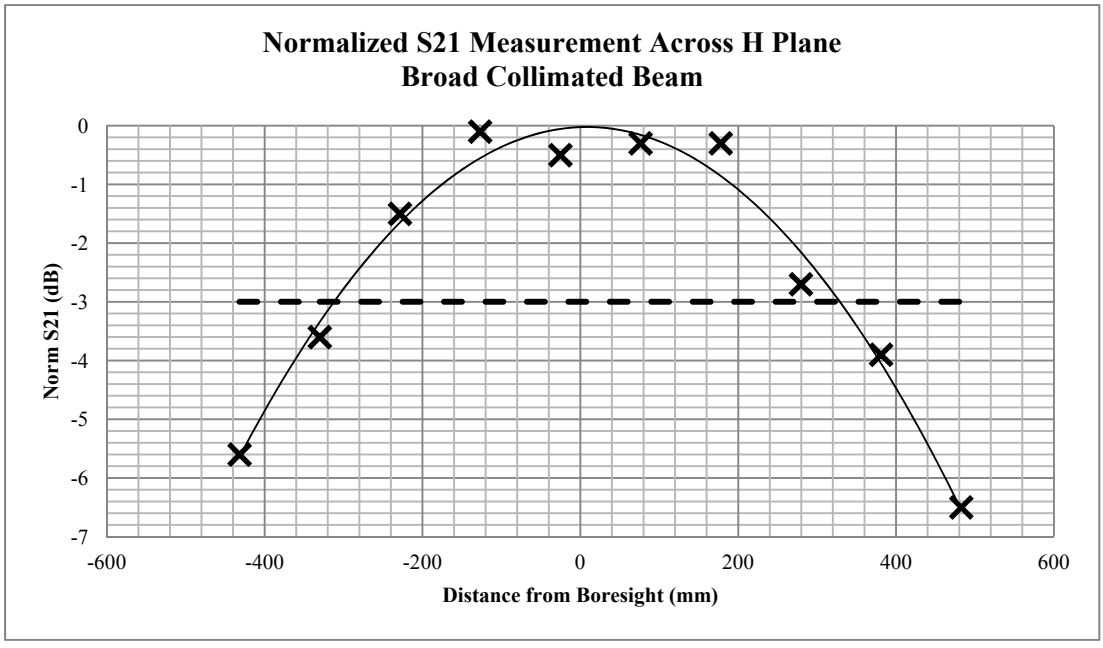

Figure 65. H-Plane Measurements (Lenses Positioned for Broad Collimated Beam)

In positioning the lenses for collimation, lens1 was first placed a distance S1 from the phase center of the feed horn antenna. S2 was then calculated from the lens equation and the second lens was initially placed a distance from lens 1 equal to the sum of S2 and the focal length of lens 2. Initial quick boresight measurements were then made by moving the receive horn away from S2 and keeping an eye on the network analyzer. Lens 2 was repositioned plus or minus a few inches from its initial placement in an attempt to optimize collimation of the beam. It was found in all cases that the final placement was within a few inches from the initial placement. Showing good agreement between experiment and theory. Of course, this was not extremely precise but represented the best one could do by eyeballing of axial alignment and orientation of the lenses and transmit and receive horns and using a plumb bob and tape measure.

4.3.3 Validation of Code: Comparison of Experimental with Simulated Results for 5GHz Lens

Figure 66 shows experimental results of measurements made across the focal plane of the 5GHz lens presented in Section 5. The data shown in Figure 66 are normalized S21 measurements that indicate the half-power beamwidth across the E-plane in the focal plane of this lens was close to 3.6". The free-space wavelength at this frequency is $\lambda = c/f = 2.36$". The results shown in this figure indicate an Airy disc diameter of very close to the theoretical diameter according to Equation [9] of 1.5 wavelengths.

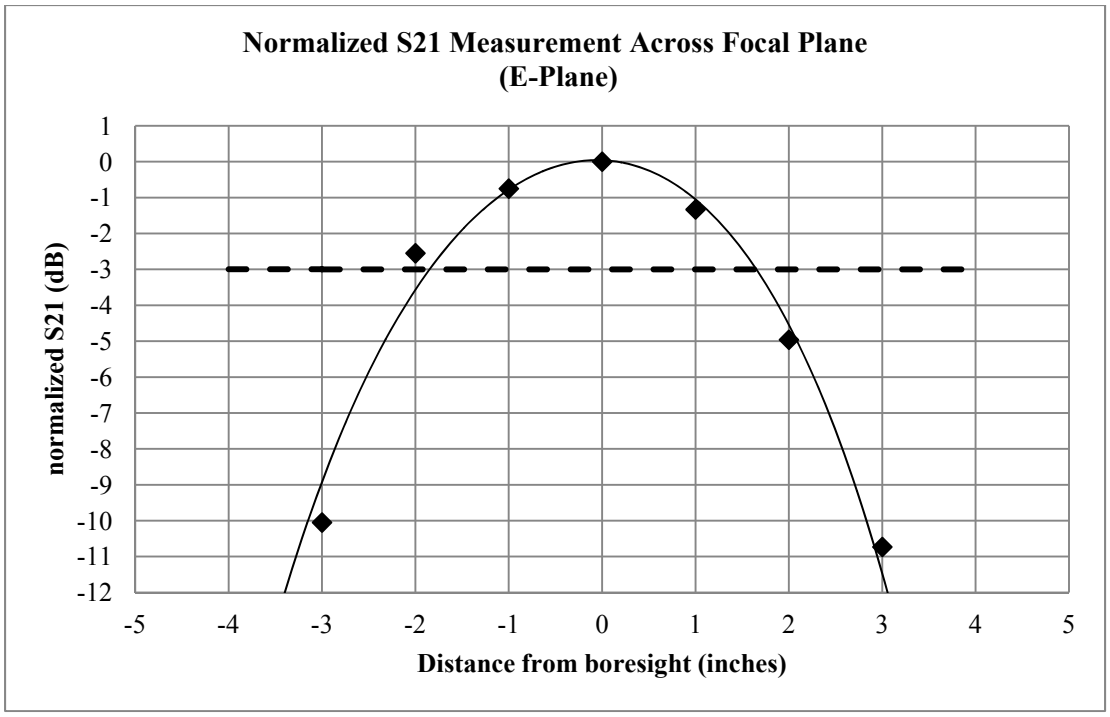

Figure 66. Experimental normalized S21 measurement across focal plane of 5GHz lens in the E-plane

These data show very good agreement with simulation, as indicated in Figure 67, which shows a simulated electric field measurement across the focal plane in the E-plane. In this case, the half power beamwidth corresponds to values that are down a factor $\sqrt{2}$ below the peak electric field, as indicated in Figure 67 by markers 2 and 3. The distance between these points is 3.72", in very good agreement with the close to 3.6" observed in experiment.

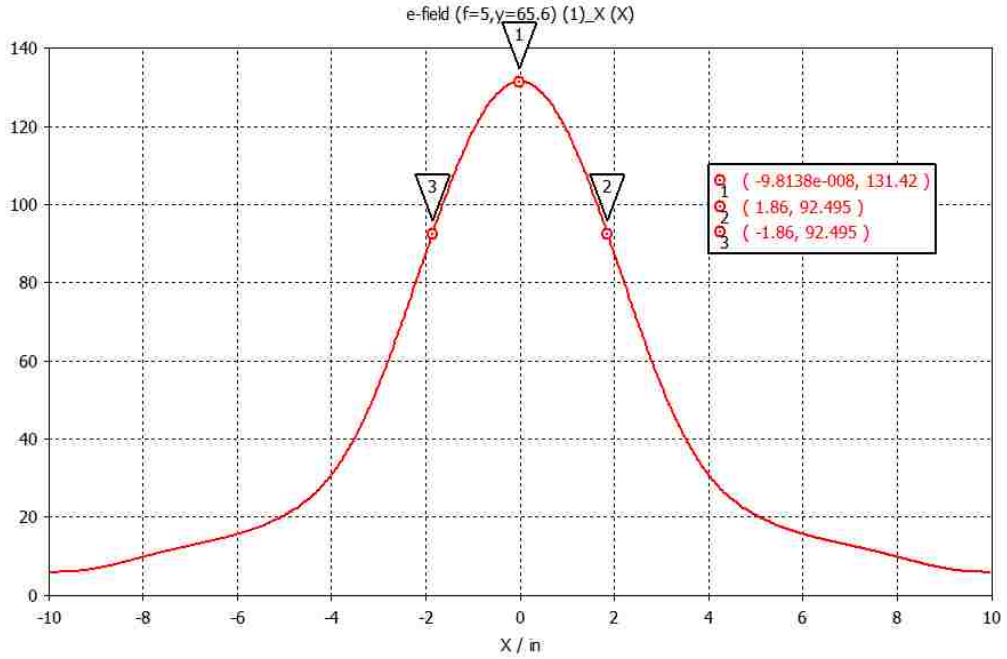

Figure 67. Simulated Electric Field Across Focal Plane for 5GHz Lens in the E-Plane

[vertical axis: Electric Field (V/m)]

To make a direct comparison of these results, the simulated measurement of electric field was shown in Figure 67 was converted to a normalized S21 measurement and the experimental data of Figure 66 were plotted on the same plot. For consistency with the rest of this document, the distance from boresight along the focal plane was converted from inches to millimeters. The results are plotted in Figure 68, excellent agreement between experimental and simulated results.

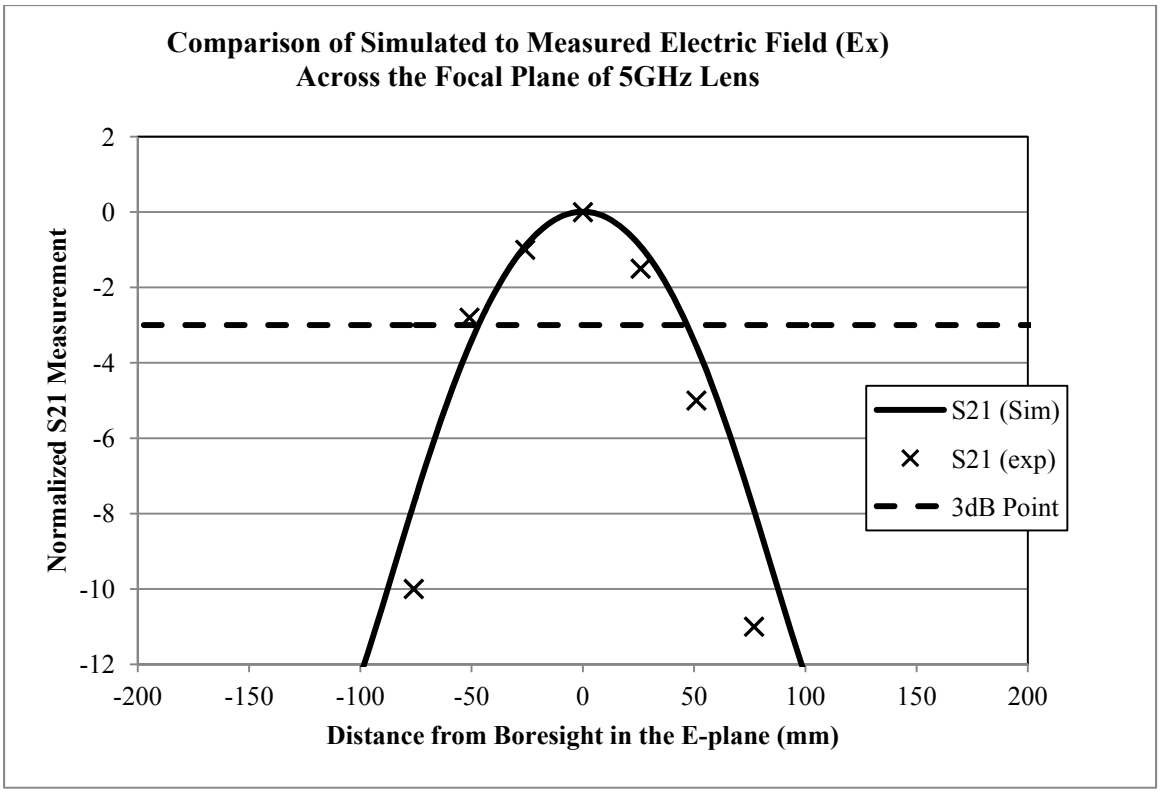

Figure 68. Comparison of Simulated to Experimental Results

4.4 High Power Demonstration: L-Band Lens

For high power demonstration, a large L-Band lens was constructed using 1.6 mm ($1/16^{th}$ inch) aluminum plates and polystyrene support rods with spacers between the plates, as shown in Figure 69. The plates were 1.74 m (6' long) and 1.2 m (4' wide). The frequency of operation was 1.3 GHz and the plate spacing was 160 mm (6.25 "), resulting in an index of refraction of $n \approx 0.6$.

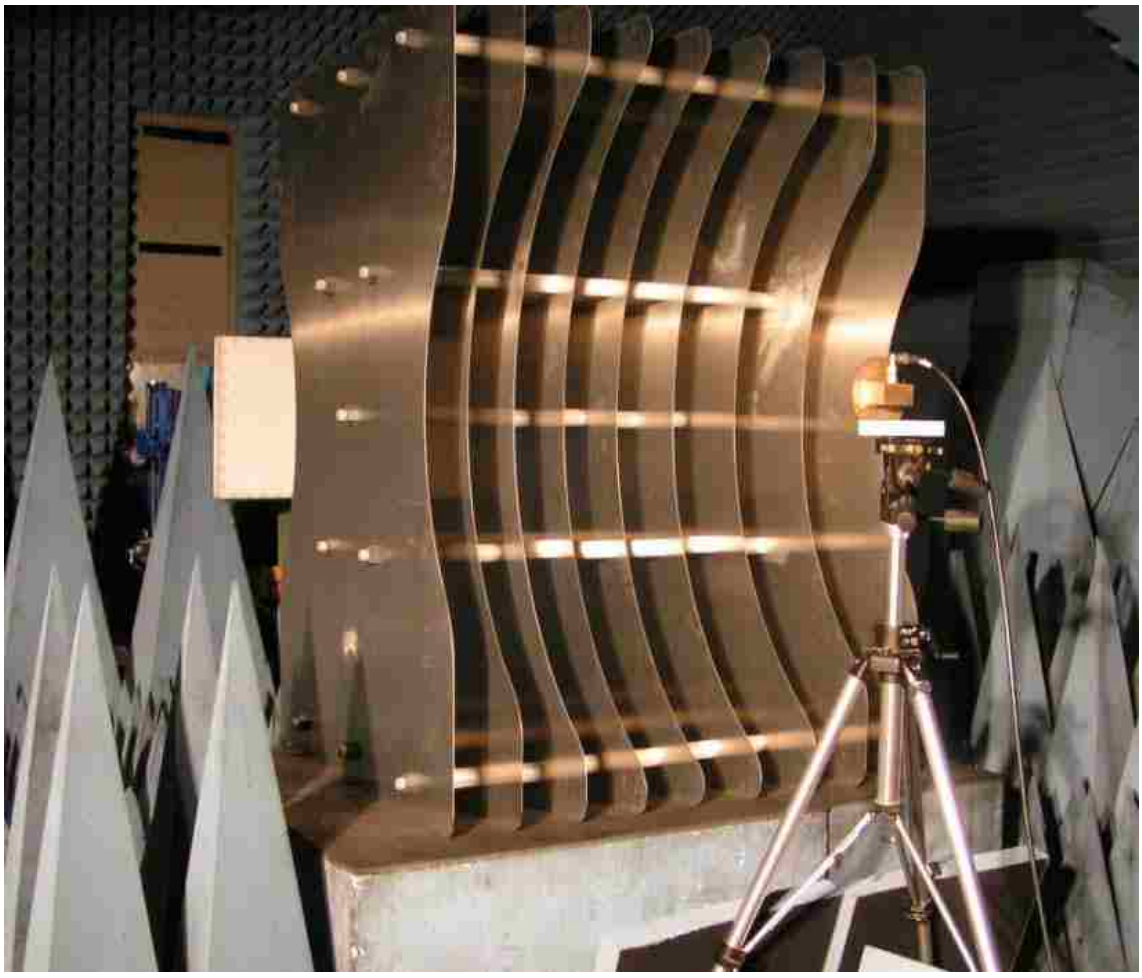

Figure 69. L-Band Lens for High Power Demonstration

This was a bi-concave spherical lens, with R1=R2=0.89 m (35”), which yielded a focal length of 1.3 m. The lens was postioned R= 2.56 meters (greater than the lens focal length) from the aperture of the horn antenna. Low power S21 measurements were made using the setup shown in Figure 59 to locate the focal plane of the lens when it was positioned 2.56 meters from the aperture of the transmit horn antenna, by moving the receive sensor along boresight away from the lens (on the far side of the lens) and finding the peak in the S21 measurement . The results are shown in Figure 70, which compares measurements with the lens in place (indicated by the upper curve) to those obtained at the same locations when the lens was removed (indicated by the lower curve.

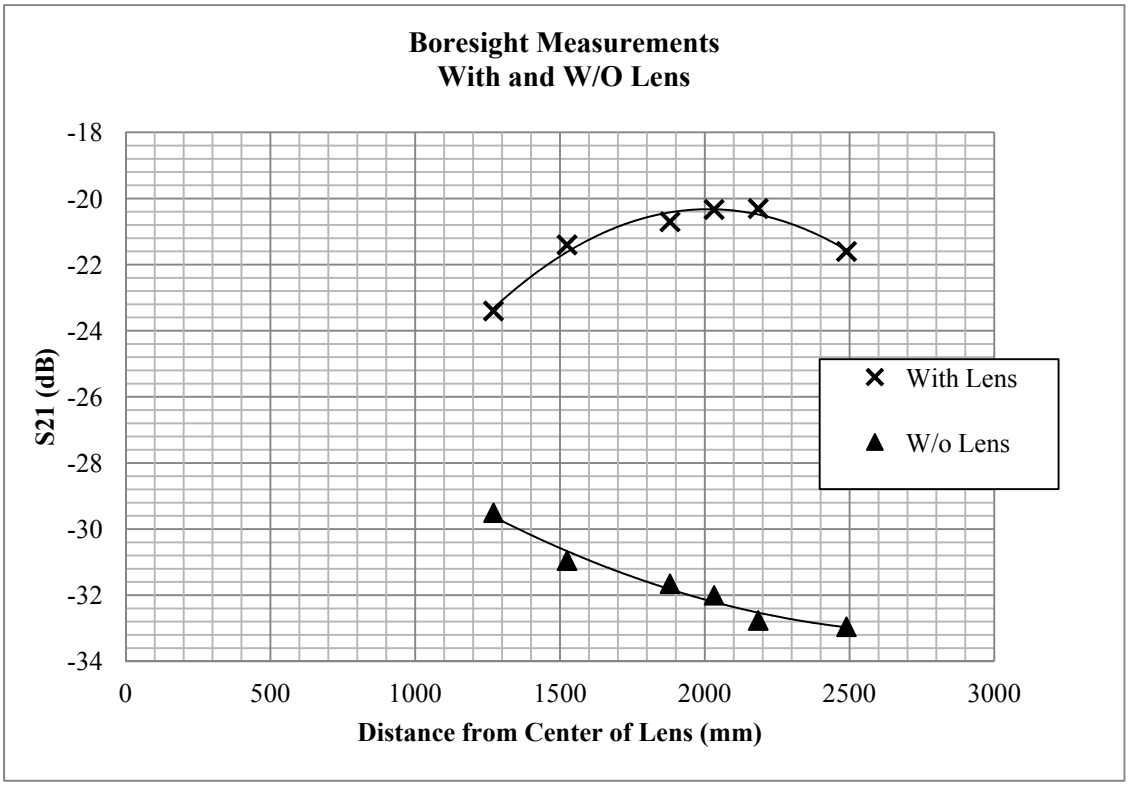

Figure 70. Boresight Measurements With and Without Lens

These measurements indicated location of the focal plane at close to 2m. At this location, S21 measurements were then made in the vertical (E-plane) direction and also in the horizontal (H-plane) direction, to explore the diameter of the Airy disc.

The results are shown in Figures 71and 72, respectively.

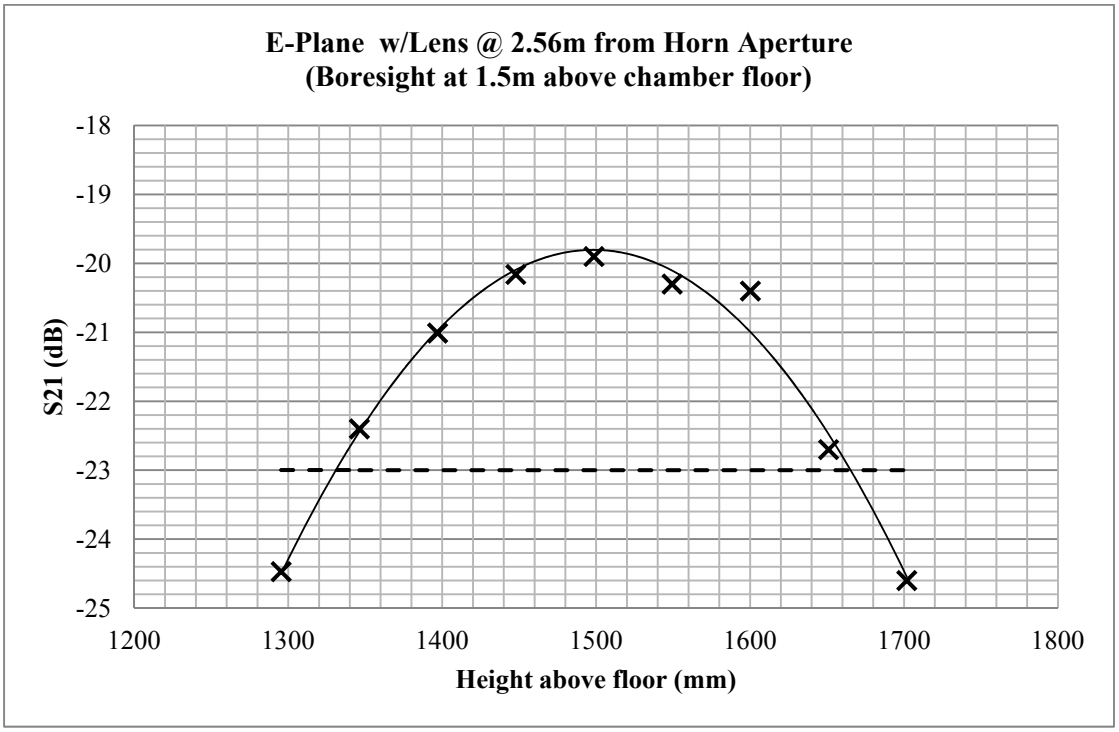

Figure 71. Low Power Measurements; Electric Field across E-Plane in the Focal Plane of the Lens

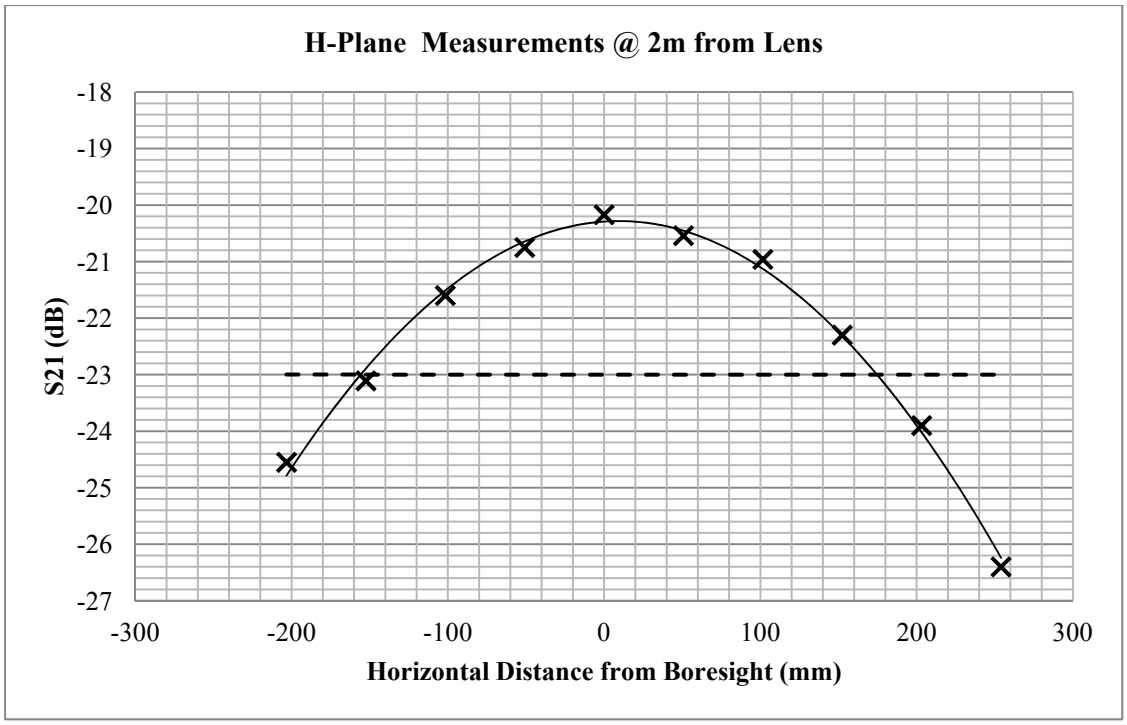

Figure 72. Low Power Measurement: Electric Field Across H-Plane in the Focal Plane of the Lens

In Figure 71, the half power beamwidth in the E-plane is close to 310mm. Figure 72 indicates that the half power beam width in the H-plane is 330mm. In both cases, this is slightly less than ½ λ.

High power measurements were then made using a 200MW source. An S-band open waveguide sensor (below cutoff); was used to measure the electric field on the far side of the lens.

Results of electric field measurements made along boresight are shown in Figure 73.

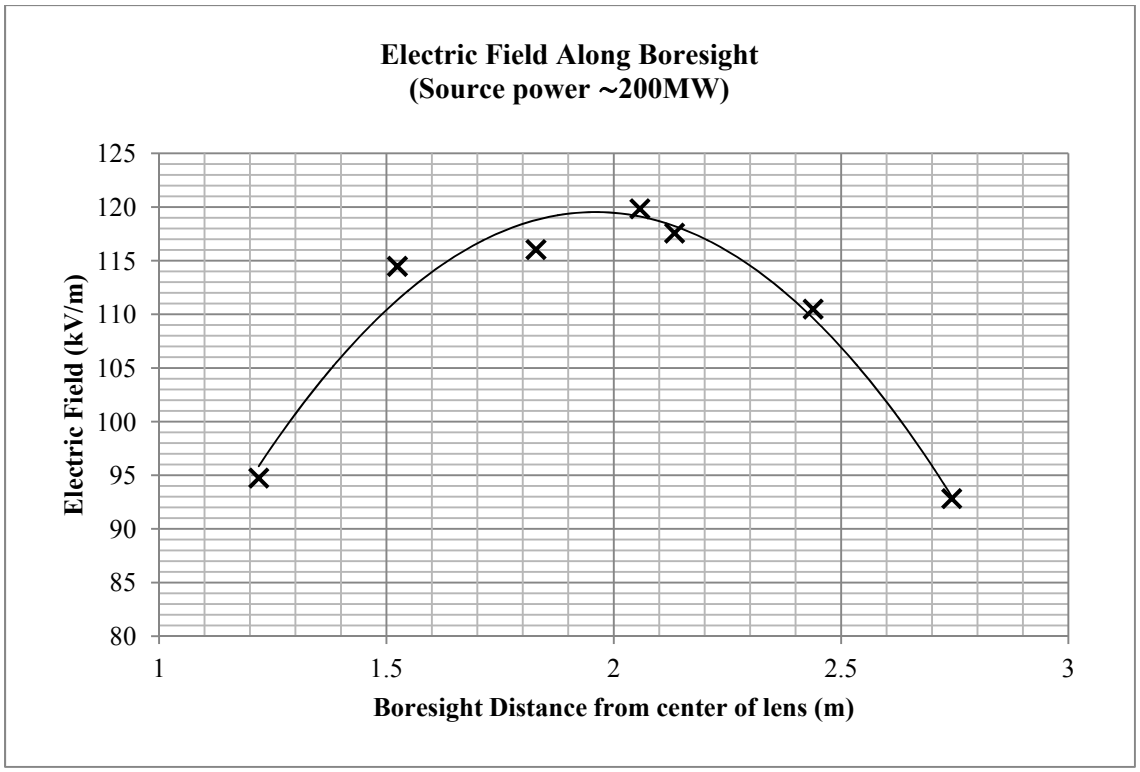

Figure 73. High Power Measurements: Boresight Electric Field Through Focal Plane

The electric field peaks at a distance of close to 2 meters from the center of the lens, indicating the location of the Airy disc. The peak electric field is on the order of 120 kV/m. This is well below the electric field required to cause air breakdown of 300kV/m. Because the electric field scales as the square root of the power, air breakdown is not expected to occur below several GW at this frequency.

Results of electric field measurements in the E- and H- planes across the focal plane for this source power are shown in Figures 74 and 75, respectively.

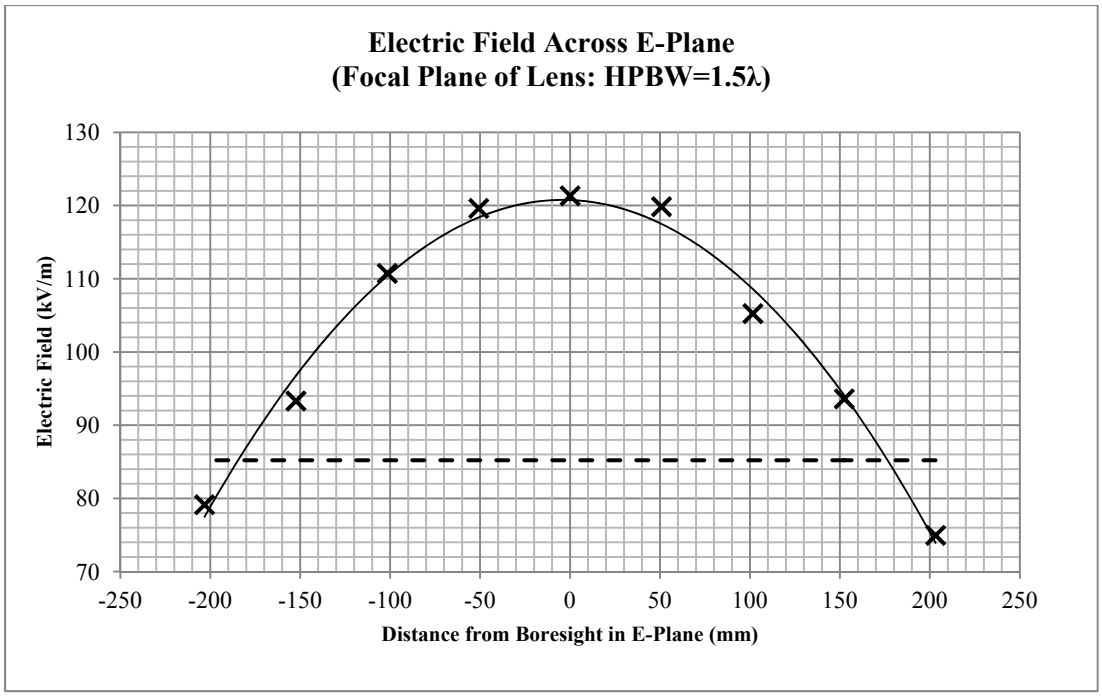

Figure 74. High Power Measurements: E-Field Across E-Plane in Focal Plane of Lens

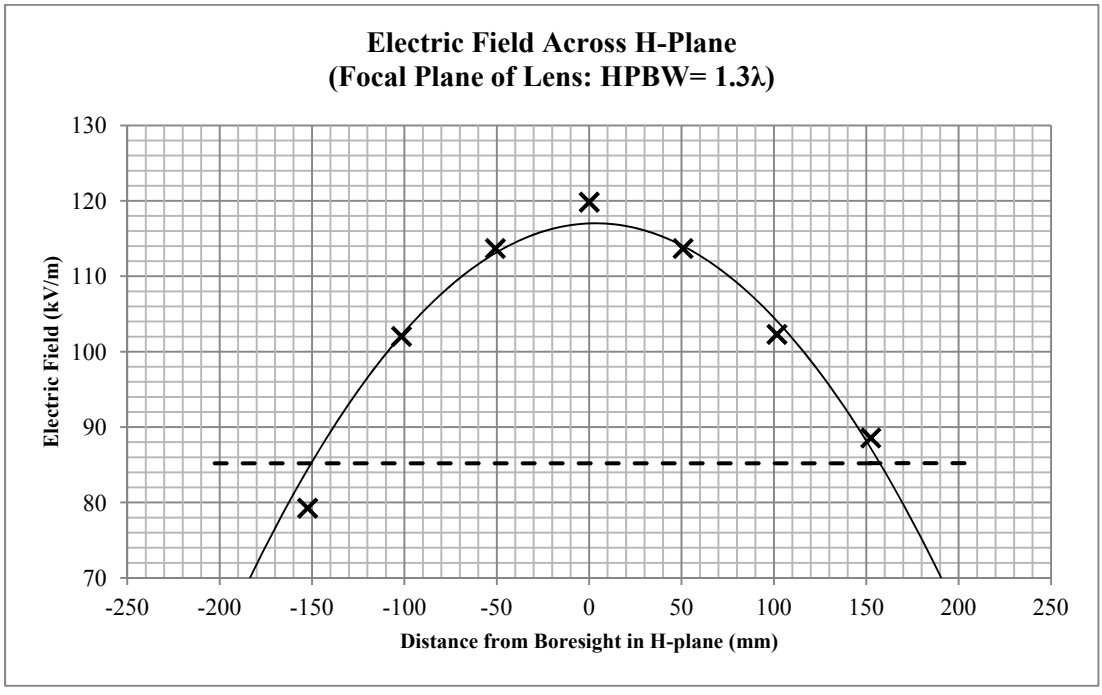

Figure 75. High Power Measurements: Electric Field Across H-plane in Focal Plane of Lens

Similar to the results for the low power measurements, the width of the Airy disc in the E- and H- planes is close to 1 ½ λ. The pattern is slightly broader in the H-plane. The peak electric field in the center of the focal plane was close to 120 kV/m, well below the 300 kV/m required for air breakdown. The maximum power handling capability of this zoom antenna is, in fact, determined by this threshold; i.e. one cannot exceed the voltage required for air breakdown in the center of the focal plane of the first lens. This is discussed further in Section 4.11.

4.5 Evaluation of Carbon Fiber Reinforced Polymer Composites

For the lens plates, it is desirable to have high conductivity, low density to minimize weight, low reactivity with air/water for outdoor applications, and sufficient rigidity and strength to maintain their shape with the type of construction shown in Figure 69; i.e., built for very high power applications, with air spacing and dielectric rod support structures.

Table 6 below lists some relevant properties of metals

Material	Resistivity (nΩ◦m)	Density (gm/cm3)
Silver	15.87	10.49
Copper	16.87	8.96
Gold	22.14	19.3
Aluminum	26.5	2.7
Iron	96.1	7.874

Table 6. Properties of Metals

Aluminum has long been the material of choice for many antenna components due to its high conductivity, relatively low reactance with air and water, light weight, and low cost.

However, newly emerging carbon fiber reinforced polymer (CFRP) composites may provide a better alternative to aluminum in terms of strength and weight. These

composites have been explored for applications that include slotted waveguide arrays and microstrip antennas [Ref. 15, 16] and their conductivity/resistivity has been evaluated analytically [Ref. 17-19] and measured experimentally [Ref. 20, 21]. These have sufficient rigidity and tensile strength to serve as lens plates, and could significantly reduce the weight of the lenses, provided they have sufficient conductivity.

Experimental impulse tests as well as simulations were conducted to explore these CFRP composites and to evaluate the minimum conductivity required for the lens plates.

4.5.1 Experimental Results: Impulse Tests

Impulse tests were conducted using the experimental setup shown in Figure 76.

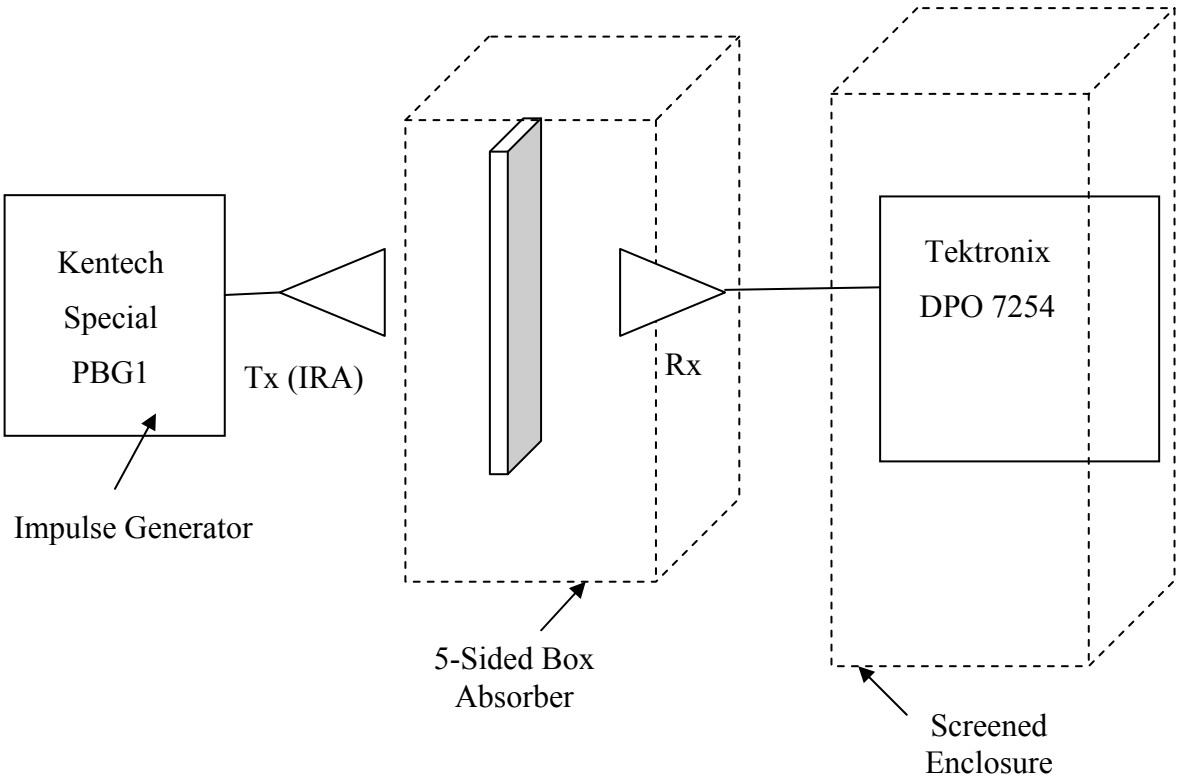

Figure 76. Test Setup for Impulse Measurements

The transmit antenna was an 18" diameter IRA antenna manufactured by Farr Research, Inc, model #FRI-IRA [Ref. 22-24] which radiates an impulse with a pencil beam radiation pattern. The receive antenna was a transmission line antenna also manufactured by Farr Research, Inc, model #FRI-TEM-02-100. It is called a "Replicating Sensor", as the time domain receive signal replicates the time domain intensity of the incident TEM wave. These antennae are shown in the photograph of Figure 77.

Figure 77. Transmit and Receive Antennae Used in Impulse Tests

The impulse was provided by a Special PBG1 pulser manufactured by Kentech, shown in the photograph of Figure 78. This source delivers a 6.5kV peak voltage impulse with an 80ns rise time into a 50 Ω load.

Figure 78. Special PBG1 Pulse Source Used in Impulse Tests

Figure 79. Tek. DPO 7254 Oscilloscope in Screened Enclosure

Data was acquired with a Tektronix DPO7254 digitizing oscilloscope (2.5GHz bandwidth, 40GS/s) in a screened enclosure to minimize noise, as shown in Figure 79. It was used in a 50 sample averaging mode; again, to increase signal-to-noise ratio.

In an additional attempt to minimize noise, a box was made out of absorber material, with a 12” opening in which various materials (thin layer) were inserted. This is illustrated in the photo of Figure 80; shown with a thin copper sheet as the sampled material.

Figure 80. Absorber Box with Copper Sample for Impulse Tests

This was a 5-sided box of absorber material with the receive antenna inserted into the opening. Thin samples of stainless steel, lead, copper, and aluminum were used and the impulse response of these metals was compared to that of several carbon fiber compounds.

The results are shown in the frequency domain Figure 81. All of the samples used in these tests appeared to provide good blocking of the impulse, compared to the free space baseline measurement shown by the curve in light green.

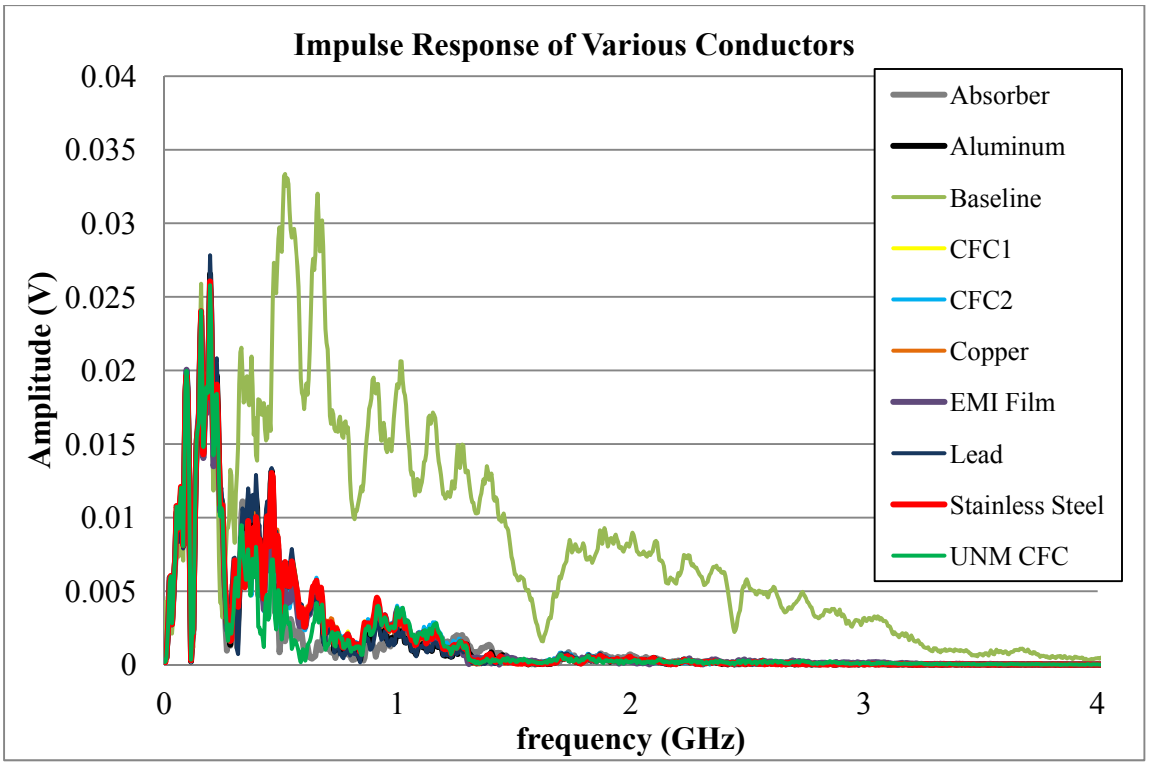

Figure 81. Results of Impulse Tests

While these measurements were too coarse to accurately quantify the effect of varying conductivity, they do yield important information on the high frequency conductivity of these materials (as opposed to the bulk conductivity) and indicate that any of these metals as well as the CFRP composite provided by UNM (denoted by "UNM CFC" in the legend of Figure 81), have sufficient conductivity to serve as antenna elements.

4.5.2 Simulations to Explore Minimum Conductivity Required for Lens Plates

Simulations were run to explore minimum bulk conductivity required for the lens plates. The setup for the simulation is shown in Figure 82. Again, the feed horn was designed to have a gain of 16dBi and had the usual waveguide feed sufficiently long to support the TE10 mode of propagation. A waveguide port was applied to the input at y = 0.

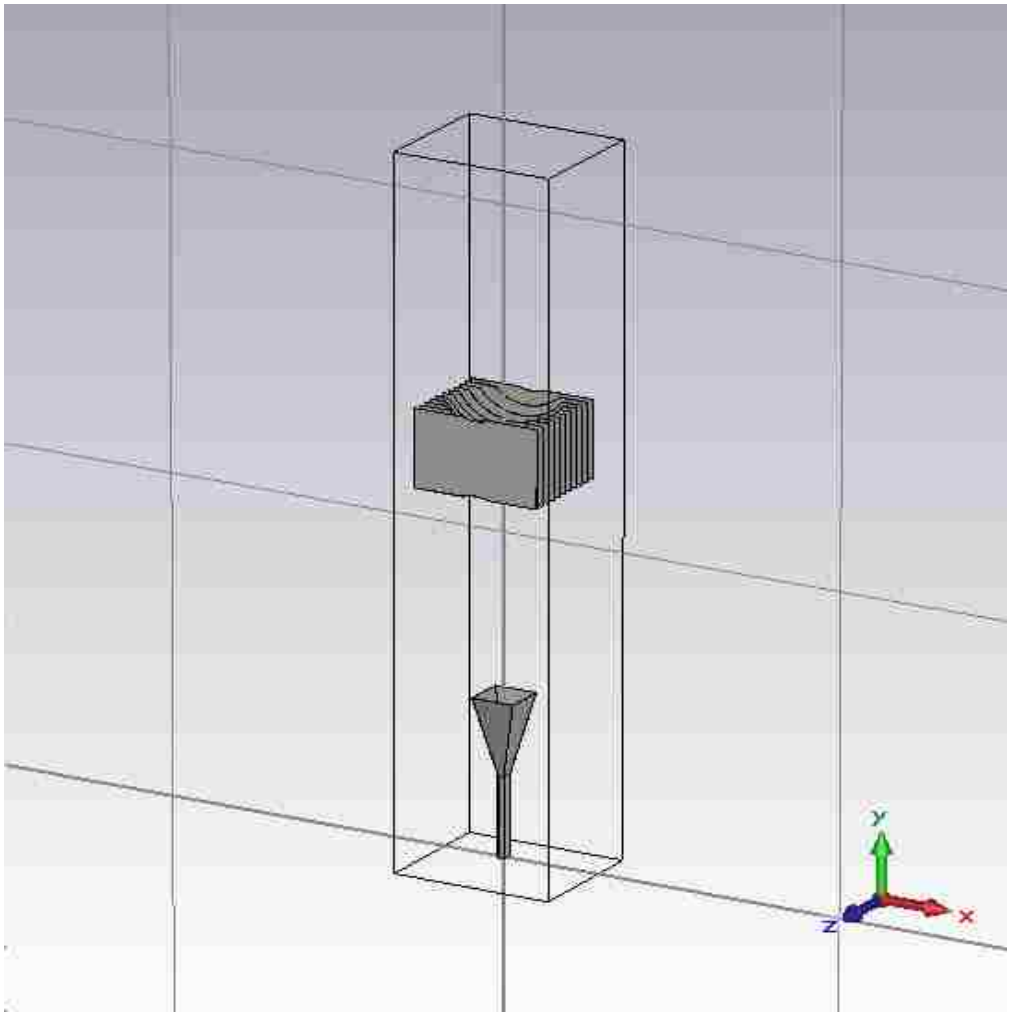

Figure 82. Simulated Design of LBand Horn and Lens to Explore Effect of Varying Conductivity of Plates

The parameters for the lens and the L-Band horn antenna are shown in Table 7.

Parameter	Dimension (mm)
Radius of curvature of lens	889
Plate spacing	147.6
Horn E	609.6
Waveguide E	82.55
Horn H	609.6
Waveguide H	165.1
Height of lens plate	1828.8
Thickness of lens plate	3.17
Width of lens plate	1219.2
Horn length	1219.2
Waveguide length	1270
Half min thickness of lens	177.8

Table 7. Design Parameters for LBand Horn and Lens

The waveguide port was then excited with a Gaussian excitation of 1-2 GHz. This frequency range was selected because weight reduction becomes more important at lower frequencies as lens size increases and because the conductivity of a material increases

with frequency (as skin depth increases). Therefore, showing sufficient conductivity at the lower end of the frequency range is sufficient to establish that this conductivity would suffice at higher frequencies. The excitation in the time and frequency domains is shown in Figures 83 and 84, respectively.

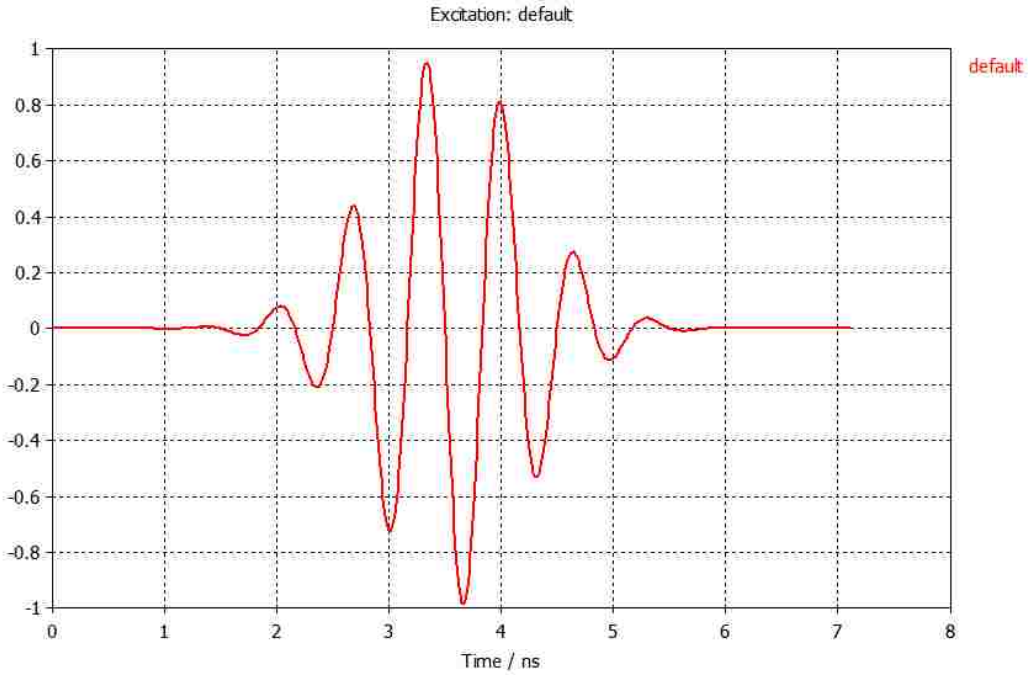

Figure 83. Gaussian Excitation (Time Domain)

[vertical axis: Amplitude (V)]

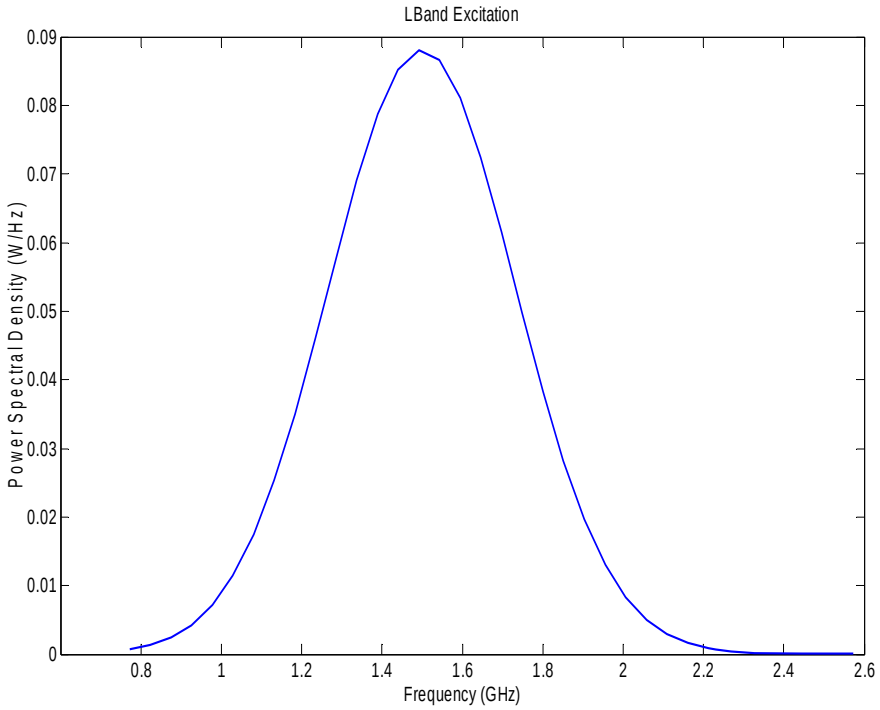

Figure 84. Power Spectral Density of Gaussian Excitation (Frequency Domain)

The conductivity of this material was provided by the manufacturer and is shown in Figure 85, relative to Aluminum plate, foil, and bulk aluminum. The conductivity was measured at 726 S/m.

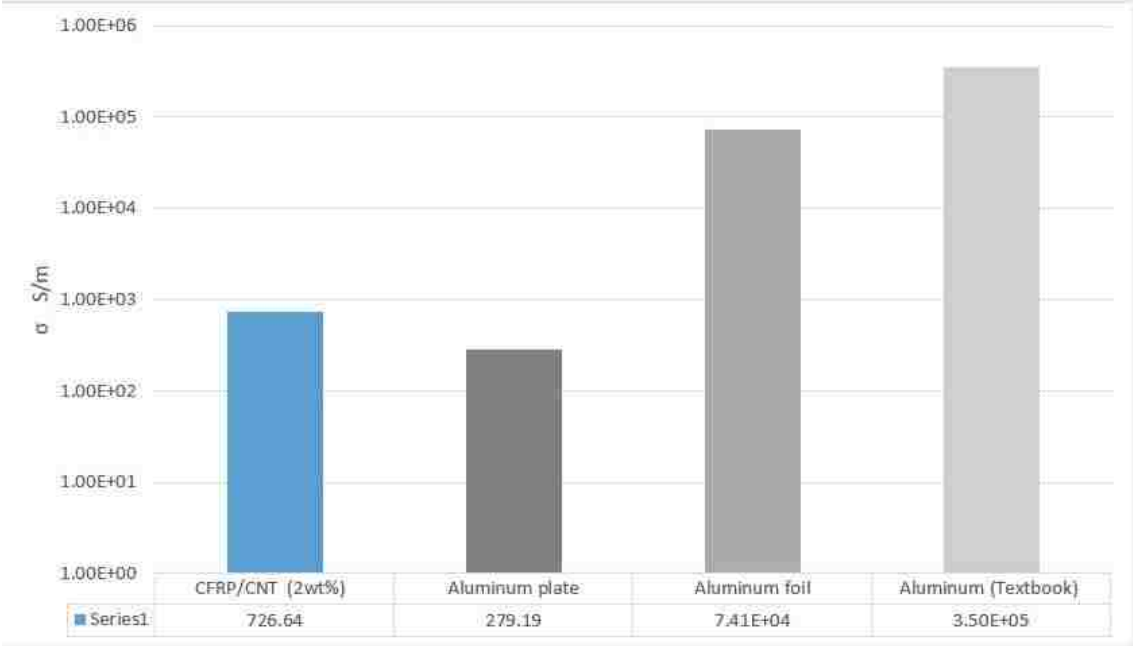

Figure 85. Conductivity of CFRP/CNT Compared to Aluminum

The thickness of the plates was arbitrarily chosen to be 3 mm (1/8th inch), although thinner plates would work just as well, limited only by the skin depth of the material at the lowest operational frequency. Figure 86 compares the skin depth of aluminum to the CFRP/CNT across the frequency range from 1 to 10 GHz.

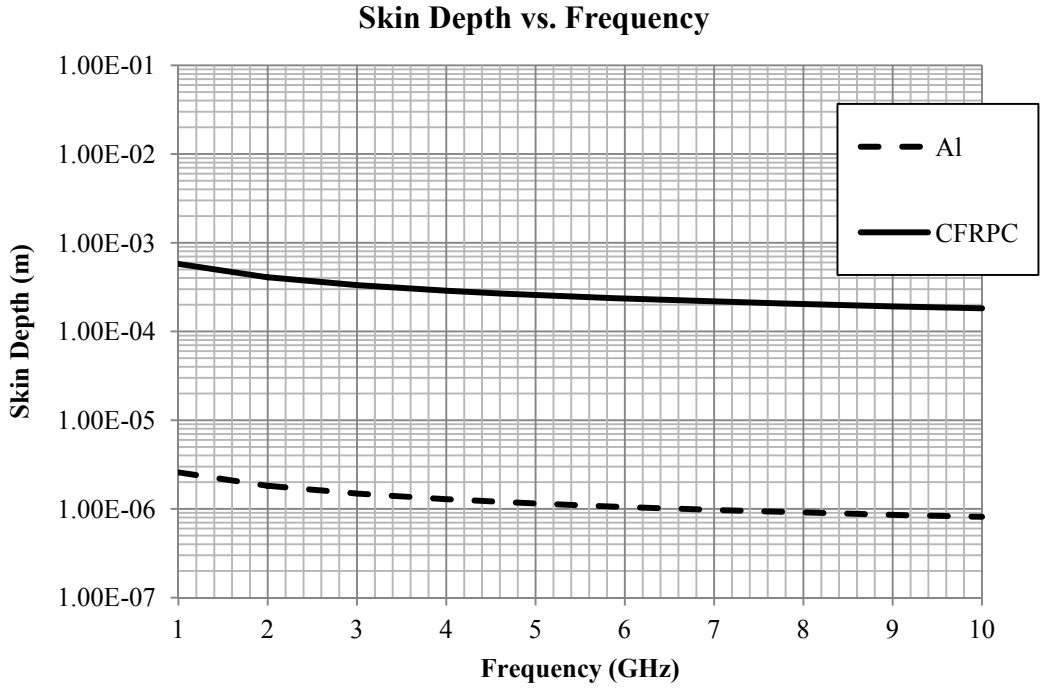

Figure 86. Skin depth of CFRPC and Aluminum

While the skin depth of the CFRPC is significantly higher than that of aluminum, it is still sufficiently small that plates having a thickness of a few mm at 1 GHz would be thick enough to work as lens elements.

Several simulations were run, each time changing the material properties to vary the conductivity of the material. Wave propagation from the horn antenna and through the lens to beyond the focal plane was simulated for infinite conductivity (corresponding to that of a PEC), with a conductivity of 726 S/m (corresponding to that of the UNM CFRP composite) , and with materials having conductivities of 10 and 100 S/m. The results are shown in Figure 87 and 88. Both of these are simulated boresight measurements.

comparing response of all 5 materials; however, Figure 88 focuses in on the focal region, with greater sensitivity for the vertical scale.

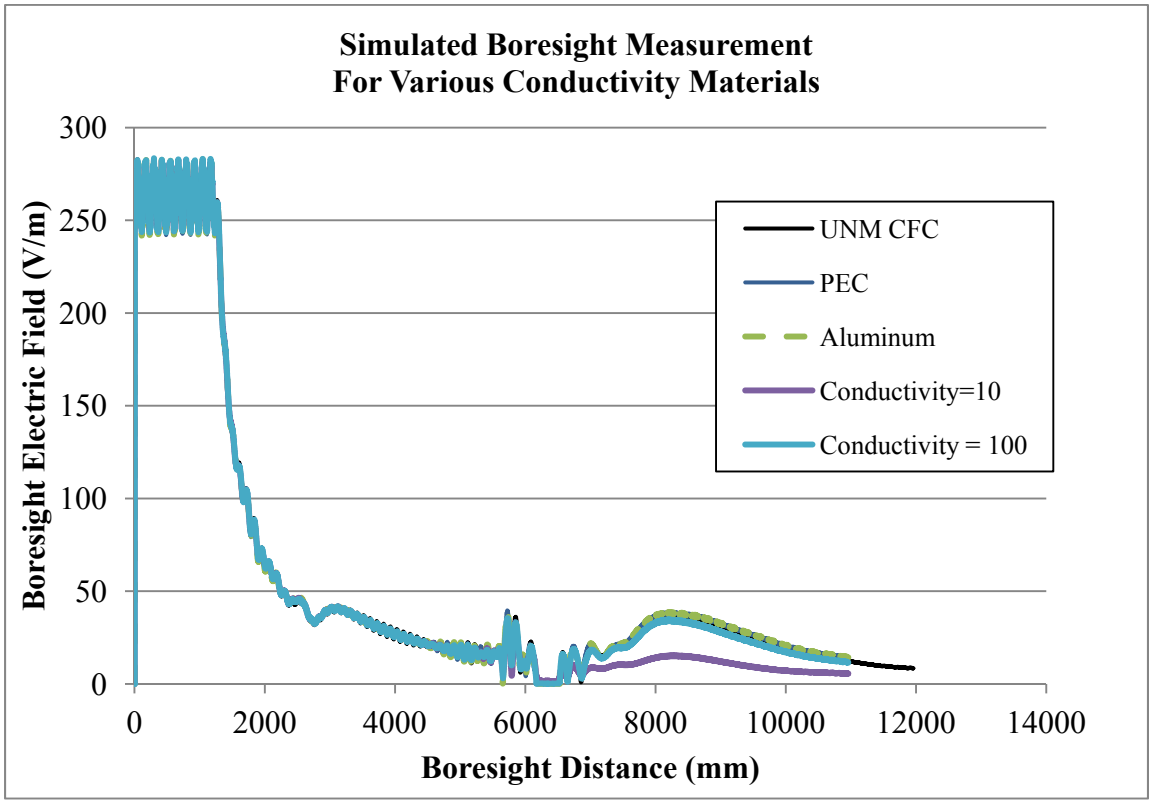

Figure 87. Simulated Boresight Measurements with Lens Plate Material of Varying Conductivity

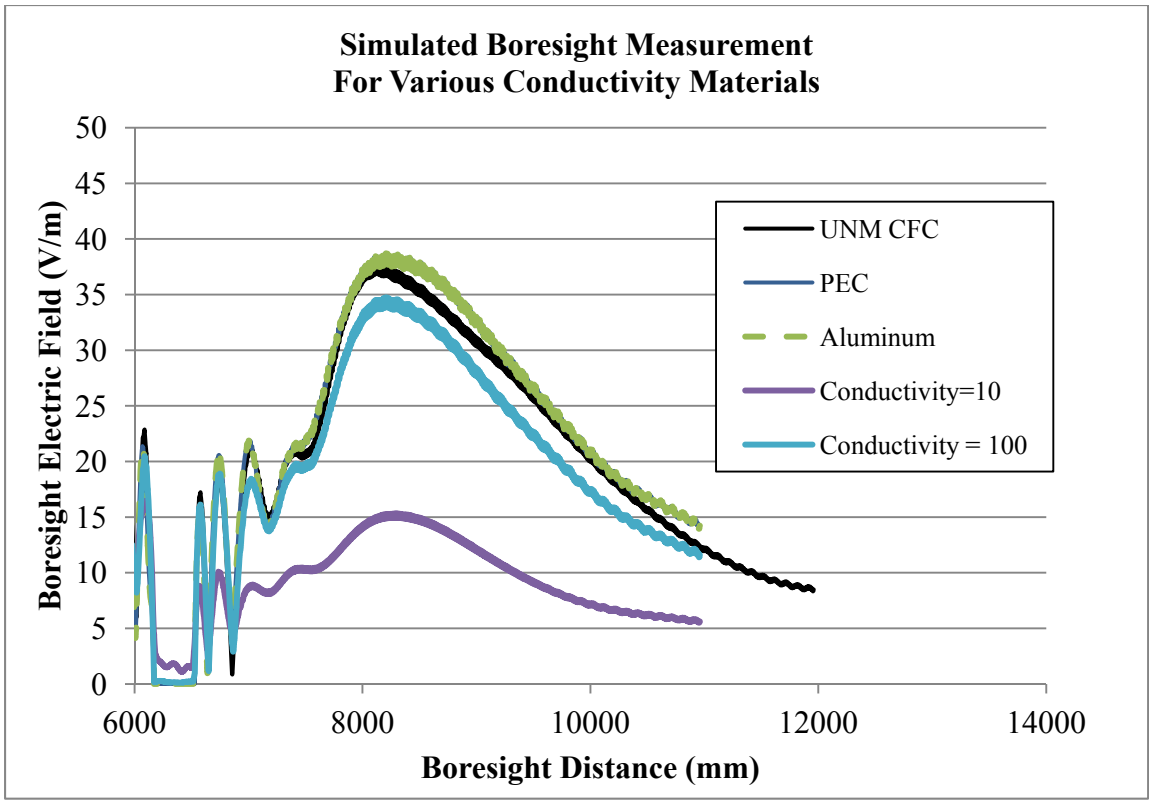

Figure 88. Simulated Boresight Measurement for Various Conductivities: Close Up of Focal Region.

The green curve, corresponding to the conductivity of Aluminum overlays the curve corresponding to PEC. The difference between the response of the lens with plates having a conductivity of 726 S/m (corresponding to the UNM CFRP compound) and that of Aluminum is not significant, in terms of peak fields or beam convergence in the focal plane, indicating that, the conductivity of the UNM CFRP composite is sufficiently high to ensure proper beam focus or collimation with this material. This material would reduce the weight of the lens by 25% or more and would have sufficient tensile strength and rigidity to replace aluminum for lens design.

The purple curve, corresponding to a conductivity of 10 S/m clearly indicates that this conductivity is too low, as the peak electric field in the focal plane is severely reduced. The blue curve, corresponding to a conductivity of 100S/m, indicates that this conductivity is almost acceptable; placing a lower bound on the conductivity for the conducting plates of about $\sigma = 200$S/m.

Simulated measurements of the x-directed electric field across the E- and H-planes is shown in Figures 89 and 90, respectively. The conductivity of the CFRP/CNT carbon fiber composite appears to have little effect on the lens' ability to focus in this plane.

While inclusion of CFRP composites in the design of the parallel plate waveguide lenses may add to the cost, the reduction in weight may be desirable. The density of the CFRP/CNT composite was approximately 25% less than the density of aluminum . Therefore the reduction in weight would be about 25%. However, since it was demonstrate d herein that lower conductivity would work well as lens plates, this weight could be reduced significantly.

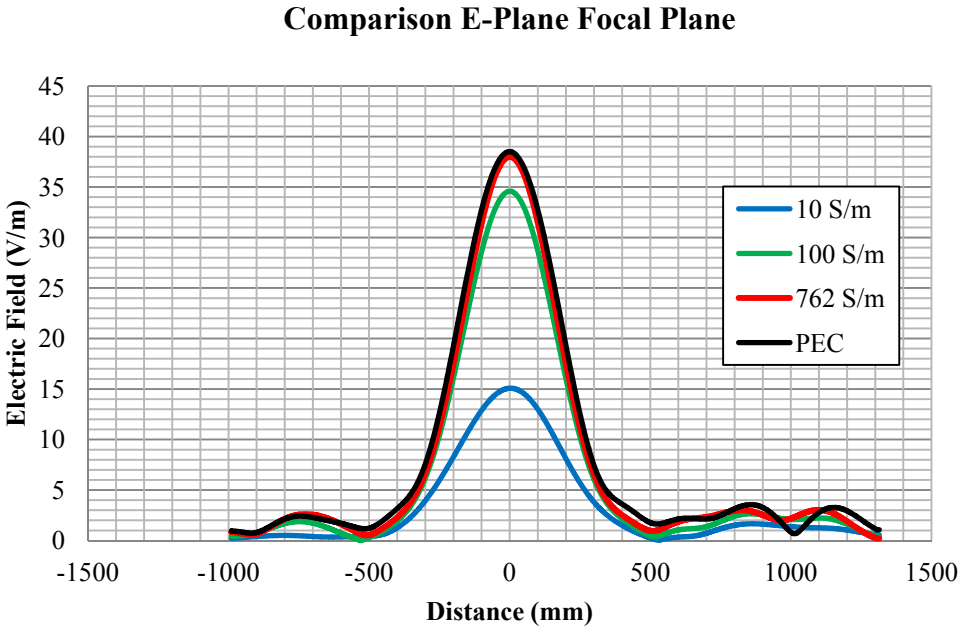

Figure 89. E-Plane Measurements Across Focal Plane

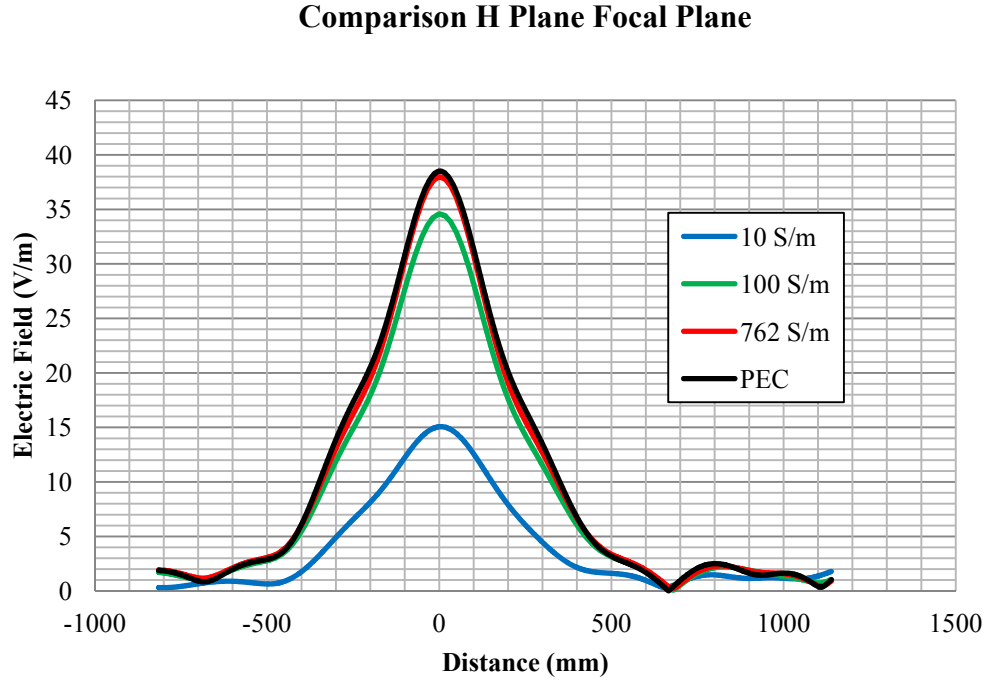

Figure 90. H-Plane Measurements Across Focal Plane

4.6 Analysis/Mitigation of Spurious Modes

Spurious modes could be induced in the parallel plate waveguide by the presence of harmonic frequencies, or by the presence of longitudinal or cross polarized fields which might exist in the near-field of the pyramidal feed horn antenna.

As mentioned previously, the plate spacing for the lens was chosen to be slightly larger than ½ λ at the center frequency, and such that the index of refraction is very close to n = 0.6. This ensures propagation in the TE10 mode, for which the cutoff frequency is

$$f_c(\mathrm{TE1}) = \frac{\mathrm{c}}{2\mathrm{a}} \qquad [14]$$

It is important to note that this is also the cutoff frequency for the TM1 mode. The next higher mode of propagation is TE2 (and TM2), which has a cutoff frequency of

$$f_c(\mathrm{TE2, TM2}) = \frac{\mathrm{c}}{\mathrm{a}} \qquad [15]$$

Or twice that of the fundamental mode.

As an example, for a 10GHz source, with bandwidth of 10% and for a plate spacing corresponding to n = 0.6, the cutoff frequency would be just under 7.9 GHz. The cutoff frequency for the next higher TE2 mode would be 15.8 GHz. Ideally there would be no

energy in the source above this frequency and the TE2 and all higher modes would be cut off. However, harmonics of the center frequency in a real source may be present. For the 10GHz source in this example, the first harmonic would occur at f = 30 GHz; which is well above the cutoff frequency for the TE2 mode. This could be a concern if the gain of the horn antenna at this frequency was significant.

The response of the 10GHz horn used in the simulations of Section 4.3 at frequencies near 30 GHz is shown in Figure 91.

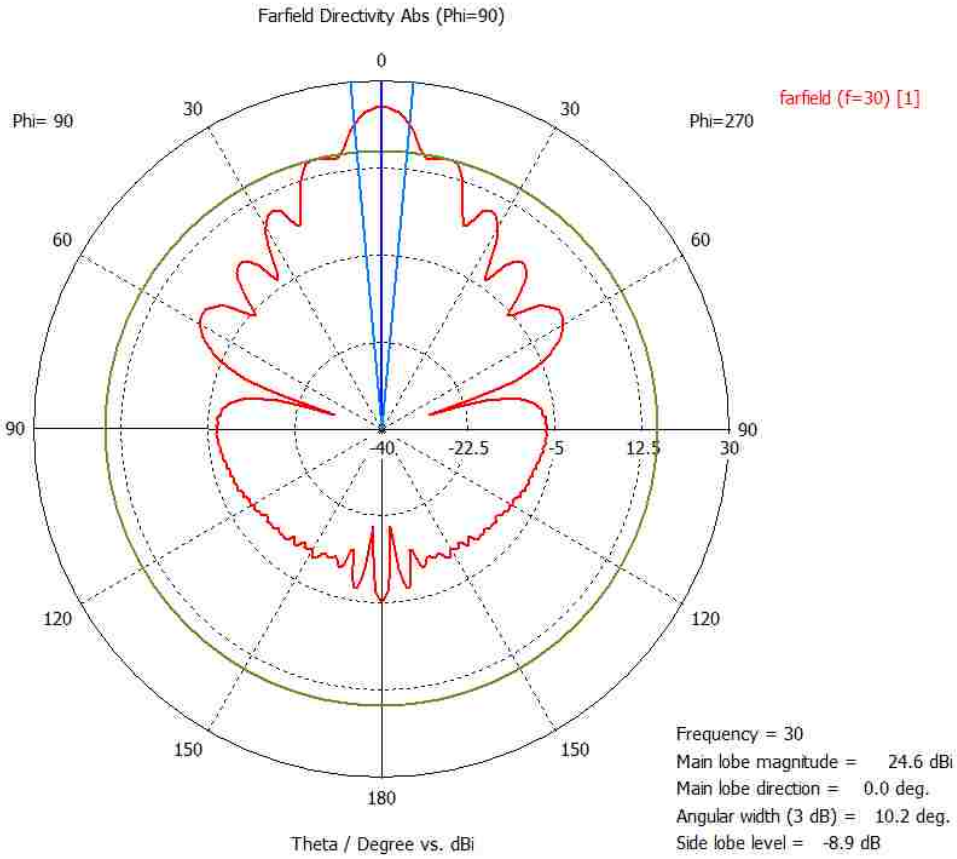

Figure 91. Gain of 10GHz Horn Antenna at 30GHz

This simulation indicates very high directivity along boresight with a half power beamwidth of 10.2°. The directivity is close to 10dB above the gain of the horn antenna at the fundamental frequency. Thus, if the high power source generates harmonics at sufficiently high levels, higher order modes could be excited in the lens and greatly interfere with focusing capability of the lens. To avoid this, the power associated with the first harmonic would need to be 30dB below that of the fundamental frequency; this would result in radiated power density at the first harmonic being 20dB down from the radiated power density at the fundamental frequency. Using a waveguide feed for the horn antenna would help to mitigate the presence of harmonics, as these harmonic frequencies are well above the cutoff frequency of the waveguide.

Another concern is that, in the near field of the horn, undesirable longitudinal and transverse electric fields (in the y- and z- directions in the simulations) could exist; exciting unwanted TM or TEM modes in the parallel plate waveguide structure of the lens.

The X-band horn used in the simulations, as described in Section 4.2.1, is shown in Figure 92 below, along with an electric field monitor placed in the near field of the horn about a wavelength away from the aperture.

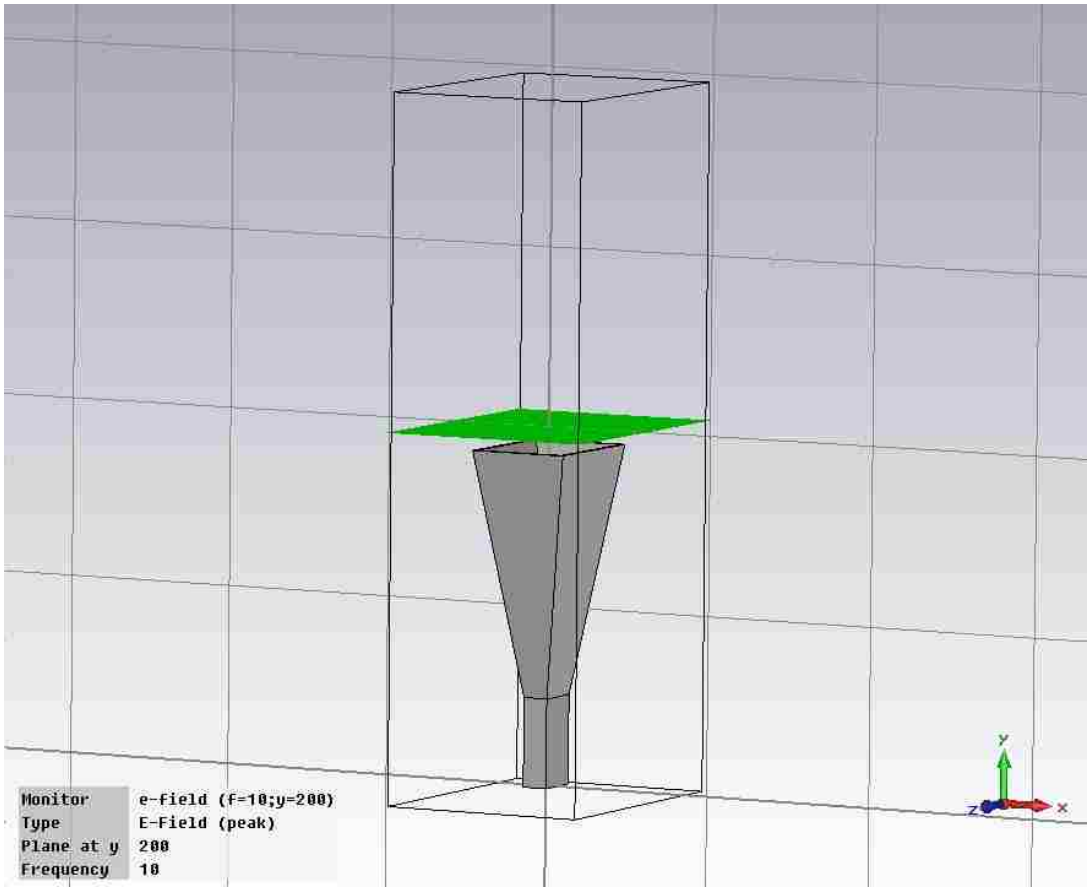

Figure 92. X-Band Horn with Field Monitor in the Near Field (y = 200mm)

Electric fields in the x-, y-, and z-directions were evaluated in the plane of this field monitor as well as in the E-plane (z = 0). The results are shown in Figures 93-96.

The magnitude of the x-directed E-field in the plane of the field monitor at y = 200mm is shown in Figure 93. It is relatively constant over a rectangular area in the x-z plane and has a magnitude of 457 V/m. This is the desirable component of the electric field and appears well behaved across the aperture of the horn.

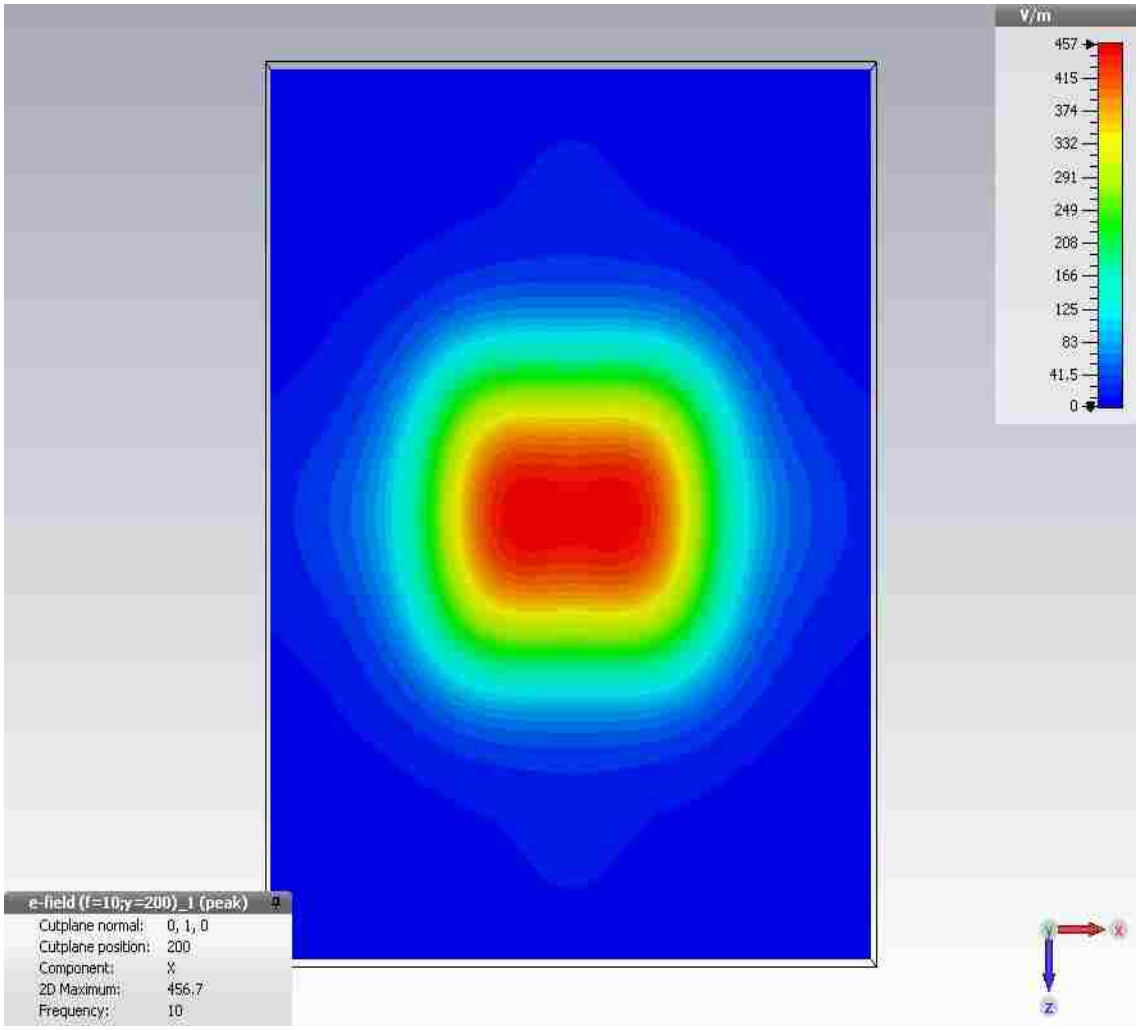

Figure 93. Near Field Electric Field (E_x)

The z-component of the electric field, which would tend to propagate through the lens in the TEM mode, is shown in the same plane at y = 200mm (about a wavelength from the horn aperture) in Figure 94. This component is on the order of a factor of 10 down from the peak x-directed E-fields and is not significant.

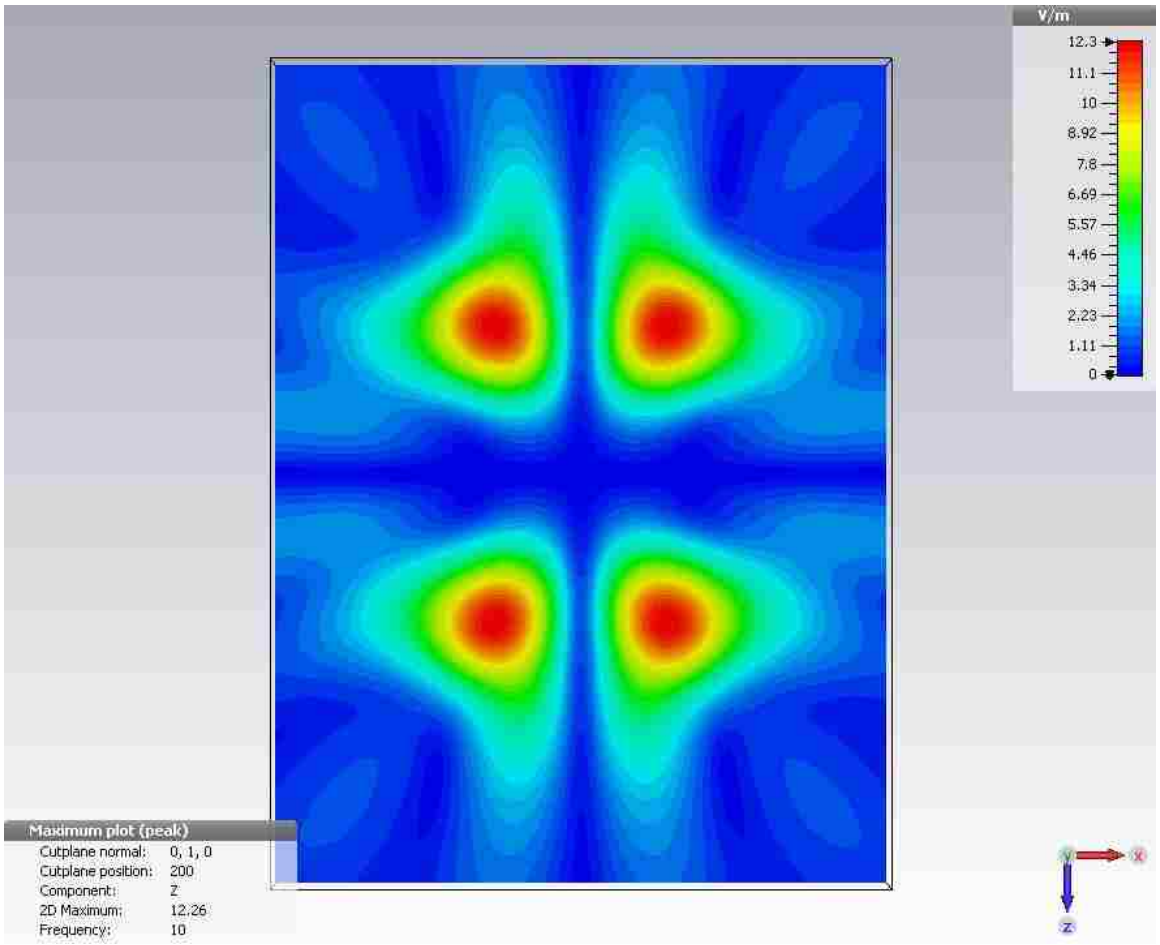

Figure 94. Transverse Electric Fields (Ez)

The y-component of the electric field in the plane of the monitor at y = 200 mm is shown in Figure 95. The peak field is split into two regions and has a peak magnitude of 155 V/m.

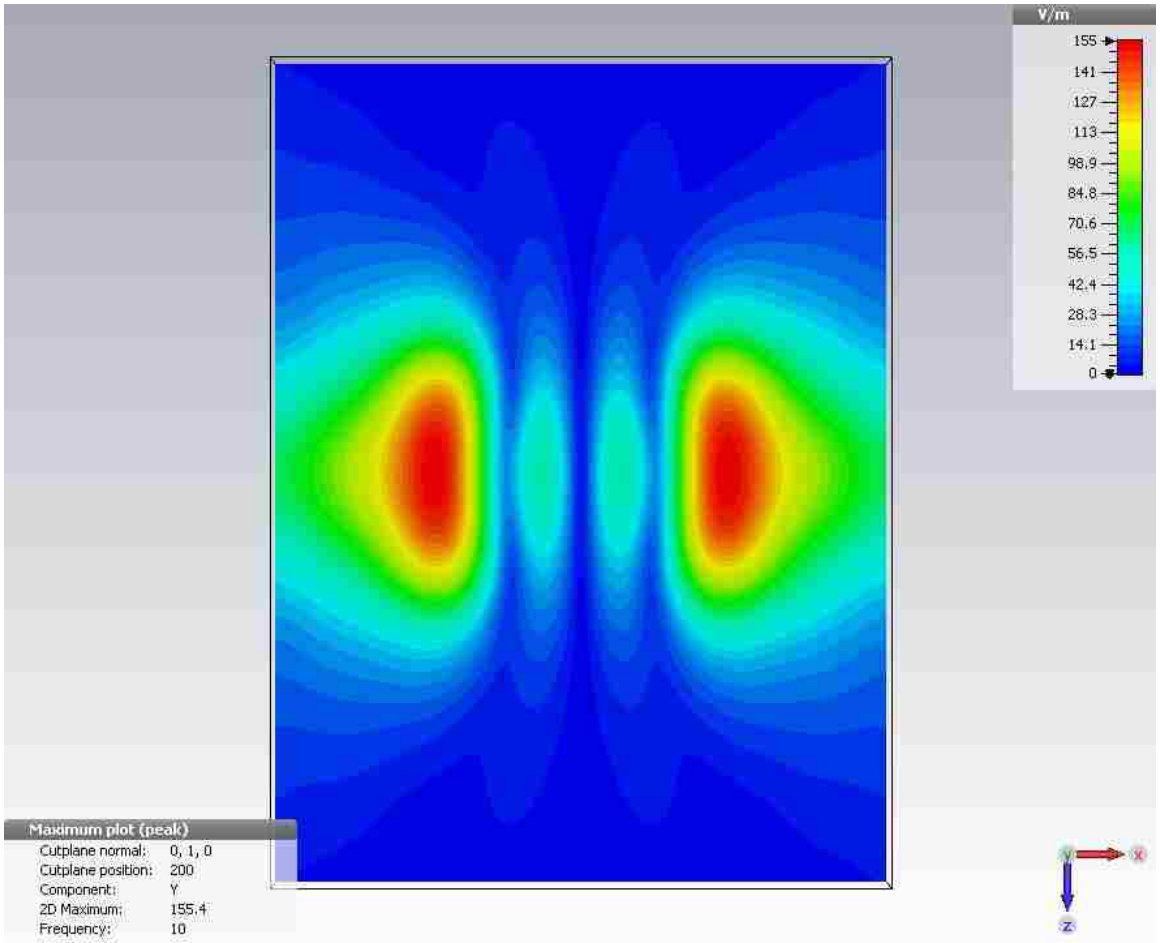

Figure 95. Longitudinal Electric Field (E_y)

In the plane of propagation x-y plane, these longitudinal electric field components diverge from the horn aperture, as can be seen in Figure 96.

This longitudinal component is significant; being only a factor of three down from the peak x-directed electric field at a distance of about a wavelength from the aperture of the horn. This has the potential to excite TM modes in the waveguide when the lens is very close to the horn aperture; the fundamental TM1 mode has the same cutoff frequency as the TE1 mode for parallel plate waveguide and hence the same propagation velocity.

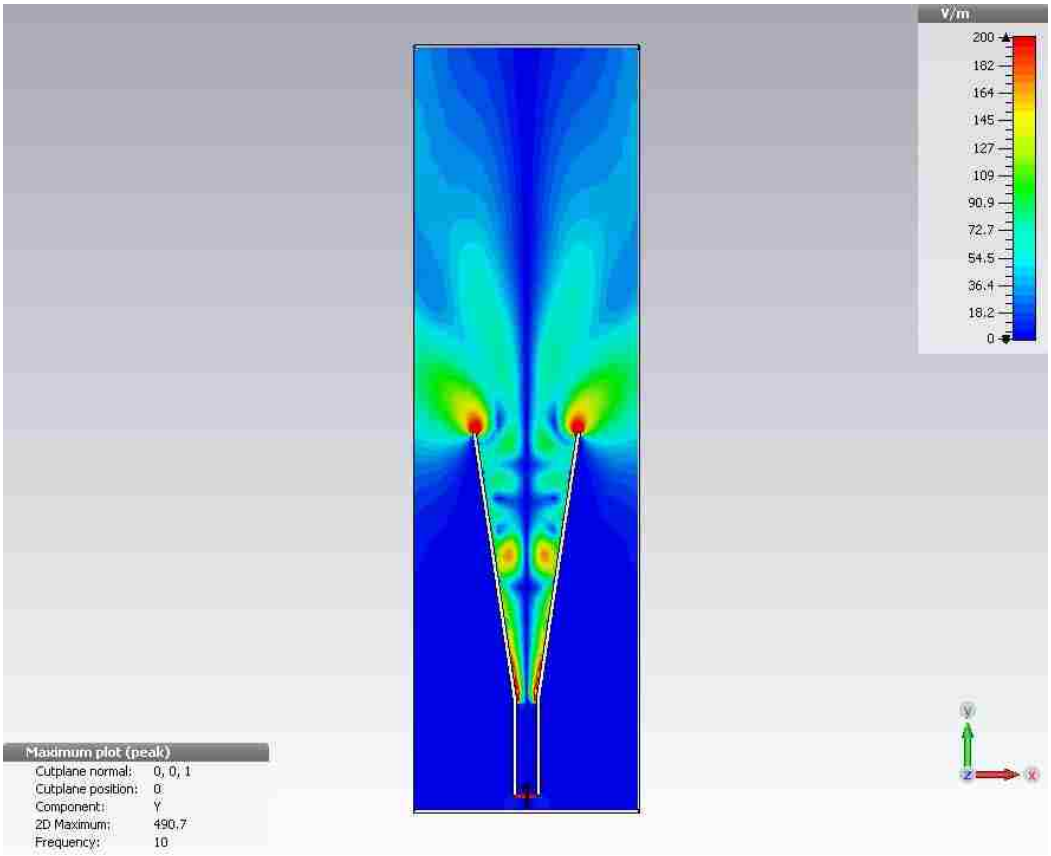

Figure 96. Longitudinal Fields Ey in the X-Y Plane

Note the high intensity electric fields observed at the edges of the horn antenna along the aperture in Figure 96. These are easily mitigated by attaching a rolled surface section to

the outside of the horn and will therefore not be discussed further here; except to say that the shape is not critical but that its radius of curvature should be larger than λ/4 [Ref. 25].

The y-directed electric fields would propagate on the outer portion of the lens and could affect the beam pattern in the focal plane of the lens. However, these fields diverge and fall rapidly as one moves away from the horn aperture. Mitigation of potential spurious modes caused by longitudinal fields in the near field of the horn is readily accomplished by designing the first lens with sufficiently long focal length so that it never has to be close enough to the horn aperture for these fields to be significant.

Additionally, some finite resistivity to the plates may also help to mitigate spurious modes induced by longitudinal fields in the near field of the horn antenna. The attenuation due to conductor loss for the TEM, TE1 and TM1 modes is presented in [Ref. 26].

According to [Ref. 26], conductor loss for the TM1 mode is significantly higher than that for the TE1 mode in parallel plate waveguide.

To quantify this effect for the 10GHz lens 1 described in Section 4.2.2, with a plate spacing of a = 19.05mm, and a frequency of 10GHz, the wave number k = 201m^{-1}. Thus, ka/π = 1.27. Referring to the curves for attenuation loss for the TE1 and TM1 modes in [Ref. 26], it is seen that

$$\alpha_c = 1.25 \frac{R_s}{\eta d} \qquad [16]$$

for the TE1 mode and

$$\alpha_c = 3\frac{R_s}{\eta d} \qquad [17]$$

for the TM1, mode, where d is the plate spacing (denoted by "a" in this document).

Table 8 below lists the attenuation due to conductor loss for the TE1 mode and TM1 mode for conductivities at 10GHz of Aluminum and for the UNM CFRP/CNT with a conductivity of 726 S/m.

material	**σ(S/m)**	**δ (m)**	**R_s(Ω)**	**α_c (Np/m) (TE1)**	**α_c (Np/m) (TM1)**
Aluminum	$2.5\text{x}10^{7}$	$1.0\text{x}10^{-6}$	0.0397	0.007	0.017
UNM CFC	$7.6\text{x}10^{2}$	$1.8\text{x}10^{-4}$	7.20	1.26	3.02

Table 8. Attenuation Due to Conductor Loss for Al and CFC

The attenuation due to conductor loss for Aluminum for either the TE1 or TM1 mode is insignificant; however it becomes significant for the conductivity of the CFRP composite. For the TE1 mode, it is clear that the attenuation due to conductivity for the CFRP/CNT composite material is not sufficient to affect the focusing properties of the lens (as is

evident in Figures 87-90). However, the higher attenuation would help to mitigate propagation of TM modes in the waveguide.

The width of the large L-Band lens near the outer edge of the lens is close to 1.2 m. The attenuation due to conductivity for the TM1 mode across this path length for aluminum would be $\alpha c = .02$ Np, or about -16dB which is negligible. For the carbon fiber compound, it would be $\alpha c = 3.63$ Np or about 6dB; which reduces the power available for radiation from the TM1 propagating mode by a factor of 4.

The conclusion is that carbon fiber reinforced polymer composites may be the material of choice over a metal for larger, lower frequency lenses because of their lower density and higher resistivity to the TM1 mode, as long as the plates are thicker than the skin depth .

4.7 Phase Error Analysis

The beam radiated from a simple horn antenna will have a spherical shape to the wave front with origin at the phase center of the horn, as shown in Figure 97. Phase error is introduced by the difference in the location of the phase center in the E- and H- planes and by the difference between the shape of the wave front and the lens, as indicated in Figure 97, which induces a path length error.

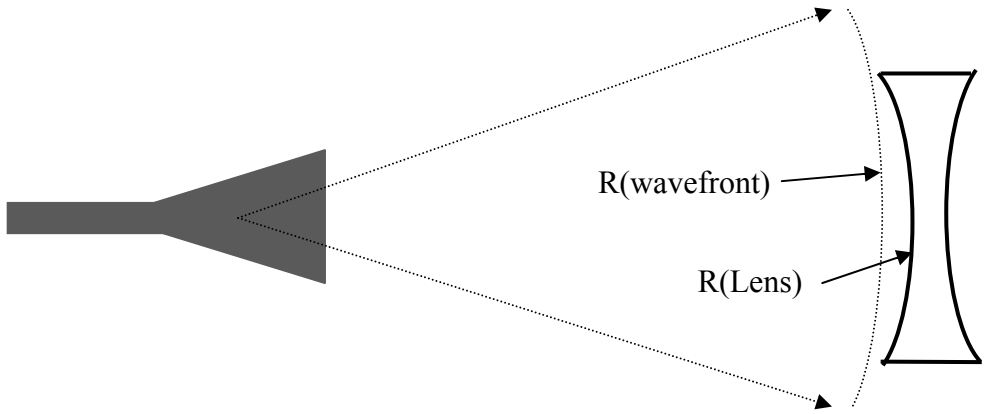

Figure 97. Illustration of Mismatch Between Radius of Curvature of Lens and Incident Phase-Front

For a moderate gain horn (on the order of 16dBi), suitable for the zoom antenna system described herein, the half power beamwidth is approximately 30°. For a lens designed

with a relatively small focal length, the greatest phase error would be introduced in the system at its farthest distance (S1) from the horn. At the nearest distance, the radius of curvature of the phase front is very close to that of the lens. Therefore, maximum phase error would be introduced with lens 1 at its farthest location from the horn (maximum S1).

Figure 98 shows the difference (in wavelengths) between the radius of curvature of the incident phase front and the radius of curvature of the lens used in the simulations in Section 4.2.2 with the lens at its farthest displacement from the horn (i.e., at y = 800mm). This difference is maximum at 15° (corresponding to the edge of the cone defined by the half power beamwidth of the horn; however, it is ½ λ at its maximum.

The fact that this phase error is not significant is evidenced in the x-directed electric field pattern across the focal plane in both the E- and H- planes.

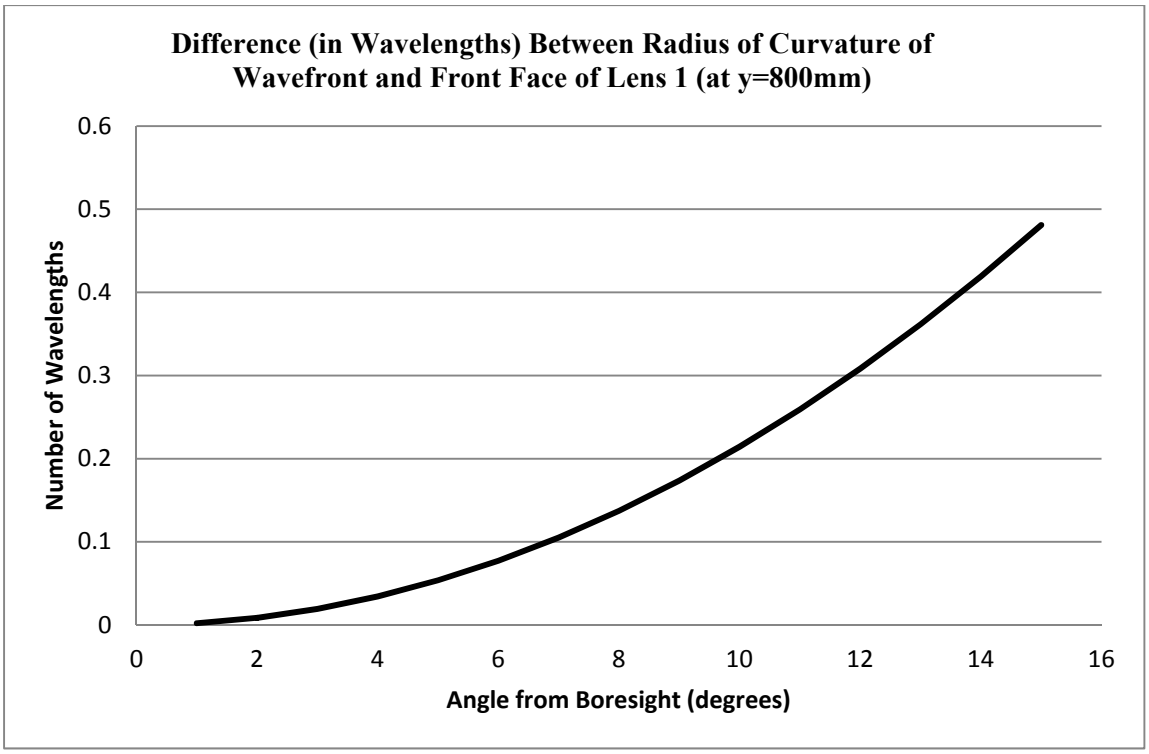

Figure 98. Difference Between Phase Front and Curvature of Lens 1

While this is significant, re-shaping of the lens to better fit the phase front at this location would introduce even greater path length difference and therefore phase error when the lens is placed closest to the horn antenna for the narrowest diameter of collimated beam at the output of the zoom antenna. It is concluded therefore, for this reason (as well as to minimize cost and complexity of fabrication) , that spherical lenses are optimal for the zoom antenna.

Furthermore, simulated results confirm that this is a valid conclusion. The simulated phase across the focal plane in the E- and H- planes with lens 1 at its maximum displacement from the horn at y = 800 mm for the 10GHz system simulated in Section

4.2, is shown in Figures 99 and 100, respectively. The phase is constant across the half power beam width of the Airy disc.

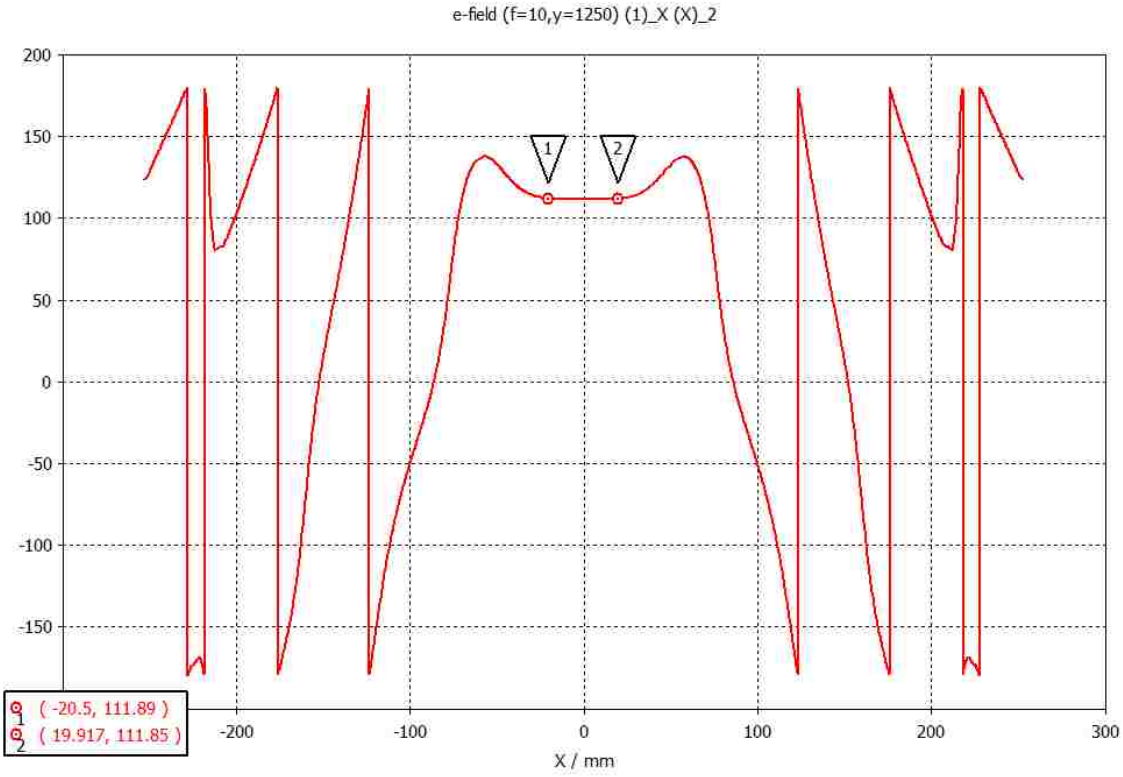

Figure 99. Phase Across E-Plane in the Focal Plane

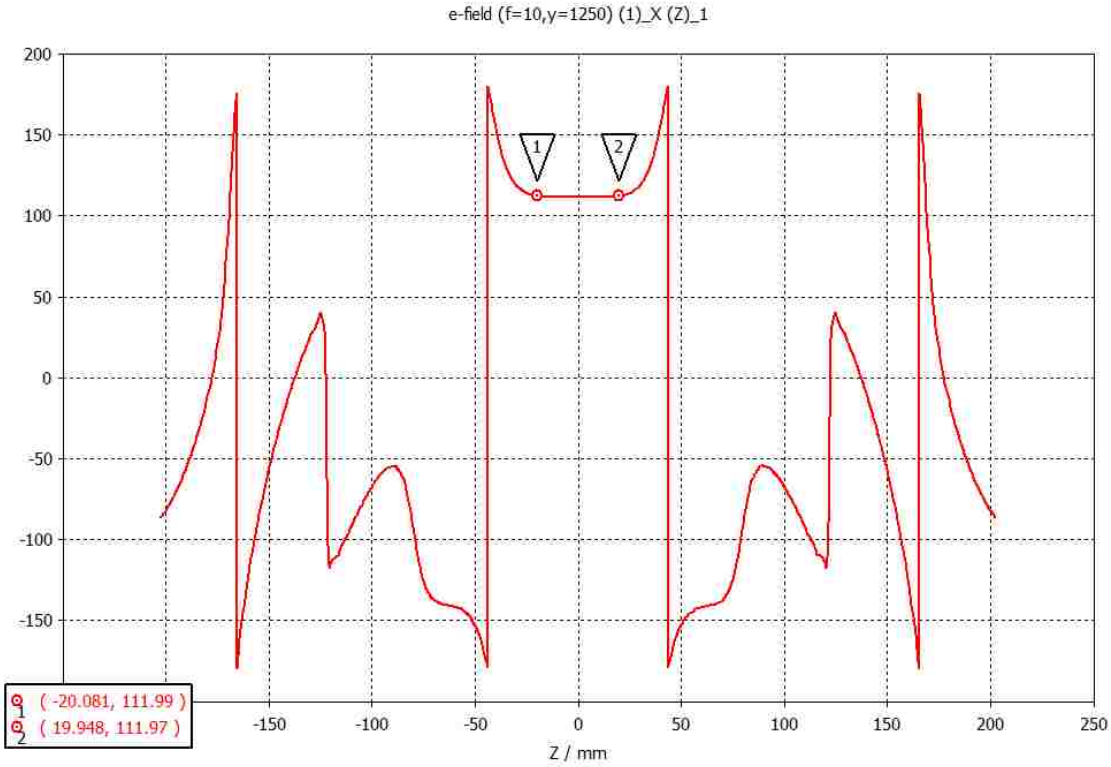

Figure 100. Phase Across H-Plane in the Focal Plane

4.8 Reflection at Air-Lens Interface

Reflection at the air-lens interface is a result of two factors: backscatter from the metal plates and the mode mismatch at the interface between the incident TEM wave with index of refraction n = 1 and the TE1 mode in the waveguide array with index of refraction n ≈ 0.6. Both the backscatter from the plates and reflection at the interface due to mode mismatch tend to focus the reflected energy to a point corresponding to the center of the sphere that defines the radius of curvature of the lens. As the lens nears the aperture of the horn, interaction with this reflected energy affects the focal length of the lens, as was observed in the simulations of Section 4.2.2.

In the realm of optics, one would mitigate the reflection due to mismatch in indices of refraction by coating the face of the lens with a material having an index of refraction given by

$$n' = \sqrt{n1 * n2} \qquad [18]$$

In this case, however, one would need a coating with an index of refraction of n' = 0.8 and such a material does not exist.

To minimize reflection due to mode mismatch, it is necessary to maximize plate spacing for maximum index of refraction at a given frequency. Doing so also minimizes backscatter from the metal plates as it reduces the number of plates for a given lens

diameter. However, the bandwidth of the system places limits on how high the index of refraction can be, as discussed in the following section.

4.9 Bandwidth

The bandwidth of the system is determined by the fact that the index of refraction of the lens is dependent on the frequency, as indicated by Equation 5; referred to in optics as "chromatic aberration". The variation in index of refraction over a range of frequencies for a lens designed to operate at 10GHz is shown in Figure 101.

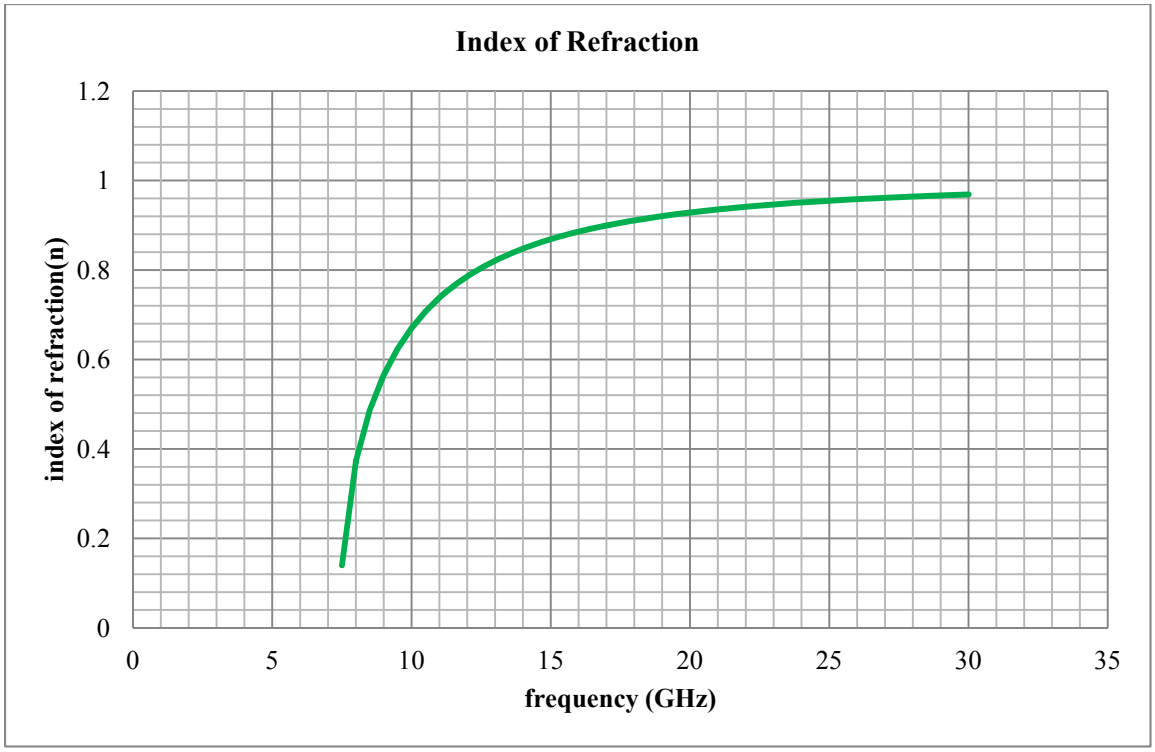

Figure 101. Variation in Index of Refraction with Frequency

At the high end of this frequency range, the index of refraction approaches 1 and this lens becomes transparent to the incident TEM wave. As the frequency decreases below 10 GHz, the index of refraction approaches n = 0 and the lens becomes opaque.

As stated in the previous section, backscatter and reflection at the air lens interface are minimized by maximizing the index of refraction. In order to maximize the bandwidth of the system, one must not design the lens with an index of refraction so close to unity at the center frequency that the lens that the lens becomes transparent to energy at the high end of the bandwidth of the system. For maximum bandwidth and minimum reflection, the optimal index of refraction (at the center frequency of the system) should be close to 0.6.

4.10 Magnification Range/ Zoom Ratio

The magnification of the zoom antenna at any given position of the lenses is determined by the ratio of the radius of the collimated beam at the output to the radius of the beam intercepted by lens 1. Figure 102 is a reproduction of an earlier figure, for ease of reference.

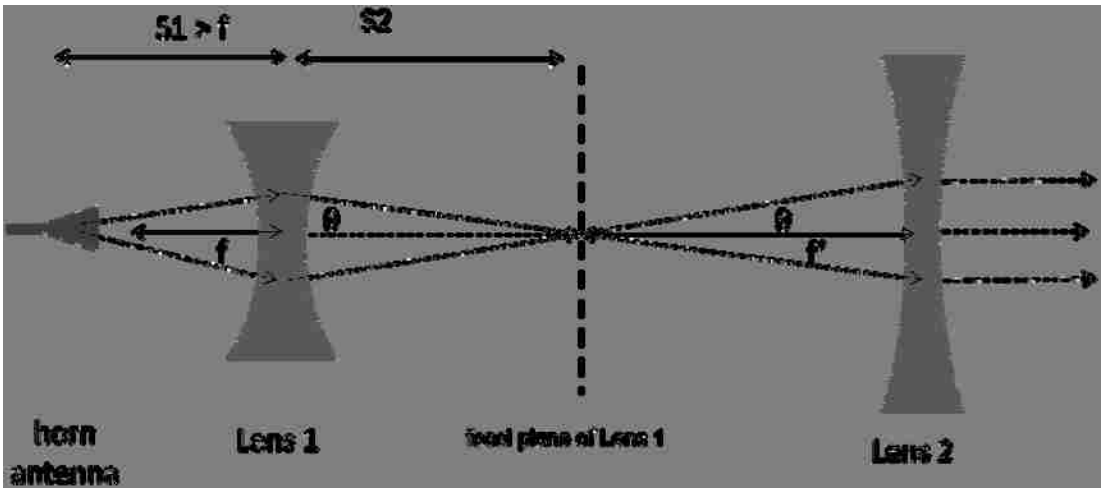

Figure 102. Zoom Antenna Concept

For a horn antenna with a half power beam width of 30 degrees, the radius of the beam intercepted by lens 1(denoted by y1 in Equation 18) at a distance of S1 from the phase center of the transmit horn antenna is given by

$$y1 = \mathrm{S1}\tan\left(15°\right) \qquad [18]$$

The angle of convergence, θ, of the beam towards the focal plane of lens 1 is equal to the angle of divergence from the focal plane of lens 1 towards lens 2 and is given by

$$\theta = \tan^{-1}(\frac{\mathrm{y1}}{\mathrm{S2}}) \quad [19]$$

Finally, the diameter of the collimated beam (denoted by y2 in Equation X0 at the output is equal to

$$y2 = \mathrm{f}'\tan(\theta) \quad [20]$$

or

$$y2 = \mathrm{f}'\frac{\mathrm{y1}}{\mathrm{S2}} \quad [21]$$

Combining [20] with [21] yields

$$M = \frac{y2}{y1} = \frac{\mathrm{f}'}{\mathrm{S2}} \quad [22]$$

Perhaps the best way to determine lens parameters for a given zoom application and explore possible range of magnification is with an Excel spreadsheet. An example of parameters explored in designing the 10GHz zoom antenna described in Section 4.3, is

shown in Table 9. Values in green are input by the user and can be varied to explore the resulting effect throughout the system. Cells corresponding to black numerical values contain appropriate formulas (e.g., lensmaker's equation, lens equation, calculation of beam diameter at the location of the lens). Thin lens approximations are useful for this phase of the design process.

To obtain a relatively small focal length for 1ens1, the most appropriate shape is a biconcave lens, with R1=R2. Therefore, the formula input to the cell corresponding to the value of R2 is simply –R1. Choose n=0.6 (optimum index of refraction for parallel plate waveguide lenses). Include formulas for the focal lengths in the appropriate cells according to Equation 7. Include formulas for calculating S2 from Equation 8 in the appropriate cells and explore what happens with the system for minimum and maximum S1. The diameter of the beam at the location of lens 1 is determined from Equation 18; however the angle must be converted from degrees to radians.

Note that the minimum beam diameter of collimated beam at the output can never be less than about 1.5λ due to diffraction limits. Note also that the diameter of lens 2 can never exceed 2*R1. These values are shown in red in this spreadsheet.

Finally, the range of magnification (or "zoom ratio") at the bottom of the spreadsheet is determined by the ratio of the beam diameter at the location of Lens2 for S1(min) and S1(max).

	A	B	C	D	E	F	G	H	I
1	Lens 1			Lens 2					
2									
3	R1	-203.20	mm	R1'	-558.80	mm			
4	R2	203.20	mm	R2'	1.00E+07	mm			
5	n	0.60		n'	0.60				
6	f	254.00	mm	f'	1396.92	mm			
7									
8									
9									
10	S1(min)	279.40		Location of Lens2 for collimation	4.47	meters			
11	S2(max)	2794.00							
12									
13				Beam Diameter (location of Lens1)	149.65	mm			
14				Beam Diameter (location of Lens2)	74.82	mm	1.5λ	0.045	mm
15				magnification	0.50				
16									
17									
18	S1(max)	673.10		Location of Lens2 for collimation	2.48	meters			
19	S2(min)	407.94							
20									
21				Beam Diameter (location of Lens1)	360.52	mm	2*R1	406.4	mm
22				Beam Diameter (location of Lens2)	1234.55	mm			
23				magnification	3.42				
24									
25				Range of Magnification	6.85				

Table 9. Excel Spreadsheet Created to Design 10GHz Zoom Antenna

The location of lens2 to achieve collimation can also be an important factor. For a system to be tested inside, dimensions of the test facility must be taken into account. For an outdoor system, it would be difficult to implement a system with lens2 at very large distances from the phase center of the transmit horn antenna (on the order of 20 meters).

Figure 103 below illustrates the effect on the magnification of the system as the ratio S1/f1 is increased, for increasing values of f2 (expressed as a multiple of f1).

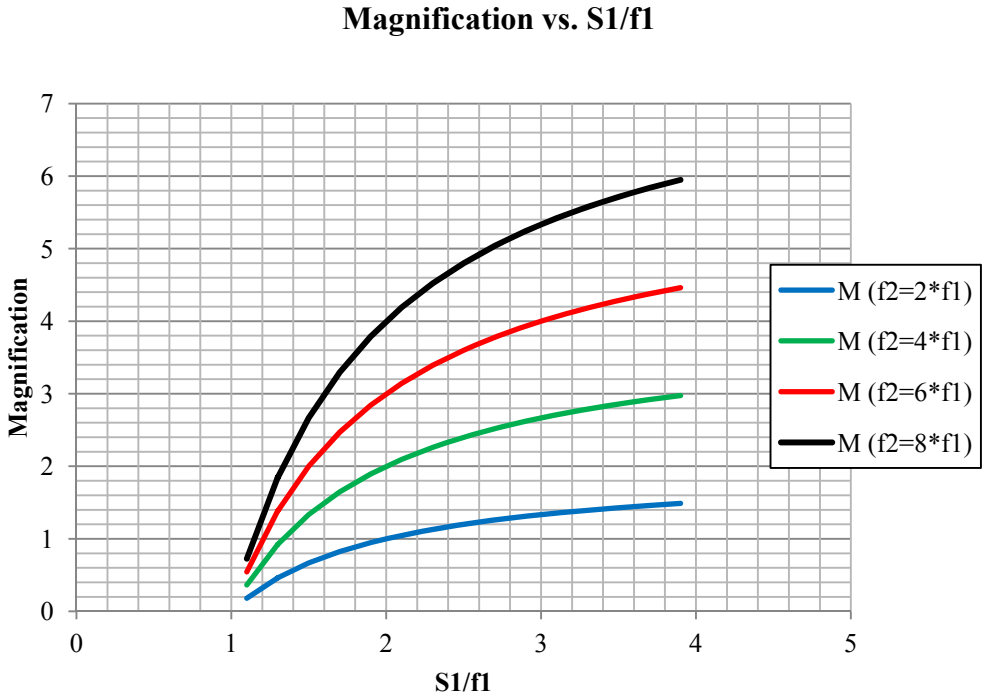

Figure 103. Magnification for Varying S1/f1 and f2/f1

The diameter of lens 1 must always be less than or equal to twice the radius of curvature of the lens. From the thin lens approximation to the lens given in Equation 7, the focal length of a biconcave lens with R1 = R2 and n = 0.6, is f1 = R1/0.8. The beam diameter at a distance S1 from the phase center of the horn is always D = 2*S1*tan 15°. This constraint places an upper bound on S1/f 1of approximately 4. The maximum magnification M is limited only by size constraints; the larger the focal length of f2, the larger lens 2 has to be and the farther it must be from lens 1 at maximum S1 to collimate the beam. The minimum magnification can be less than 1 and is limited only by the diffraction limited Airy disc diameter. It is important to note here that this minimum

magnification cannot be achieved through the use of reflector antennas. The maximum zoom ratio for a realistic system is therefore on the order of 10:1.

4.11 Maximum Power Handling Capability

The power handling capability of the system is limited, for pulsed operation, by the dielectric strength of air, or 3 x 10^3 kV/m. High electric fields exist within the focal region created by lens 1and are a maximum at the center of the this focal plane.

If all of the source power (P_s) were to be concentrated over the area of the Airy disc created by lens 1, the average power density in this disc, $S_{ave,}$ assuming 70% efficiency of the lens, would be:

$$S_{ave} = \frac{0.7P_s}{A} \quad [20]$$

where A is the area of the Airy disc. The diameter of this disc was demonstrated through experiment and simulation spanning 1-10GHz to have a diameter of close to 1.5λ, so that the area of this disc is.

$$A = 4\pi(.75\lambda)^2 \quad [21]$$

Since the diameter of this disc is defined as the half power beamwidth, , the peak power density in the center of the disc, S_p would be twice the average power density, or $S_p = 2S$.

The peak electric field in air (having an impedance of 377 Ω), is then determined from

$$E = \sqrt{377S_p} \quad [22]$$

Or

$$E = \sqrt{377(2S)} \quad [23]$$

So that the peak electric field in the center of the disc is

$$E = \sqrt{377\frac{0.7 * 2 * \mathrm{P}_s}{4\pi(.75\lambda)^2}} \quad [24]$$

where the factor of 0.7 is included to account for the efficiency of the lens. Therefore, the source power required to cause air breakdown in the center of the disc is determined from

$$P_s = \frac{\mathrm{E}^2(4\pi(.75\lambda)^2)}{(377)(1.4)} \quad [25]$$

This curve is shown in Figure 104.

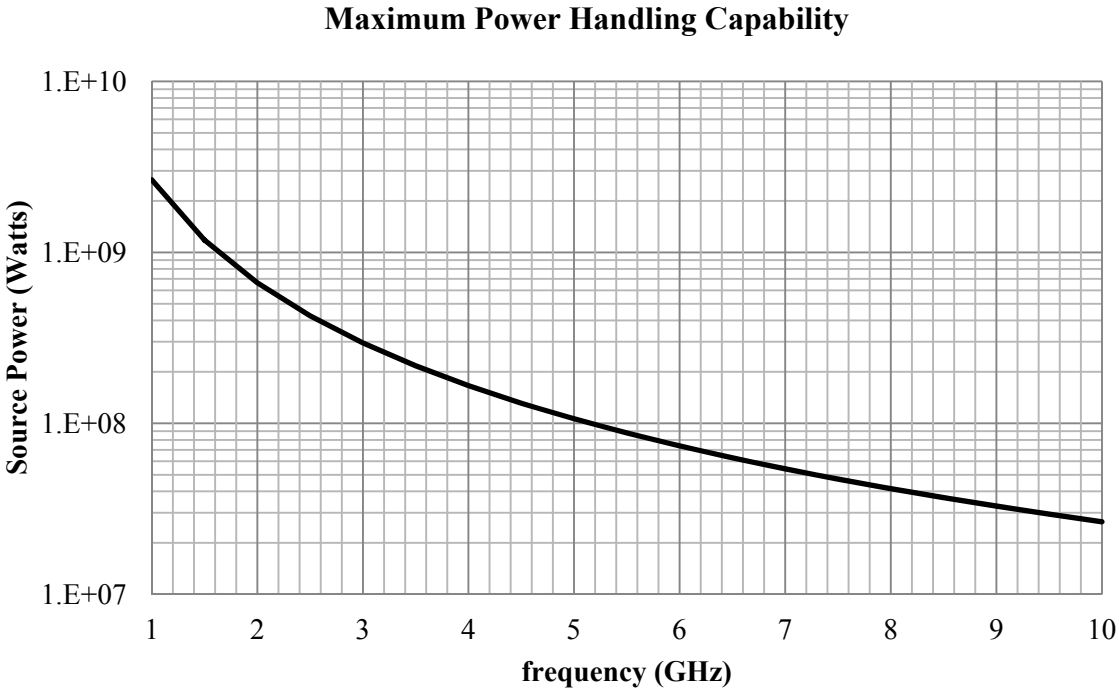

Figure 104. Source Power Requred to Induce Air Breakdown in the Focal Region

5. SUMMARY AND CONCLUSIONS

A high power microwave zoom antenna comprising a moderate gain feed horn antenna and two parallel plate waveguide antennas has been successfully designed and demonstrated through experiment and simulation. This is a novel concept; there is nothing else in existence that can provide this capability for high power microwave applications. The antenna radiates a collimated beam of linearly polarized electromagnetic waves with continuously variable diameter with an achievable zoom ratio of 10:1.

This zoom antenna works with any HPM source with as much as 10% bandwidth that can produce a TE10 mode into a waveguide output.

The parallel plate waveguide lenses have relatively high tolerance to warping and twisting and are sufficiently lightweight to employ in a fieldable system. Simple spherical lenses were demonstrated to work well in this application, resulting in low complexity and therefore low cost in design. For minimal cost, aluminum is a preferable material for the lens, with dielectric rods and spacers to provide the support structure. Sixteenth inch aluminum plates are sufficiently rigid with this construction to employ in even very large lenses.

If overall weight is a more important consideration than cost, the plates can be constructed of special carbon fiber reinforced polymer composites, which could reduce the weight by at least 25% and conceivably by as much as a factor of 5, depending on the material. In fact, the lower conductivity of the carbon fiber compounds would aid in

mitigating spurious modes that may be significant for very close spacing between the feed horn aperture and the first lens in the overall system.

6. REFERENCES

[1] Lu, Howard Ho Shu.; Variable Beamwidth and Zoom Contour Beam Antenna Systems, U.S. Patent 6,414,646, July 2, 2002.

[2] Schmidt, Richard F., Variable Beamwidth Antenna, U.S. Patent 3938162, February 10, 1976

[3] DeSize, Lorne K.; McInnes, Peter A.; Skahill, George E.; "Reflector Antenna Zoom Techniques", Airborn Instruments Lab Deer Park, NY, Feb 1967

[4] W. E. Koch, "Metal-Lens Antennas," Proceedings of the I.R.E. (34) 1 , pp. 828–836, November 1946

[5] ESA Telecomunications and Integrated Applications, "Waveguide Lens Antennas": http://telecom.esa.int/telecom/www/object/index.cfm?fobjectid=10028, May 2009

[6] Krauss, John D., "Antennas", 2nd Ed., McGraw Hill, New York, pp. 661-683

[7] Silver, Samuel, MIT Radiation Laboratory Seres, "Microwave Antenna Theory and Design" Volume 12, Ch. 11, pp. 389-412

[8] C.J. Sletten, Reflector and Lens Antennas; Analysis and Design Using Personal Computers, 1st ed., MA: Artech House, 1988, pp. 262-272

[9] Blake, Lamont V., and Long, Maurice W., Antennas: Fundamentals, Design, Measurement, 3rd Edition, SciTech Publishing, Inc. Raleigh North Carolina 2009, pp. 264-266

[10] Krauss, John D., "Antennas for All Applications", 3rd Ed., McGraw Hill, New York, pp. 626

[11] P. Wade, N1BWT, and M. Reilly, KB1VC, "Metal Lens Antennas for 10 GHz," Proceedings of the 18th Eastern VHF/UHF Conference, ARRL, May 1992, pp. 71-78.

[12] Bentley, Julie and Olson, Craig, "Field Guide to Lens Design", SPIE Press, WA 2012, p. 48

[13] Teichman, M, "Determination of Horn Antenna Phase Centers by Edge Diffraction Theory", IEEE Transactions on Aerospace and Electronic Systems, Nov 1973, Vol AES-9, Issue 6, pp. 875-882

[14] Walther, A., "The Ray and Wave Theory of Lenses", Caimbridge Studies in Modern Optics, Caimbridge University Press, UK, 1995, p. 310

[15] Bojovschi A, Shariati N. and Ghorbani K., "Analysis of a Carbon Fibre Reinforced Polymer Slotted Waveguide Array Fed By a Loop Type End Launcher", Microwave Conference Proceedings (APMC), 2013 Asia-Pacific, pp. 476-478

[16] Seidel, T.J., Galehdar A., Rowe W.S.T., John S., Callus P.J. and Ghorband K., "The Anisotropic Conductivity Unidirectional Carbon Fibre Reinforced Polymer Laminates and Its Effect on Microstrip Antennas", Proceedings of Asia-Pacific Microwave Conference, 2010.

[17] Akhtar M.j., Feher L., Thumm M.A., "A Multi-Layered Waveguide Technique for Determining Permittivity and Conductivity of Composite Materials"., Proceedings German Microwave Conference (2005), April 5-7, pp. 37-40

[18]Holloway C.L., Sarto M.S., and Johansson M.; "Analysing Carbon-Fiber Composite Materials with Equivalent Layer Models", IEEE Trans. Electromagnetic Compatibility, Vol. 47, No. 4, pp. 833-844, November 2005

[19] Kim Y.J., Shin T.S., Choi H.D., Kwon J.H, Chung Y., Yoon H.G.; "Electrical Conductivity of Chemically Modified Multiwalled Carbon Nanotube/Epoxy Composites", Carbon 2005; 43(1), pp. 23-30

[20] Bojovshi A., Scott J., and Ghorbani K., "The Reflectivity of Carbon Fiber Reinforced Polymer Short Circuit Illuminated by Guided Microwaves", Applied Physics Letters, 103, 111910 (2013)

[21] Dai H., Wong E.W., and Lieber C.M.; "Probing Electrical Transport in Nanomaterials: Conductivity of Individual Carbon Nanotubes", Science, 272-5261, pp. 523-526

[22] Farr, Everett G and Bowen, Leland H, "Results of Optimization Experiments on a Solid Reflector IRA", Sensor and Simulation Notes # 463, January, 2002

[23] C.E. Baum, "Radiation of impulse-like transient fields," Sensor and Simulation Notes #321, Nov. 1989

[24] C.E. Baum and E.G. Farr, "Impulse radiating antennas," in Ultra-Wide-band, Short-Pulse Electromagnetics, H.L.Bertoni, L. Carin and I. B. Felson, Ed. New York: Plenum, pp. 131-144, 1993.

[25] Burnside, W.D., and C. W. Chuang, “An Aperture-Matched Horn Design,” IEEE Transactions on Antennas and Propagation., AP-30, pp. 790-796, July 1982

[26] Pozar, David M., “Microwave Engineering”, 3rd Ed, John Wiley and Sons, Inc., New Jersey, 2005, p. 105